USE OF FLUORESCENT BI-FUNCTIONAL LINKERS IN MAKING METAL ORGANIC COORDINATION NETWORKS

Karan Pratap Singh Yadav

A dissertation submitted for the partial fulfilment of
BS-MS dual degree in Science

Indian Institute of Science Education and Research Mohali

April 2014

Certificate of Examination

This is to certify that the dissertation titled "Use of fluorescent bi-functional linkers in making Metal Organic Coordination Networks" submitted by Mr. Karan Pratap Singh Yadav (Reg. No. MS09070) for the partial fulfilment of BS-MS dual degree programme of the Institute has been examined by the thesis committee members duly appointed by the Institute. The committee finds the work done by the candidate satisfactory and recommends that the thesis be accepted.

Prof. Ramesh Kapoor	Dr. Ramesh Ramachandran	Dr. Sanjay Mandal
(Member)	(Member)	(Convener & Supervisor)

Dated: April 25, 2014

Declaration

The work presented in this dissertation has been carried out by me under the guidance of Dr. Sanjay Mandal at the Indian Institute of Science Education and Research Mohali. This work has not been submitted in part or in full for a degree, a diploma, or a fellowship to any other university or institute. Whenever contributions of others are involved, every effort is made to indicate this clearly, with due acknowledgement of collaborative research and discussions. This thesis is a bonafide record of original work done by me and all sources listed within have been detailed in the bibliography.

Karan Pratap Singh Yadav

Dated: April 25, 2014

In my capacity as the supervisor of the candidate's project work, I certify that the above statements by the candidate are true to the best of my knowledge.

Dr. Sanjay Mandal

Dated: April 25, 2014

Acknowledgements

I sincerely thank my project supervisor Dr. Sanjay Mandal for giving me this opportunity to explore an interesting facet of MOCNs. I am grateful for his keen supervision, valuable advice and open-minded approach. I highly appreciate the amount of freedom given to design the project so as to cultivate my curiosities in this amazing field of chemistry.

I am highly indebted to Navnita Kumar for her consistent guidance, timely assistance and encouragement during the entire duration of the project. I thank all of my labmates for their support and lively workplace company.

I would like to thank IISER Mohali for providing all the facilities for research work. CIL at NIPER Mohali is acknowledged for elemental analysis. An INSPIRE fellowship from the MHRD, Govt. of India, is gratefully appreciated during the BS-MS program for the past five years.

Lastly, I thank my friends and family for their love and care at all times.

List of Figures

Figure 1. Schematic representations of 1D, 2D and 3D MOCNs 1

Figure 2. Jablonski diagram depicting the luminescence phenomenon 8

Figure 3. Representation of emission possibilities in MOCN 8

Figure 4. Schematic representation of antenna effect 9

Figure 5. Structure of perylene-3,4,9,10-tetracarboxylic dinahydride (PTCDA) 11

Figure 6. Structure of Perylene diimide 11

Figure 7. TGA of linkers L1-L4 19

Figure 8. TGA of L1 and metal complexes **1-4** 19

Figure 9. TGA of L2 and metal complexes **5-8** 20

Figure 10. TGA of L3 and metal complexes **9-12** 20

Figure 11. TGA of L4 and metal complexes **13-16** 21

Figure 12. FTIR spectrum of L1 22

Figure 13. FTIR spectrum of L2 23

Figure 14. FTIR spectrum of L3 23

Figure 15. FTIR spectrum of L4 24

Figure 16. FTIR spectrum of $[Cu(Ala\text{-}Per)(H_2O)]_2 \cdot 6H_2O$ (**1**) 24

Figure 17. FTIR spectrum of $[Ni(Ala\text{-}Per)(H_2O)]_2 \cdot 3H_2O$ (**2**) 25

Figure 18. FTIR spectrum of $[Cd(Ala\text{-}Per)(H_2O)]_2$ (**3**) 25

Figure 19. FTIR spectrum of $[Zn(Ala\text{-}Per)(H_2O)]_2 \cdot 4H_2O$ (**4**) 26

Figure 20. FTIR spectrum of $[Cu(Phe\text{-}Per)(H_2O)]_2 \cdot 5H_2O$ (**5**) 26

Figure 21. FTIR spectrum of $[Ni(Phe\text{-}Per)(H_2O)]_2 \cdot 6H_2O$ (**6**) 27

Figure 22. FTIR spectrum of $[Cd(Phe\text{-}Per)(H_2O)]_2$ (**7**) 27

Figure 23. FTIR spectrum of $[Zn(Phe\text{-}Per)(H_2O)]_2 \cdot 2H_2O$ (**8**) 28

Figure 24. FTIR spectrum of $[Cu(Tyr\text{-}Per)(H_2O)]_2 \cdot 8H_2O$ (**9**) 28

Figure 25. FTIR spectrum of $[Ni(Tyr\text{-}Per)(H_2O)]_2 \cdot 8H_2O$ (**10**) 29

Figure 26. FTIR spectrum of $[Cd(Tyr\text{-}Per)(H_2O)]_2 \cdot 7H_2O$ (**11**) 29

Figure 27. FTIR spectrum of $[Zn(Tyr\text{-}Per)(H_2O)]_2 \cdot 8H_2O$ (**12**) 30

Figure 28. FTIR spectrum of $[Cu_2(Glu\text{-}Per)(H_2O)_2]_2 \cdot 5H_2O$ (**13**) 30

Figure 29. FTIR spectrum of $[Ni_2(Glu\text{-}Per)(H_2O)_2]_2 \cdot 7H_2O$ (**14**) 31

Figure 30. FTIR spectrum of $[Cd_2(Glu\text{-}Per)(H_2O)_2]_2 \cdot 5H_2O$ (**15**) 31

Figure 31. FTIR spectrum of $[Zn(Glu\text{-}Per)(H_2O)]_2 \cdot 3H_2O$ (**16**) 32

Figure 32. Emission spectra for L3 and metal complexes **9**, **10**, **11**; λ_{ex} = 410 nm 33

Figure 33. Emission spectrum of L1; λ_{ex} = 525 nm 34

Figure 34. Emission spectrum of $[Cu(Ala\text{-}Per)(H_2O)]_2 \cdot 6H_2O$ (**1**); λ_{ex} = 525 nm 34

Figure 35. Emission spectrum of $[Ni(Ala\text{-}Per)(H_2O)]_2 \cdot 3H_2O$ (**2**); λ_{ex} = 525 nm 35

Figure 36. Emission spectrum of $[Cd(Ala\text{-}Per)(H_2O)]_2$ (**3**); λ_{ex} = 525 nm 35

Figure 37. Emission spectrum of $[Zn(Ala\text{-}Per)(H_2O)]_2 \cdot 4H_2O$ (**4**); λ_{ex} = 525 nm 36

Figure 38. Emission spectrum of L2; λ_{ex} = 599 nm 36

Figure 39. Emission spectrum of $[Cu(Phe\text{-}Per)(H_2O)]_2 \cdot 5H_2O$ (**5**); λ_{ex} = 599 nm 37

Figure 40. Emission spectrum of $[Ni(Phe\text{-}Per)(H_2O)]_2 \cdot 6H_2O$ (**6**); λ_{ex} = 599 nm 37

Figure 41. Emission spectrum of $[Cd(Phe\text{-}Per)(H_2O)]_2$ (**7**); λ_{ex} = 599 nm 38

Figure 42. Emission spectrum of $[Zn(Phe\text{-}Per)(H_2O)]_2 \cdot 2H_2O$ (**8**); λ_{ex} = 599 nm 38

Figure 43. Emission spectrum of L3; λ_{ex} = 531 nm 39

Figure 44. Emission spectrum of $[Cu(Tyr\text{-}Per)(H_2O)]_2 \cdot 8H_2O$ (**9**); λ_{ex} = 261 nm 39

Figure 45. Emission spectrum of $[Cu(Tyr\text{-}Per)(H_2O)]_2 \cdot 8H_2O$ (**9**); λ_{ex} = 531 nm 40

Figure 46. Emission spectrum of $[Ni(Tyr\text{-}Per)(H_2O)]_2 \cdot 8H_2O$ (**10**); λ_{ex} = 491 nm 40

Figure 47. Emission spectrum of $[Ni(Tyr\text{-}Per)(H_2O)]_2 \cdot 8H_2O$ (**10**); λ_{ex} = 531 nm 41

Figure 48. Emission spectrum of $[Cd(Tyr\text{-}Per)(H_2O)]_2 \cdot 7H_2O$ (**11**); λ_{ex} = 531 nm 41

Figure 49. Emission spectrum of $[Zn(Tyr\text{-}Per)(H_2O)]_2 \cdot 8H_2O$ (**12**); λ_{ex} = 531 nm 42

Figure 50. Emission spectrum of L4; λ_{ex} = 524 nm 42

Figure 51. Emission spectrum of $[Cu_2(Glu\text{-}Per)(H_2O)_2]_2 \cdot 5H_2O$ (**13**); λ_{ex} = 254 nm 43

Figure 52. Emission spectrum of $[Cu_2(Glu\text{-}Per)(H_2O)_2]_2 \cdot 5H_2O$ (**13**); λ_{ex} = 524 nm 43

Figure 53. Emission spectrum of $[Ni_2(Glu\text{-}Per)(H_2O)_2]_2 \cdot 7H_2O$ (**14**); λ_{ex} = 524 nm 44

Figure 54. Emission spectrum of $[Cd_2(Glu\text{-}Per)(H_2O)_2]_2 \cdot 5H_2O$ (**15**); λ_{ex} = 524 nm 44

Figure 55. Emission spectrum of $[Zn(Glu\text{-}Per)(H_2O)]_2 \cdot 3H_2O$ (**16**); λ_{ex} = 524 nm 45

Figure 56. CD spectra for L3 and metal complexes **9**, **10** and **11** 45

Figure 57. PXRD patterns of L1 and metal complexes **1-4** 46

Figure 58. PXRD patterns of L2 and metal complexes **5-8** 47

Figure 59. PXRD patterns of L3 and metal complexes **9-12** 47

List of Tables

Table 1. Metal complexes generated using perylene based linkers 11

Table 2. FTIR stretching frequencies for metal complexes 22

List of Schemes

Scheme 1: Synthesis of perylene based linkers 17

Scheme 2: Synthesis of metal complexes 18

Contents

List of Figures	i
List of Tables	iii
List of Schemes	iii
Abstract	v
Introduction	1
Experimental Section	12
Results and Discussion	17
Conclusion and Future directions	48
References	49

Abstract

Perylene-3,4,9,10-tetracarboxylic dianhydride (PTCDA) is employed to synthesize four bi-functional fluorescent linkers (L1-L4) by reacting it with amino acids, such as L-Alanine, L-Phenylalanine, L-Tyrosine and L-Glutamic acid, respectively. All four linkers are characterized by FTIR, ^{1}H NMR, circular dichroism and fluorescence spectroscopy, thermogravimetric analysis (TGA) and powder X-ray diffractometry. Metal complexes (**1-16**) were prepared for different ratios (1:1 or 1:2) of transition metal ions, such as Cu^{2+}, Ni^{2+}, Cd^{2+} and Zn^{2+}, and one of the linkers. All metal complexes are characterized by elemental analysis, FTIR, circular dichroism and fluorescence spectroscopy, TGA and powder X-ray diffractometry. TGA shows that linkers as well as the complexes are thermally stable up to 300 ^{0}C. PXRD patterns strongly suggest their isostructural nature, although being low in intensity hinting at limited crystalline nature. These frameworks can have various non-covalent interactions, like hydrogen bonding, π-π interactions, etc., along with coordination bonds to form supramolecular coordination networks. These type of metal organic coordination networks (MOCNs) have inherent fluorescent property and therefore are tested for photoluminescence based sensing applications, with quenching phenomenon being predominant in the solution state.

Chapter I

INTRODUCTION

Metal Organic Coordination Networks (MOCNs), an emerging class of materials, is the power of an idea to pursue interdisciplinary research, blending two often disparately regarded streams of inorganic and organic chemistry.[1] Theoretically speaking, combination of two fundamental units of every MOCN, i.e. the metal ion and the organic linker, provide endless possibilities. MOCNs can be broadly classified into three categories based on the type of interactions present in them, leading to different dimensionality and functionality (Figure 1).

1. Coordination polymers: 1D, 2D, 3D non porous coordination materials.
2. Metal Organic Frameworks (MOFs): 1D, 2D, 3D porous coordination frameworks.
3. Supramolecular Assemblies: 1D, 2D, 3D non porous/porous frameworks. In this case, the interactions of concern are hydrogen bonding and π-π interactions that are responsible for the generation of the porous frameworks.

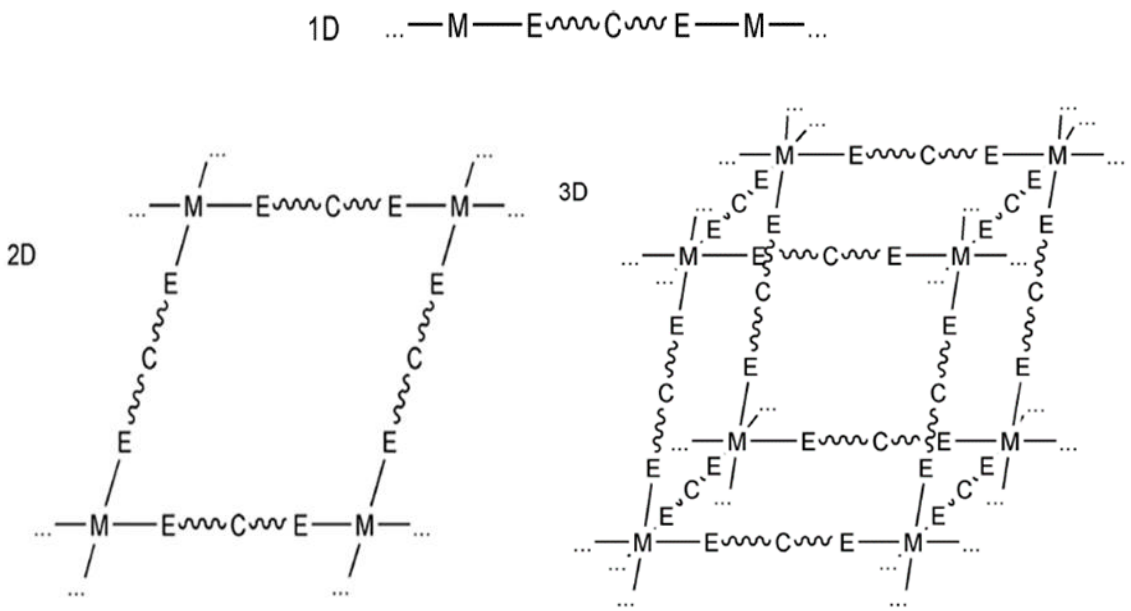

Figure 1. Schematic representations of 1D, 2D and 3D MOCNs.[2]
(M = metal centre; C = carbon; E = donor atoms, i.e., O, N, S, etc.)

Dimensionality of any MOCN is governed by the number of coordination sites on the metal ion and the denticity of the organic linker. Metal ions generally used are transition metal ions

or lanthanide metal ions providing a huge range of coordination number leading to multiple possibilities. Organic linker molecules with varying degrees of denticity occupy some of the coordination sites of a metal ion, leaving others for other coordinating species, thereby helping in progression of framework structure. Combination of a metal ion with a linker molecule is generally referred as Secondary Building Unit (SBU).[3] All of above subsets of MOCNs have common building blocks differing in their organisation around the metal centre and other types of interactions within the structure. Thus, components of MOCNs, in totality, are:

1. Metal ions: Generally transition metal ions are used. Lanthanides have also been examined.

2. Linkers: Organic species that serves as a bridge between two metal centres. Anionic (generally oxygen containing, e.g. carboxylates) and neutral (generally nitrogen containing, e.g. 4,4'-bipyridine, pyrazine) linkers are common.[2] Cationic linkers, such as bipyridinium derivatives, are also known. Linkers provide extreme scopes of topological and functional diversity in MOCNs.

3. Ligands: Organic species localised on one metal centre. These help to tune the physical properties of the MOCNs and therefore its applications.

4. Counter ions: Anions/Cations to balance the charge. Anions are more common.

5. Guest molecules: Porosity in the framework leads to trapping of solvent molecules in the structure. Species other than solvent medium could be trapped too.

Earlier work dates back to 1965 when metal frameworks of zinc, nickel, iron, aluminium, etc. with aromatic di- or tri-carboxylate were prepared. A new wave came along with the concept of reticular design and some ground breaking results from the group of O. M. Yaghi,[4] S. Kitagawa,[5] G. Ferey,[6] etc. Several comparisons with oxides, molecular sieves, porous carbon and hetero-polyanion salts have been made. Self-assembly of metal ions, which act as coordination centres, linked together with a variety of polyatomic organic bridging ligands, resulted in tailored nano-porous host materials as robust solids with high thermal and mechanical stability. Unlike other solid matter, e.g. zeolites, carbons and metal oxides, a number of coordination compounds are known to exhibit high framework flexibility and shrinkage/expansion due to interactions with guest molecules. The total lack of non-accessible bulk volume in MOF structures is a huge advantage over earlier materials. All advantages can be attributed to the huge amount of tunability of structure and properties in case of MOCNs by

varying the components. Theoretically, it provides an option to develop compounds with all the desired properties by adopting the correct methodology. Diversity of organic component allows us to target various physical properties and therefore, foray into multitudes of applications, such as catalysis,[7,8,9] sensors,[10-13] gas purification, gas separation and gas storage,[14-17] light harvesting materials,[18] drug delivery systems,[19] and so on.

Synthesis of MOCNs

Since the structural and physical properties of MOCNs are largely dependent on the nature of components and their interactions, synthesis becomes challenging, and also interesting. In order to formulate the exact synthetic strategy, the understanding of possible topologies, functionality of organic linker molecules, and also the metal coordination environment becomes essential. Challenge is to come up with reaction conditions which secure the organic moiety while forming the defined framework with desired particle size and properties.

Conventional synthetic method[20] is to take metal ion and organic linker in a solution, and stir them for few hours at room temperature, allowing self-assembly of the components involved. Sheer simplicity of this one pot synthetic method has led to it's widespread use. This synthesis could also be performed at elevated temperatures. As far as synthetic requirements are below or at the boiling point under ambient pressure, the reaction is classified under Non-solvothermal method. However, due to solubility constraints of MOCNs generated, additional steps have to be performed for crystallization, such as layering of solutions, slow diffusion of reactants into each other or solvent evaporation are employed. All of them exploit the principle of concentration gradient. Temperature gradient can also be used to generate concentration gradient. However, it must be taken into account that temperature can have strong influence on the crystal morphology and stability. MOF-5, MOF-177, HKUST-1, ZIF-8 are some examples synthesized using this strategy.[20-23]

Solvothermal reactions as defined by Rabenau,[24] are the reactions occurring in closed vessels under autogenous pressure above the boiling point of the solvent. In this method, all the reactants are mixed together along with the solvent in a solvothermal bomb and placed in a programmable oven under high temperature for few days. Once the reaction time is over, the bomb is allowed to cool slowly by providing a temperature gradient, generating crystals of MOFs directly. Stringent temperature and pressure conditions reduce the simple nature as compared to non-solvothermal reactions, but the ability to generate crystals without any extra step makes this method desirable.

Methods have been borrowed from other fields so as to increase the efficiency of the reaction by getting better yield and the ability to scale up, reduce reaction time and also improve the quality of thus obtained product. Microwave-assisted synthesis, electrochemical synthesis, sonochemical synthesis and mechanochemical synthesis are some of the techniques employed.[20] Alternative routes are important as they lead to generation of products with different size and morphology, which has huge impact on it's properties.

Microwave-assisted synthesis utilize the phenomenon of interaction of electromagnetic waves with electronic charge carriers. Microwave assisted method focus on accelerating the rate, obtaining nanoscale product, improving the product quality and generation of selective polymorphs. Direct interaction of the microwave radiation with the solvent/reactant makes it an energy-efficient method. Ni and Masel[25] were the first to use microwave irradiation to synthesize MOFs. They made IRMOF-1 (also known as MOF-5), IRMOF−2 and IRMOF−3 with reaction times greatly reduced and products being microcrystalline. Starting materials may interact strongly with radiation, therefore choice of solvents and energy input should be well thought of.

Electrochemical synthesis method was developed in 2005 by researchers at BASF with the aim of excluding anions, such as nitrate, perchlorate or chloride, which get incorporated into the framework during the synthesis, especially during large scale production. Direct introduction of the metal ions through anionic dissolution, into the reaction medium composed of the organic linker and a conducting salt is carried out, instead of using the metal salts. Electrochemical route is advantageous as it runs as continuous process and gives a higher solid content, when compared to batch processes. Researchers from BASF reported various combinations of anode materials (Zn, Cu, Mg, Co) and linkers (1,3,5-H_3BTC, 1,2,3-H_3BTC, H_2BDC).[26]

Sonochemical synthesis method involves the application of high-energy ultrasound waves to reaction mixtures. There is no direct interaction between ultrasound waves and the molecules, as the wavelength of ultrasound is much larger than the molecular dimensions. Very high and very low pressure zones are formed upon sonochemical irradiation, resulting in cavitation, the formation and collapse of bubbles in solution. Generation of very high local temperatures (greater than 5000 K), results in extremely fast heating and cooling rates. Crystals of MOF-5 in 1-methyl-2-pyrrolidinone (NMP) has been obtained using this method.[27] Sonochemical

synthesis is a fast, energy-efficient, environmentally friendly method that can easily be carried out at room temperature. Nano-crystalline particles are often obtained via this method.

Mechanochemical synthesis method, also known as solid-state synthesis, involves grinding of components together to get the product. In 2006, Pichon et al.[28] first reported the synthesis of a copper-isonicotinic acid MOF using this method. Hydrated metal salts enhance the reactivity due to the release of H_2O molecules which assists the grinding process leading to Liquid-assisted grinding (LAG), a modification involving use of very small amount of solvent. 1D, 2D, and 3D coordination polymers by varying the solvent added to a mixture of fumaric acid and ZnO have been reported.[29]

Other aspects of synthesis, such as control of catenation, in-situ synthesis of linker molecules, role of solvents and other structure directing agents must be taken into account along with reaction parameters to get the desired product.

In case the MOCNs generated are robust and porous, a large number of post synthetic modification steps are possible, allowing late-stage transformations without having substantial impact on the framework. Postsynthetic modifications[30,31] are basically chemical derivatization of MOCNs after their formation. Some of the advantages offered are:

1. Possibility to include more diverse functional groups, earlier restricted by synthetic conditions.
2. Chemical derivatization is performed directly on crystalline solids (e.g. heterogeneous) leading to facile purification and isolation of modified products.
3. Generation of a pool of topologically identical, but functionally diverse MOCNs, as a given structure can be modified with different reagents.
4. Control over both the type of substituent and the degree of modification, allowing introduction of multiple functional units into a single framework, thus enabling an effective way to systematically fine-tune and optimize properties.

Applications of MOCNs

MOCNs are expanding to every possible facet known to material science, whether it be sensors, storage materials, catalysis, biomedicine, gas separation and purification and several other aspects of host-guest chemistry. It would only be possible to discuss a few of them here.

Catalysis: MOCNs have graduated to advanced levels when it comes to catalysis because of higher porosity as compared to other materials. Although not as stable as zeolites, they have

developed a niche in field of enantioselective catalysis, production of fine chemicals and delicate molecules. Different type of concepts have been demonstrated ranging from heterogenization of well defined homogeneous catalysts, framework encapsulation of molecular catalysts, coupling of catalysis to chemical separation and to substrate size selective catalysis. Multi-catalyst architectures and reactivity defining microenvironments are some of the fields which are yet to be explored. MOF-5, reported by Ravon et. al. catalyzes the Friedal-Craft tert-butylation of both toluene and biphenyl. Para-alkylation is strongly favoured over ortho alkylation, which reflects the encapsulation of reactants by MOF-5. $AlCl_3$ on the other hand is nonselective to alkylation, as there are no well defined cavities like MOF-5.[32]

Gas storage, separation and purification: High framework flexibility and total lack of inaccessible volume have revolutionised the field of storage materials. Properties like the drastically increased velocity of molecular traffic through these open structures are closely related to the regularity of pores in nanometre size. Porosity along with high surface area facilitate such purposes.

Gas purification: Structures with accessible open metal sites are well suited to strongly (>30 kJ mol^{-1}) chemisorb electron-rich, odour-generating molecules, like amines, phosphines, oxygenates, alcohols, water, or sulphur containing molecules. Removal of ppm traces of sulphur components from various gases have been achieved. e.g.: removal of tetrahydrothiophene (THT, odorant) from natural gas. At room temperature, traces of 10–15 ppm sulphur were fully captured down to less than 1 ppm using an electrochemically prepared shaped Cu-EMOF in a fixed bed reactor.[33] The overall capacity of the MOF material outperformed the commercially available activated carbon materials as adsorbents by about an order of magnitude.

Gas separation: In gas separation processes, the gas mixtures usually consist of components having concentrations in the same order of magnitude. Usually, either distillation or pressure and/or thermal swing adsorption–desorption are used to separate the mixtures. Examples of existing technologies are nitrogen–oxygen (air), nitrogen–methane, and noble gas (e.g. Kr–Xe) separations. Interestingly, small pore MOFs are able to separate molecules by size or kinetic diameter, e.g., while water uptake occurs, slightly larger molecules such as N_2, O_2, CO_2, and methane are occluded from adsorption. e.g.: the adsorption isotherms of nitrogen and hydrogen for the small-pore Mg-MOF (Basolite M050)[34] show preferential adsorption of hydrogen over nitrogen.

Gas storage: Due to the absence of dead volume, there is increase in specific gas storage. This effect depends on the type, temperature and pressure of the gas, as well as on the specific MOF material being used. MOF-storage for hydrogen works fully reversibly, avoids complicated heat treatments, and recharging proceeds within seconds or minutes. This clearly is an advantage over metal hydrides as storage materials. In MOF-5 even the distinct locations of adsorbed hydrogen molecules have been elucidated using inelastic neutron scattering, while density functional theory (DFT) studies have proposed a storage capacity of 16–20 molecules of H_2 per Zn_4O cluster.[35]

Medicine: Given the host-guest interactions present in the cavities in MOCNs they have the potential to act as excellent carriers of drug molecules for targeted delivery. Tunability of pore size and shape, chemical composition, microenvironment facilitates the selectivity of guest molecule and release mechanism. Apart from that given the luminescent nature of some MOCNs they can also be used in bio-imaging. e.g.: Paramagnetism helps to increase the relaxation rate of water protons in the tissues being imaged. Lanthanides, being highly paramagnetic, are often used as contrast agents in magnetic resonance imaging (MRI). $Gd(1,4\text{-}BDC)_{1.5}$, a nanoMOF by Reiter et al.[36] was found to be better enhancer of water signals as compared to other commercially available contrast agents.

Luminescent MOCNs

MOCNs showing luminescent behaviour are an important subset of the bigger family because of huge potential in fields of chemical and biological sensing, imaging, optoelectronics, energy storage and conversion, etc.[10] Luminescence can simply be defined as emission of light upon absorption of energy. Fluorescence the common form, is a spin allowed transition from lowest singlet excited state to singlet ground state, having lifetime in nanoseconds. Photoluminescence is a spin forbidden transition from lowest triplet excited state, having varying lifetimes from milliseconds to few seconds (Figure 2).

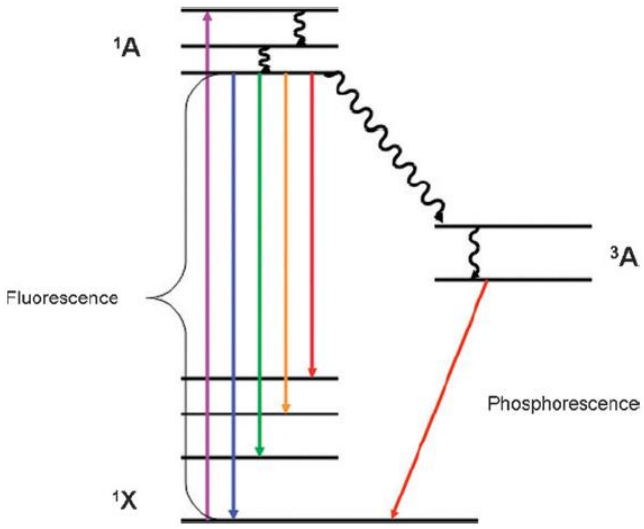

Figure 2. Jablonski diagram depicting the luminescence phenomenon.[10]
(^{1}X: singlet ground state, ^{1}A: singlet excited state, ^{3}A: triplet excited state)

Building blocks of MOCNs: organic linkers and/or the metal ions are the major cause of luminescence (Figure 3). Guest molecule entrapped in the framework may also contribute to luminescence.

Generally organic linkers lead to fluorescence. The π electrons due to extended π networks or presence of an aromatic moiety in these linkers contribute heavily to luminescence. This can be classified as linker based luminescence or ligand-to-ligand charge transfer (LLCT). Organic fluorophores are immobilized in an ordered arrangement and are in close proximity with one another in a MOCN structure, thereby invoking different intermolecular interactions. As a result photoemission may be different from free form.

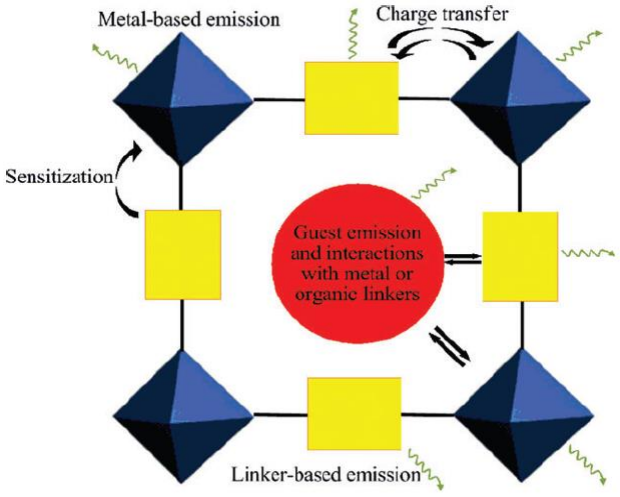

Figure 3. Representation of emission possibilities in MOCN.[10]

The d^{10} transition metal based MOCNs show phenomena of ligand to metal charge transfer (LMCT) and metal to ligand charge transfer (MLCT). LMCT is often observed in Zn(II) and Cd(II) compounds while MLCT is generally seen in Cu(I) and Ag(I) compounds. These mechanisms are not mutually exclusive. More than one emission pathway can coexist in a competitive manner with another. Ligand-field transitions (d–d) in case of paramagnetic transition metal complexes may lead to strong reabsorption and/or quenching of fluorescence arising because of the organic moiety, which can occur via electron or energy transfer through the partially filled d-orbitals. Lanthanide MOCNs show metal-centered luminescence, generally phosphorescence. Antenna effects (Figure 4) leads to transfer of energy from triplet excited state of linkers to lanthanide's emissive states.

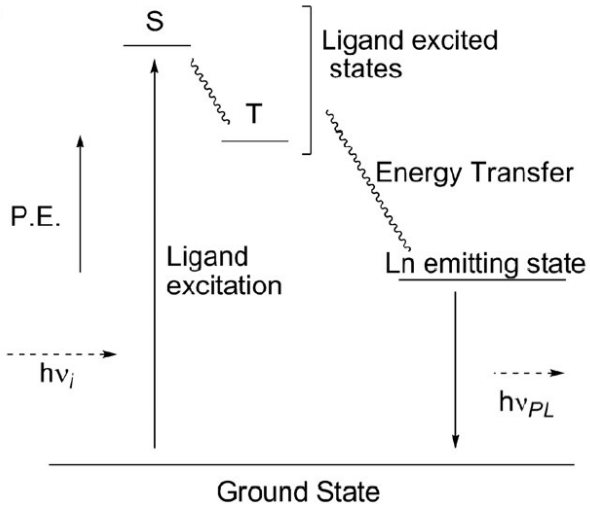

Figure 4. Schematic representation of antenna effect.[10]

Role of luminescent MOCNs as sensors

Photoluminescence based sensors are the most widely explored till date because of its simplicity, involving a signal which a normal human eye can detect. Advancements in fluorescence spectroscopy with detection limits reaching to single molecule level and also the ability to analyse powdered samples directly, without the need of film fabrication or any other processing steps further strengthen their ground. Signal quenching or enhancement, both are possible depending on the analyte molecule and it's interaction with molecular probe. Different type of sensing are discussed below:

Chemical sensing (size-selective): Luminescent Zn_3btc_2 (btc = benzenetricarboxylate) was tested for diffusion of different amines. Following exposure to amines of different sizes, a

decrease in the fluorescence was observed for amines that were small enough to easily diffuse into the MOF pores, including ethylamine, dimethylamine, and propylamine. In contrast, aniline and butylamine showed no quenching, due to size exclusion. Large surface areas combined with confinement of analyte inside the MOF cavities lead to high sensitivity.[37,38]

Explosive sensing: $Zn_2(bpdc)_2bpee$ (bpdc = 4,4'-biphenyldicarboxylate; bpee = 1,2-bipyridylethene), a MOF containing a linker with the potential to fluoresce, was screened for the detection of 1,4-dinitrotoluene (DNT), which is a byproduct of the formation of 2,4,6-trinitrotoluene (TNT) and 2,3-dimethyl-2,3-dinitrobutane (DMNB). The latter is an additive used to facilitate detection of plastic explosives. In both the cases electron transfer from the framework to guest molecule lead to decrease in intensity. Within 10s the fluorescence intensity dropped by 85%, showcasing a very fast and efficient detection of nitroexplosives.[39,40]

Biosensing: Detection of Dipicolinic acid (DPA) helps in prevention of *Bacillus anthracis* related biological attacks. $Eu_2(fma)_2(ox)(H_2O)_4 \cdot 4H_2O$, a nano MOF, was used recently for the effective turn-on detection of DPA.[41] Nanoscale particle size enhances the sensitivity for the detection of DPA along with ensuring uniform dispersion into the solvent. Addition of a small amount of DPA (2 ppm) to the MOF suspension significantly increases the luminescent intensity of the mixture (90 times of its original emission intensity). Preferential binding of DPA at the Eu^{+3} center, which can largely facilitate the intramolecular energy transfer leads to high sensitivity, which is shown by negligible effect on emission intensity upon exposure to other components that coexist within the bacterial endospores.

Present work

Perylene (Figure 5) dye has been known as highly photostable pigments or vat dyes.[42-44] Perylene derivatives have been studied because of their brilliant colour, strong absorption and fluorescence and good thermal, chemical, photochemical and electrochemical stability making them highly promising materials for applications in organic solar cells, photovoltaic devices, and for dye lasers.[45-47] Although synthesis of chiral perylenediimides[48] have been done, the synthesis of macromolecules with inherently strong chiral properties remains as a challenge. It is important to strike a balance between good solubility and the ability to form stacks with extensive intermolecular orbital overlap, for various applications. This could be achieved by substituent tuning the face-to-face interaction of perylene dye. Also, enhancement of structural stability should be taken into account in order to provide efficient chiroptical switching.

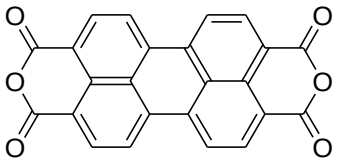

Figure 5. Structure of Perylene-3,4,9,10-tetracarboxylic dinahydride (PTCDA).

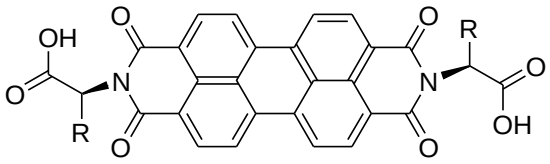

Figure 6. Structure of Perylene diimide.

Above mentioned linker molecule (Figure 6) is generated by reacting PTCDA with the desired amino acid.[48-51] In this work L-Alanine, L-Phenylalanine, L-Tyrosine and L-Glutamic acid are used to make four different linkers, which are Ala-Per (L1), Phe-Per (L2), Tyr-Per (L3) and Glu-Per (L4), respectively. Apart from inherent fluorescent property, these linker molecules also have chiral centers which enhances the functionality and possible applications. Sixteen transition metal complexes of Cu^{+2}, Ni^{+2}, Cd^{+2} and Zn^{+2} were prepared with these linkers.

Table 1. Metal complexes generated using perylene based linkers.

	Ala-Per (L1)	Phe-Per (L2)	Tyr-Per (L3)	Glu-Per (L4)
Cu^{+2}	**1**	**5**	**9**	**13**
Ni^{+2}	**2**	**6**	**10**	**14**
Cd^{+2}	**3**	**7**	**11**	**15**
Zn^{+2}	**4**	**8**	**12**	**16**

All complexes were characterised by elemental analysis, FTIR, circular dichroism spectroscopy and fluorescence spectroscopy, thermo gravimetric analysis and powder X-ray diffractometry.

Chapter II

EXPERIMENTAL SECTION

Materials and Methods

All chemicals and solvents required in synthesis were obtained from commercial sources and used as received without any purification. FTIR spectra were collected for compounds prepared as KBr pellets using Perkin Elmer Spectrum RX I FT-IR spectrometer in the 400-4000 cm^{-1} range. Thermal Gravimetric Analysis was done using Shimadzu DTG-60H analyser in a range from 30-500 ^{0}C. UV-Vis spectra were recorded on Agilent technologies Cary 5000 UV-Vis-NIR spectrophotometer for the range 300-800 nm. Circular dichroism (CD) spectra were recorded on Appliedphotophysics Chirascan CD spectrophotometer. Solution state fluorescence spectra were recorded on Perkin Elmer LS 55 fluorescence spectrometer. Powder X-ray experiments were carried on a Rigaku Ultima IV diffractometer. Elemental analysis was carried out at Central Instrumentation Lab, NIPER Mohali. Melting point was measured on Buchi M-565 melting point apparatus. ^{1}H NMR spectra were recorded at room temperature using Bruker ARX 400 spectrometer. Solid state fluorescence was performed on Shimadzu RF-5301 PC spectrofluorophotometer.

Synthesis

General procedure for synthesis of Perylene-3,4,9,10-tetracarboxylic dianhydride based bi-functional linkers

In a 25 mL RB flask (2 neck), L form of amino acid, Perylene-3,4,9,10-tetracarboxylic dianhydride (PTCDA) and imidazole were taken. Mixture was then purged with Nitrogen (2-3 cycles). The RB was then filled with Nitrogen for 15 minutes and then the mixture was heated. Reaction mixture was then cooled to 100 ^{0}C. Distilled water (10 mL) was added under Nitrogen atmosphere. Dark red solution was filtered by addition of water (20 mL) on crucible. Solution obtained upon filtration was then acidified with 2M HCl solution till pH was close to 1 (no more precipitate formation). Precipitate formed was then collected via filtration and washed with water till neutral pH. Thus obtained red solid was dried in a desiccator and then analysed.

Ala-Per (L1). It is prepared following the general procedure where 190 mg (2.1 mmol) L-Alanine, 392 mg (1 mmol) PTCDA and 2.8 g (41 mmol) of imidazole were used. Heating was

carried out at 130 ^{0}C for 30 minutes. Yield: 98%. Melting point: 336 ^{0}C. FTIR (KBr, cm^{-1}): 3498 (s), 1745 (vs), 1697 (vs), 1344 (vs), 1179 (s).

Phe-Per (L2). It is prepared following the general procedure where 346.5 mg (2.1 mmol) L-Phenylalanine, 392 mg (1 mmol) PTCDA and 2.8 g (41 mmol) of imidazole were used. Heating was carried out at 130 ^{0}C for 2 hours. Yield: 98%. Melting point: 350 ^{0}C. FTIR (KBr, cm^{-1}): 3469 (m), 1732 (m), 1697 (vs), 1344 (s), 1169 (m).

Tyr-Per (L3). It is prepared following the general procedure where 362 mg (2 mmol) L-Tyrosine, 392 mg (1 mmol) PTCDA and 1.36 g (20 mmol) of imidazole were used. Heating was carried out at 130 ^{0}C for 5 hours. Yield: 97%. Melting point: 290 ^{0}C. FTIR (KBr, cm^{-1}): 3421 (s), 1729 (s), 1694 (vs), 1345 (s), 1171 (s).

Glu-Per (L4). It is prepared following the general procedure where 294 mg (2 mmol) L-Glutamic acid, 392 mg (1 mmol) PTCDA and 2.8 g (41 mmol) of imidazole were used. Heating was carried out at 130 ^{0}C for 8 hours. Yield: 85%. Melting point: 363 ^{0}C. FTIR (KBr, cm^{-1}): 3450 (m), 1752 (vs), 1696 (vs), 1342 (s), 1167 (s).

General procedure for room temperature synthesis of metal complexes of linkers L1-L4

In a 10 ml RB flask linker and 5 ml of H_2O were taken and stirred for 10 min. Metal acetate was then added and the mixture was stirred for next 24 hours. Resulting precipitate was filtered via suction (washing with water). Obtained product was dried overnight in a desiccator and then analysed.

[Cu(Ala-Per)(H_2O)]$_2$·6H_2O (1). $Cu(OAc)_2·H_2O$ (19 mg, 0.1 mmol) was used as the metal salt with Ala-Per (50 mg, 0.1 mmol) as the linker. Intense red solid was obtained. Yield: 90%. FTIR (KBr, cm^{-1}): $\boldsymbol{\nu}_{CO}$ (carboxylic, asymmetric) = 1651; $\boldsymbol{\nu}_{CO}$ (carboxylic, symmetric) = 1367; $\boldsymbol{\nu}_{OH}$ (water, coordinated) = 3217; $\boldsymbol{\nu}_{OH}$ (water, free) = 3399. Elemental analysis (CHN) for $C_{60}H_{48}N_4O_{24}Cu_2$ (MW = 1335); calculated: 53.93, 3.59, 4.19; found: 53.60, 3.12, 4.17.

[Ni(Ala-Per)(H_2O)]$_2$·3H_2O (2). $Ni(OAc)_2·4H_2O$ (23.5 mg, 0.1 mmol) was used as the metal salt with Ala-Per (50 mg, 0.1 mmol) as the linker. Intense red solid was obtained. Yield: 94%. FTIR (KBr, cm^{-1}): $\boldsymbol{\nu}_{CO}$ (carboxylic, asymmetric) = 1652; $\boldsymbol{\nu}_{CO}$ (carboxylic, symmetric) = 1367;

ν_{OH} (water, coordinated) = 3208; ν_{OH} (water, free) = 3402. Elemental analysis (CHN) for $C_{60}H_{42}N_4O_{21}Ni_2$ (MW = 1272); calculated: 56.60, 3.30, 4.40; found: 56.29, 3.39, 4.30.

[Cd(Ala-Per)(H_2O)]$_2$ (3). $Cd(OAc)_2 \cdot 2H_2O$ (25 mg, 0.1 mmol) was used as the metal salt with Ala-Per (50 mg, 0.1 mmol) as the linker. Intense red solid was obtained. Yield: 90%. FTIR (KBr, cm^{-1}): ν_{CO} (carboxylic, asymmetric) = 1648; ν_{CO} (carboxylic, symmetric) = 1367; ν_{OH} (water, coordinated) = 3209; ν_{OH} (water, free) = 3434. Elemental analysis (CHN) for $C_{60}H_{36}N_4O_{18}Cd_2$ (MW = 1324); calculated: 54.38, 2.71, 4.22; found: 54.91, 3.16, 4.14.

[Zn(Ala-Per)(H_2O)]$_2 \cdot 4H_2O$ (4). $Zn(OAc)_2 \cdot 2H_2O$ (20.6 mg, 0.1 mmol) was used as the metal salt with Ala-Per (50 mg, 0.1 mmol) as the linker. Intense red solid was obtained. Yield: 87%. FTIR (KBr, cm^{-1}): ν_{CO} (carboxylic, asymmetric) = 1648; ν_{CO} (carboxylic, symmetric) = 1367; ν_{OH} (water, coordinated) = 3213; ν_{OH} (water, free) = 3430. Elemental analysis (CHN) for $C_{60}H_{44}N_4O_{22}Zn_2$ (MW = 1302); calculated: 55.29, 3.37, 4.30; found: 55.70, 3.35, 4.11.

[Cu(Phe-Per)(H_2O)]$_2 \cdot 5H_2O$ (5). $Cu(OAc)_2 \cdot H_2O$ (14.6 mg, 0.073 mmol) was used as the metal salt with Phe-Per (50 mg, 0.073 mmol) as the linker. Intense red solid was obtained. Yield: 81%. FTIR (KBr, cm^{-1}): ν_{CO} (carboxylic, asymmetric) = 1654; ν_{CO} (carboxylic, symmetric) = 1367; ν_{OH} (water, coordinated) is not clear; ν_{OH} (water, free) = 3447. Elemental analysis (CHN) for $C_{84}H_{62}N_4O_{23}Cu_2$ (MW = 1621); calculated: 62.18, 3.82, 3.45; found: 62.76, 4.00, 3.55.

[Ni(Phe-Per)(H_2O)]$_2 \cdot 6H_2O$ (6). $Ni(OAc)_2 \cdot 4H_2O$ (18.2 mg, 0.073 mmol) was used as the metal salt with Phe-Per (50 mg, 0.073 mmol) as the linker. Intense red solid was obtained. Yield: 86%. FTIR (KBr, cm^{-1}): ν_{CO} (carboxylic, asymmetric) = 1654; ν_{CO} (carboxylic, symmetric) = 1367; ν_{OH} (water, coordinated) = 3208; ν_{OH} (water, free) = 3434. Elemental analysis (CHN) for $C_{84}H_{64}N_4O_{24}Ni_2$ (MW = 1630); calculated: 61.84, 3.92, 3.44; found: 62.40, 4.01, 3.54.

[Cd(Phe-Per)(H_2O)]$_2$ (7). $Cd(OAc)_2 \cdot 2H_2O$ (19.4 mg, 0.073 mmol) was used as the metal salt with Phe-Per (50 mg, 0.073 mmol) as the linker. Intense red solid was obtained. Yield: 89%. FTIR (KBr, cm^{-1}): ν_{CO} (carboxylic, asymmetric) = 1654; ν_{CO} (carboxylic, symmetric) = 1366; ν_{OH} (water, coordinated) is not clear; ν_{OH} (water, free) = 3447. Elemental analysis (CHN) for $C_{84}H_{52}N_4O_{18}Cd_2$ (MW = 1628); calculated: 61.91, 3.19, 3.44; found: 62.08, 3.79, 3.51.

[Zn(Phe-Per)(H_2O)]$_2 \cdot 2H_2O$ (8). $Zn(OAc)_2 \cdot 2H_2O$ (16 mg, 0.073 mmol) was used as the metal salt with Phe-Per (50 mg, 0.073 mmol) as the linker. An intense red solid was obtained. Yield: 89%. FTIR (KBr, cm^{-1}): ν_{CO} (carboxylic, asymmetric) = 1654; ν_{CO} (carboxylic, symmetric) =

1367; ν_{OH} (water, coordinated) = 3213; ν_{OH} (water, free) = 3466. Elemental analysis (CHN) for $C_{84}H_{56}N_4O_{20}Zn_2$ (MW = 1570); calculated: 64.20, 3.57, 3.57; found: 64.30, 3.66, 3.61.

[Cu(Tyr-Per)(H$_2$O)]$_2$·8H$_2$O (9). $Cu(OAc)_2 \cdot H_2O$ (14 mg, 0.07 mmol) was used as the metal salt with Tyr-Per (50 mg, 0.07 mmol) as the linker. Intense red solid was obtained. Yield: 92%. FTIR (KBr, cm^{-1}): ν_{CO} (carboxylic, asymmetric) = 1647; ν_{CO} (carboxylic, symmetric) = 1362; ν_{OH} (water, coordinated) = 3178; ν_{OH} (water, free) = 3373. Elemental analysis (CHN) for $C_{84}H_{68}N_4O_{30}Cu_2$ (MW = 1739); calculated: 58.09, 3.34, 3.22; found: 58.05, 3.57, 3.54.

[Ni(Tyr-Per)(H$_2$O)]$_2$·8H$_2$O (10). $Ni(OAc)_2 \cdot 4H_2O$ (17.5 mg, 0.07 mmol) was used as the metal salt with Tyr-Per (50 mg, 0.07 mmol) as the linker. Intense red solid was obtained. Yield: 90%. FTIR (KBr, cm^{-1}): ν_{CO} (carboxylic, asymmetric) = 1651; ν_{CO} (carboxylic, symmetric) = 1366; ν_{OH} (water, coordinated) = 3182; ν_{OH} (water, free) = 3400. Elemental analysis (CHN) for $C_{84}H_{68}N_4O_{30}Ni_2$ (MW = 1730); calculated: 58.40, 3.98, 3.24; found: 58.38, 3.83, 3.52.

[Cd(Tyr-Per)(H$_2$O)]$_2$·7H$_2$O (11). $Cd(OAc)_2 \cdot 2H_2O$ (18.6 mg, 0.07 mmol) was used as the metal salt with Tyr-Per (50 mg, 0.07 mmol) as the linker. Intense red solid was obtained. Yield: 92%. FTIR (KBr, cm^{-1}): ν_{CO} (carboxylic, asymmetric) = 1651; ν_{CO} (carboxylic, symmetric) = 1366; ν_{OH} (water, coordinated) = 3193; ν_{OH} (water, free) = 3405. Elemental analysis (CHN) for $C_{84}H_{66}N_4O_{29}Cd_2$ (MW = 1818); calculated: 55.56, 3.63, 3.08; found: 55.98, 3.63, 3.35.

[Zn(Tyr-Per)(H$_2$O)]$_2$·8H$_2$O (12). $Zn(OAc)_2 \cdot 2H_2O$ (15.4 mg, 0.07 mmol) was used as the metal salt with Tyr-Per (50 mg, 0.07 mmol) as the linker. Intense red solid was obtained. Yield: 86%. FTIR (KBr, cm^{-1}): ν_{CO} (carboxylic, asymmetric) = 1648; ν_{CO} (carboxylic, symmetric) = 1368; ν_{OH} (water, coordinated) = 3221; ν_{OH} (water, free) = 3422. Elemental analysis (CHN) for $C_{84}H_{68}N_4O_{30}Zn_2$ (MW = 1742); calculated: 57.86, 3.90, 3.21; found: 57.90, 3.73, 3.40.

[Cu$_2$(Glu-Per)(H$_2$O)$_2$]$_2$·5H$_2$O (13). $Cu(OAc)_2 \cdot H_2O$ (30.8 mg, 0.154 mmol) was used as the metal salt with Glu-Per (50 mg, 0.077 mmol) as the linker. Intense red solid was obtained. Yield: 91%. FTIR (KBr, cm^{-1}): ν_{CO} (carboxylic, asymmetric) = 1643; ν_{CO} (carboxylic, symmetric) = 1364; ν_{OH} (water, coordinated) = 3178; ν_{OH} (water, free) = 3393. Elemental analysis (CHN) for $C_{68}H_{54}N_4O_{33}Cu_4$ (MW = 1708); calculated: 47.77, 3.39, 3.27; found: 47.69, 3.01, 3.41.

[Ni$_2$(Glu-Per)(H$_2$O)$_2$]$_2$·7H$_2$O (14). $Ni(OAc)_2 \cdot 4H_2O$ (38.3 mg, 0.154 mmol) was used as the metal salt with Glu-Per (50 mg, 0.077 mmol) as the linker. Intense red solid was obtained. Yield: 88%. FTIR (KBr, cm^{-1}): ν_{CO} (carboxylic, asymmetric) = 1642; ν_{CO} (carboxylic,

symmetric) = 1364; ν_{OH} (water, coordinated) = 3178; ν_{OH} (water, free) = 3382. Elemental analysis (CHN) for $C_{68}H_{58}N_4O_{35}Ni_4$ (MW = 1726); calculated: 47.27, 3.59, 3.24; found: 47.06, 3.40, 3.31.

$[Cd_2(Glu\text{-}Per)(H_2O)_2]_2 \cdot 5H_2O$ (15). $Cd(OAc)_2 \cdot 2H_2O$ (41 mg, 0.154 mmol) was used as the metal salt with Glu-Per (50 mg, 0.077 mmol) as the linker. Intense red solid was obtained. Yield: 90%. FTIR (KBr, cm^{-1}): ν_{CO} (carboxylic, asymmetric) = 1647; ν_{CO} (carboxylic, symmetric) = 1362; ν_{OH} (water, coordinated) = 3195; ν_{OH} (water, free) = 3422. Elemental analysis (CHN) for $C_{68}H_{54}N_4O_{33}Cd_4$ (MW = 1902); calculated: 42.90, 3.04, 2.94; found: 42.64, 2.88, 3.03.

$[Zn(Glu\text{-}Per)(H_2O)]_2 \cdot 3H_2O$ (16). $Zn(OAc)_2 \cdot 2H_2O$ (33.9 mg, 0.154 mmol) was used as the metal salt with Glu-Per (50 mg, 0.077 mmol) as the linker. Intense red solid was obtained. Yield: 95%. FTIR (KBr, cm^{-1}): ν_{CO} (carboxylic, asymmetric) = 1643; ν_{CO} (carboxylic, symmetric) = 1366; ν_{OH} (water, coordinated) = 3172; ν_{OH} (water, free) = 3446. Elemental analysis (CHN) for $C_{68}H_{50}N_4O_{29}Zn_2$ (MW = 1516); calculated: 53.83, 3.30, 3.69; found: 54.07, 3.24, 3.71.

Chapter III

RESULTS AND DISCUSSION

Synthetic Strategy

Present work is an attempt to create chiral, fluorescent Metal Organic Coordination Networks (MOCNs). A huge amount of tunability of structure and properties in case of MOCNs by varying the components is exploited to achieve the goal. L form of amino acids is used to provide chirality, whereas aromatic moiety is employed to give fluorescent behaviour. L-Alanine, L-Phenylalanine, L-Tyrosine and L-Glutamic acid are the amino acids, whereas Perylene-3,4,9,10-tetracarboxylic dianhydride (PTCDA) is the aromatic moiety used in the present work. Desired linker molecules were generated by reacting various amino acids with perylene moiety. Sixteen metal complexes were then prepared using these linkers and transition metal ions, which are Cu^{2+}, Ni^{2+}, Cd^{2+} and Zn^{2+}.

Perylene based linkers, which are Ala-Per (L1), Phe-Per (L2), Tyr-Per (L3) and Glu-Per (L4) were prepared as mentioned in Scheme 1. Preparation of metal complexes (**1-16**) was the conventional one pot synthesis at room temperature wherein reactants were mixed together and stirred to give the product via self-assembly of starting materials as a solid (Scheme 2).

For reactions of amino acid with Perylene-3,4,9,10-tetracarboxylic dianhydride the molar ratio was 2:1. Linker molecules were obtained as intense red solid.

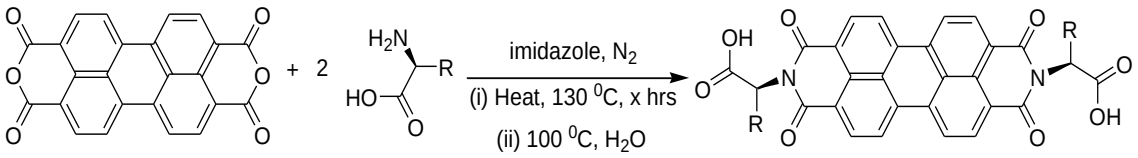

Perylene-3,4,9,10-tetracarboxylic dianhydride | Amino acid | Linker (L1-L4)

Linker	R group	Time (x hrs)
Ala-Per (L1)	CH_3	0.5
Phe-Per (L2)	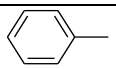	2
Tyr-Per (L3)	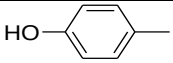	5
Glu-Per (L4)	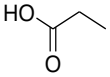	8

Scheme 1. Synthesis of perylene based linkers.

For the synthesis of metal complexes (**1-16**), the molar ratio of metal acetate hydrate and linker was 1:1 for L1-L3 and 2:1 in the case of L4. Metal complexes were obtained with a general formula $[M_xL_z(H_2O)_m]_p{\cdot}nH_2O$ and were all found to be red solid because of the inherent intense red colour of the perylene moiety.

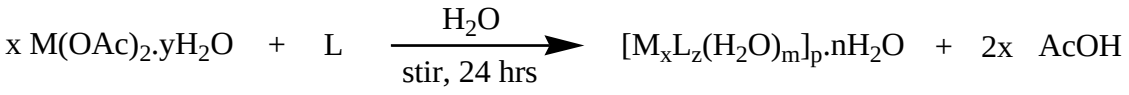

Metal acetate hydrate $M(OAc)_2{\cdot}yH_2O$	x	Linker (L)	Metal complex $[M_xL_z(H_2O)_m]_p{\cdot}nH_2O$
$Cu(OAc)_2{\cdot}H_2O$	1	Ala-Per (L1)	$[Cu(Ala\text{-}Per)(H_2O)]_2{\cdot}6H_2O$ **(1)**
$Ni(OAc)_2{\cdot}4H_2O$	1	Ala-Per (L1)	$[Ni(Ala\text{-}Per)(H_2O)]_2{\cdot}3H_2O$ **(2)**
$Cd(OAc)_2{\cdot}2H_2O$	1	Ala-Per (L1)	$[Cd(Ala\text{-}Per)(H_2O)]_2$ **(3)**
$Zn(OAc)_2{\cdot}2H_2O$	1	Ala-Per (L1)	$[Zn(Ala\text{-}Per)(H_2O)]_2{\cdot}4H_2O$ **(4)**
$Cu(OAc)_2{\cdot}H_2O$	1	Phe-Per (L2)	$[Cu(Phe\text{-}Per)(H_2O)]_2{\cdot}5H_2O$ **(5)**
$Ni(OAc)_2{\cdot}4H_2O$	1	Phe-Per (L2)	$[Ni(Phe\text{-}Per)(H_2O)]_2{\cdot}6H_2O$ **(6)**
$Cd(OAc)_2{\cdot}2H_2O$	1	Phe-Per (L2)	$[Cd(Phe\text{-}Per)(H_2O)]_2$ **(7)**
$Zn(OAc)_2{\cdot}2H_2O$	1	Phe-Per (L2)	$[Zn(Phe\text{-}Per)(H_2O)]_2{\cdot}2H_2O$ **(8)**
$Cu(OAc)_2{\cdot}H_2O$	1	Tyr-Per (L3)	$[Cu(Tyr\text{-}Per)(H_2O)]_2{\cdot}8H_2O$ **(9)**
$Ni(OAc)_2{\cdot}4H_2O$	1	Tyr-Per (L3)	$[Ni(Tyr\text{-}Per)(H_2O)]_2{\cdot}8H_2O$ **(10)**
$Cd(OAc)_2{\cdot}2H_2O$	1	Tyr-Per (L3)	$[Cd(Tyr\text{-}Per)(H_2O)]_2{\cdot}7H_2O$ **(11)**
$Zn(OAc)_2{\cdot}2H_2O$	1	Tyr-Per (L3)	$[Zn(Tyr\text{-}Per)(H_2O)]_2{\cdot}8H_2O$ **(12)**
$Cu(OAc)_2{\cdot}H_2O$	2	Glu-Per (L4)	$[Cu_2(Glu\text{-}Per)(H_2O)_2]_2{\cdot}5H_2O$ **(13)**
$Ni(OAc)_2{\cdot}4H_2O$	2	Glu-Per (L4)	$[Ni_2(Glu\text{-}Per)(H_2O)_2]_2{\cdot}7H_2O$ **(14)**
$Cd(OAc)_2{\cdot}2H_2O$	2	Glu-Per (L4)	$[Cd_2(Glu\text{-}Per)(H_2O)_2]_2{\cdot}5H_2O$ **(15)**
$Zn(OAc)_2{\cdot}2H_2O$	2	Glu-Per (L4)	$[Zn(Glu\text{-}Per)(H_2O)]_2{\cdot}3H_2O$ **(16)**

Scheme 2. Synthesis of metal complexes.

Thermogravimetric Analysis

In order to study the thermal properties of prepared linkers and their metal complexes compounds were examined via Thermogravimetric Analysis using Shimadzu DTG-60H analyser in a range from 30-500 ^{0}C. In TGA spectra of linkers initial drop is for the lattice water molecules. All of the linkers are pretty much stable up to 300 ^{0}C, after which they dissociate. In case of metal complexes initial drop is because of lattice water molecules, followed by a smaller drop in magnitude because of coordinated water molecules to the metal centre. All metal complexes were also found to be stable up to 300 ^{0}C.

Amongst the linkers, L2 was found to be most stable. L1 and L2 showed similar profile, differing from L3 and L4 because the latter have heteroatom in the R group of amino acid

which accounts for the difference in interactions. Amongst the metal complexes, Cu^{+2} complex was least stable, while the other three showed similar stability in all the cases.

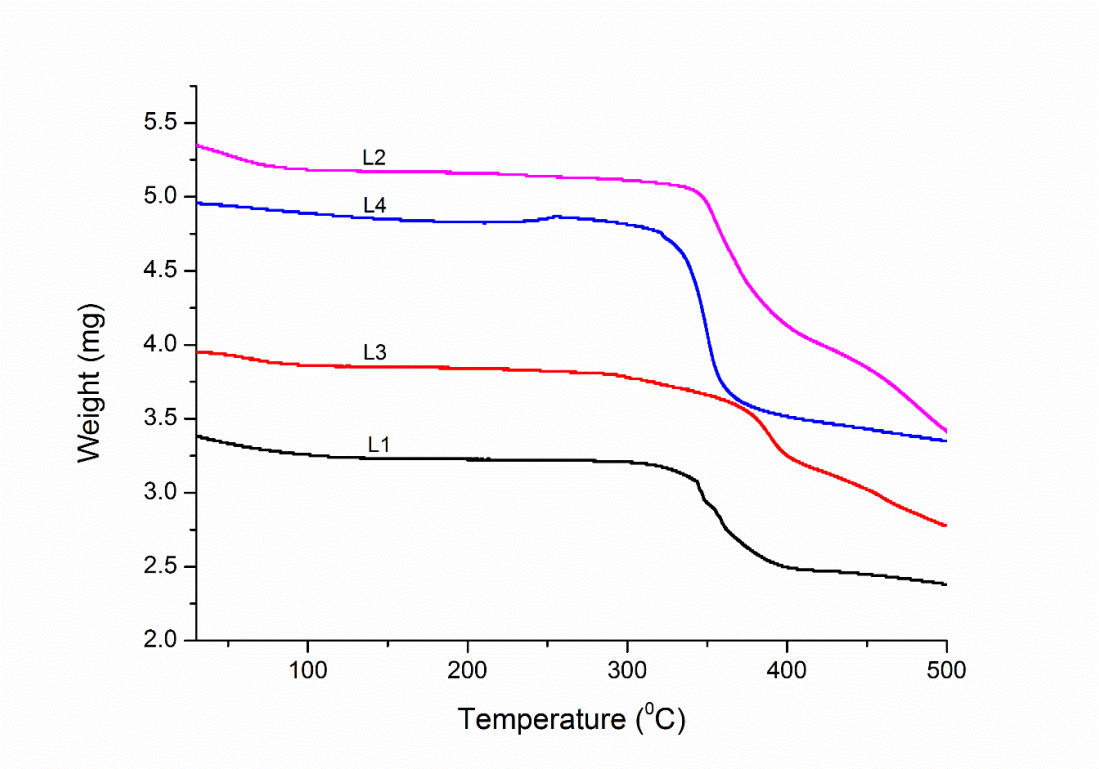

Figure 7. TGA of linkers L1-L4.
(L1: Ala-Per, L2: Phe-Per, L3: Tyr-Per, L4: Glu-Per)

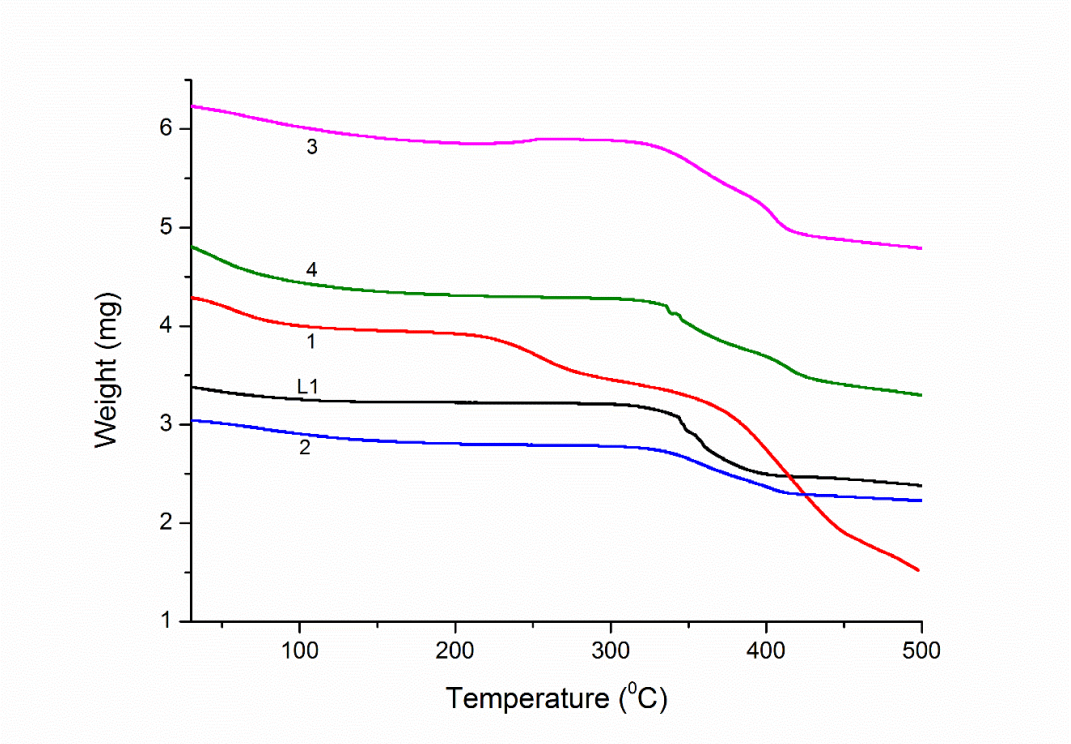

Figure 8. TGA of L1 and metal complexes **1-4**.

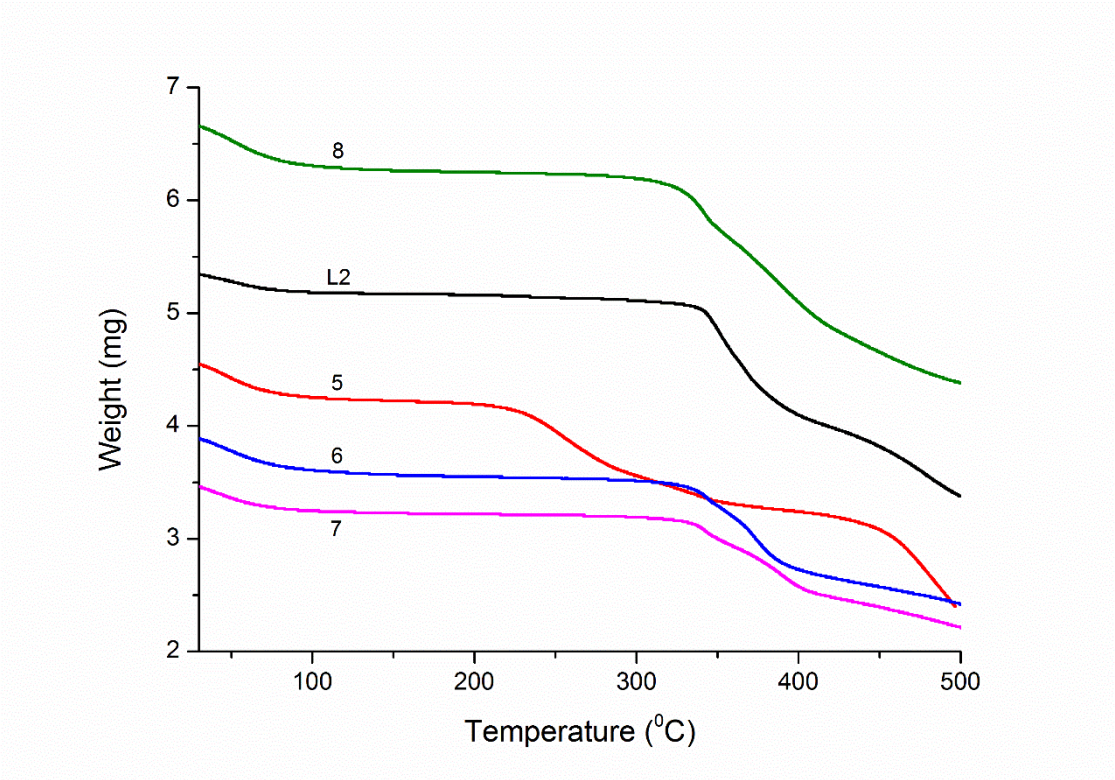

Figure 9. TGA of L2 and metal complexes **5-8**.

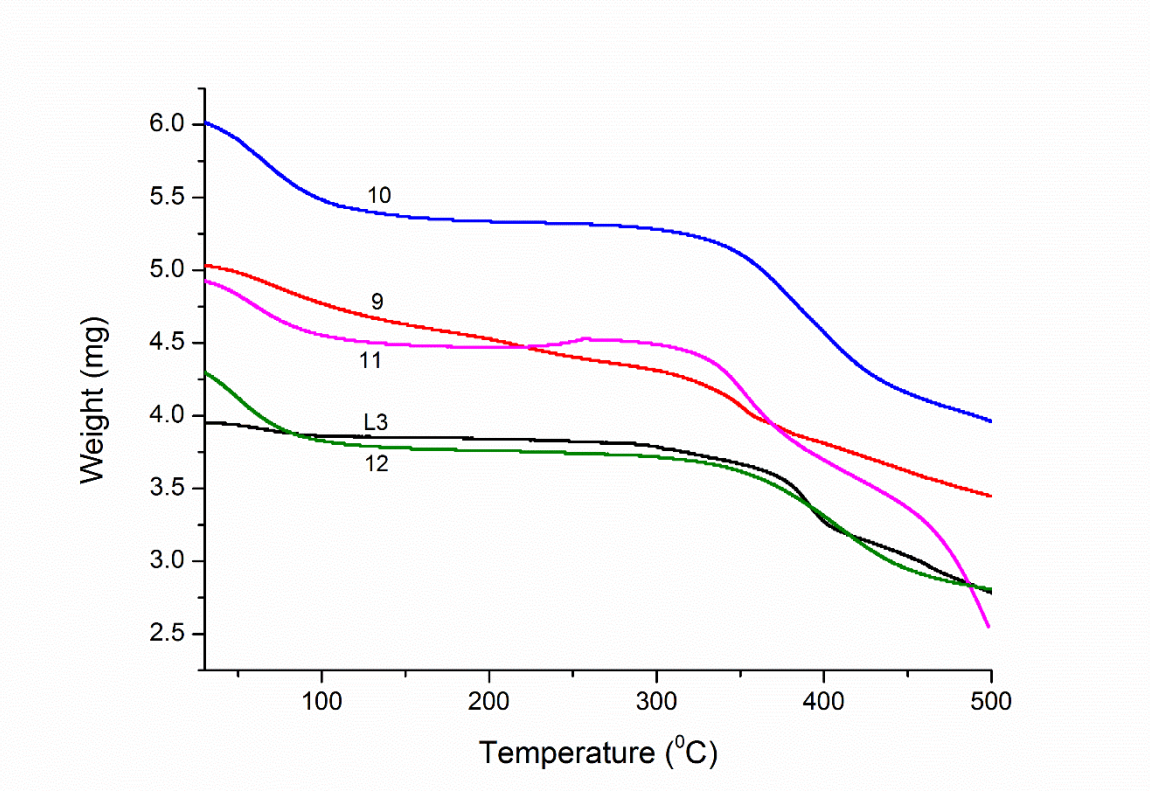

Figure 10. TGA of L3 and metal complexes **9-12**.

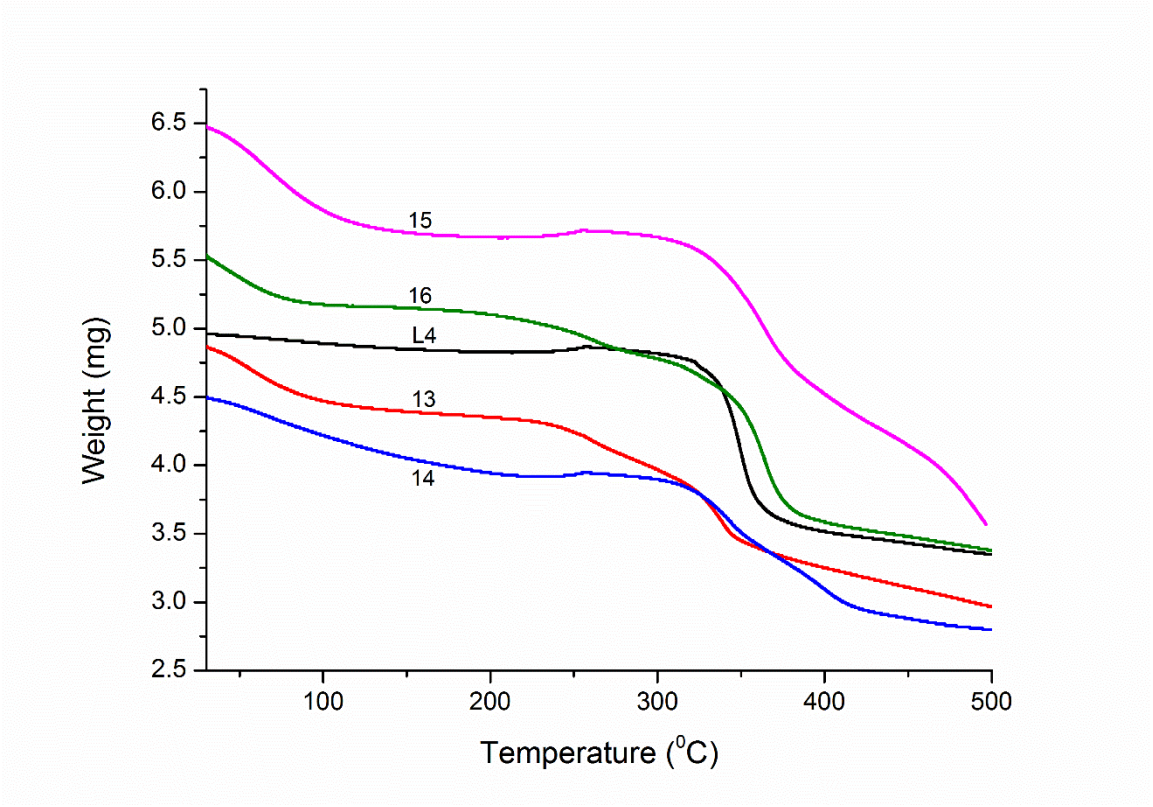

Figure 11. TGA of L4 and metal complexes **13-16**.

FTIR Spectroscopy

FTIR spectra were collected for compounds as KBr pellets using a Perkin Elmer Spectrum RX I FT-IR spectrometer in the 400-4000 cm^{-1} range. IR spectra of all compounds show a broad band around 3400 cm^{-1} which is a feature of O-H stretching frequency for water molecules. A slight hump is observed in case of metal complexes at around 3200 cm^{-1} which accounts for OH stretching frequency for the coordinated water molecules. In case of linkers features at around 1750 cm^{-1} show the carboxylate peak from the anhydride and at around 1180 cm^{-1} show the amine group.

Strong carboxylate peaks around 1640 and 1360 cm^{-1} are observed which are due to asymmetric and symmetric carboxylate stretch, respectively. This difference in the stretching frequency of about 280 cm^{-1} suggests that the binding between metal centre and the linker is monodentate type. Table 2 shows the stretching frequencies for the carboxylate groups in the metal complexes.

Table 2. FTIR stretching frequencies for metal complexes

Metal complex $[M_xL_z(H_2O)_m]_p{\cdot}nH_2O$	FTIR peaks (carboxylate) (cm^{-1})		
	$\nu_{asymmetric}$	$\nu_{symmetric}$	$\Delta\nu$
$[Cu(Ala\text{-}Per)(H_2O)]_2{\cdot}6H_2O$ **(1)**	1651	1367	284
$[Ni(Ala\text{-}Per)(H_2O)]_2{\cdot}3H_2O$ **(2)**	1652	1367	285
$[Cd(Ala\text{-}Per)(H_2O)]_2$ **(3)**	1648	1367	281
$[Zn(Ala\text{-}Per)(H_2O)]_2{\cdot}4H_2O$ **(4)**	1648	1367	281
$[Cu(Phe\text{-}Per)(H_2O)]_2{\cdot}5H_2O$ **(5)**	1654	1367	287
$[Ni(Phe\text{-}Per)(H_2O)]_2{\cdot}6H_2O$ **(6)**	1654	1367	287
$[Cd(Phe\text{-}Per)(H_2O)]_2$ **(7)**	1654	1366	288
$[Zn(Phe\text{-}Per)(H_2O)]_2{\cdot}2H_2O$ **(8)**	1654	1367	287
$[Cu(Tyr\text{-}Per)(H_2O)]_2{\cdot}8H_2O$ **(9)**	1647	1362	285
$[Ni(Tyr\text{-}Per)(H_2O)]_2{\cdot}8H_2O$ **(10)**	1651	1366	285
$[Cd(Tyr\text{-}Per)(H_2O)]_2{\cdot}7H_2O$ **(11)**	1651	1366	285
$[Zn(Tyr\text{-}Per)(H_2O)]_2{\cdot}8H_2O$ **(12)**	1648	1368	280
$[Cu_2(Glu\text{-}Per)(H_2O)_2]_2{\cdot}5H_2O$ **(13)**	1643	1364	279
$[Ni_2(Glu\text{-}Per)(H_2O)_2]_2{\cdot}7H_2O$ **(14)**	1642	1364	278
$[Cd_2(Glu\text{-}Per)(H_2O)_2]_2{\cdot}5H_2O$ **(15)**	1647	1362	285
$[Zn(Glu\text{-}Per)(H_2O)]_2{\cdot}3H_2O$ **(16)**	1643	1366	277

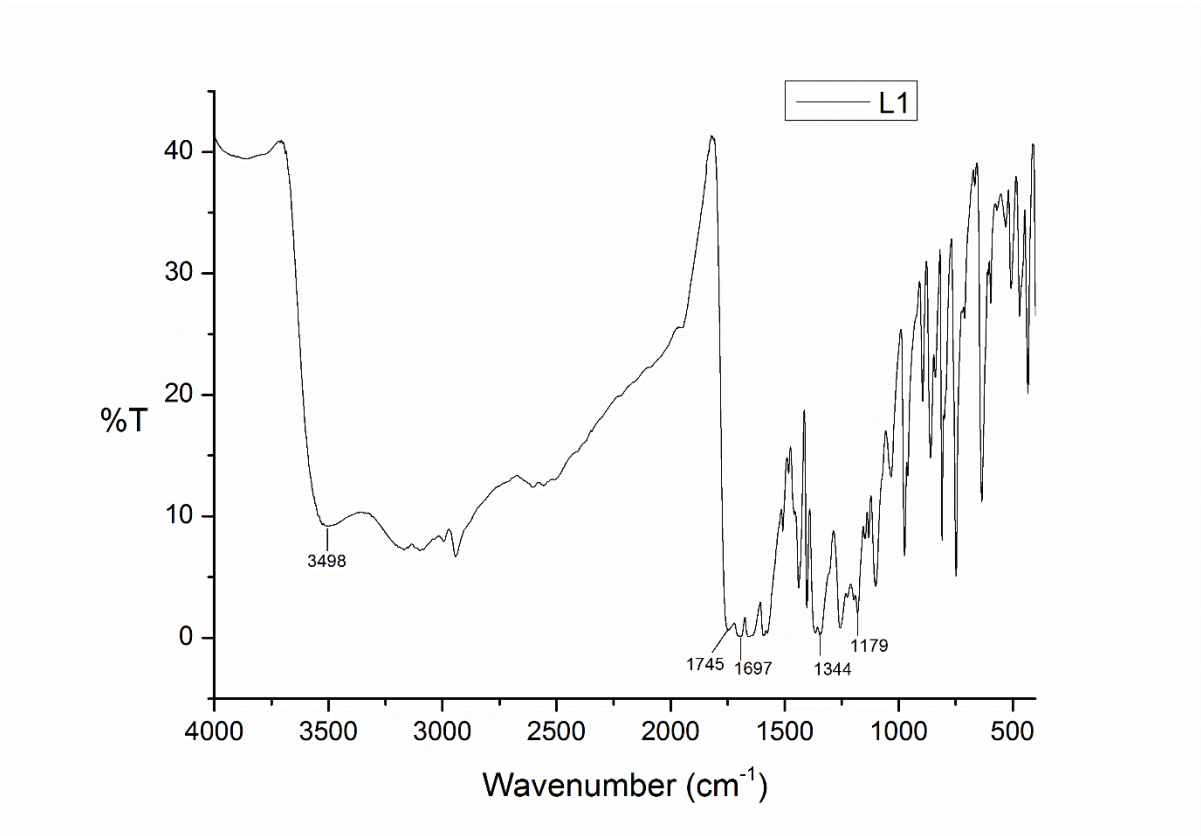

Figure 12. FTIR spectrum of L1.

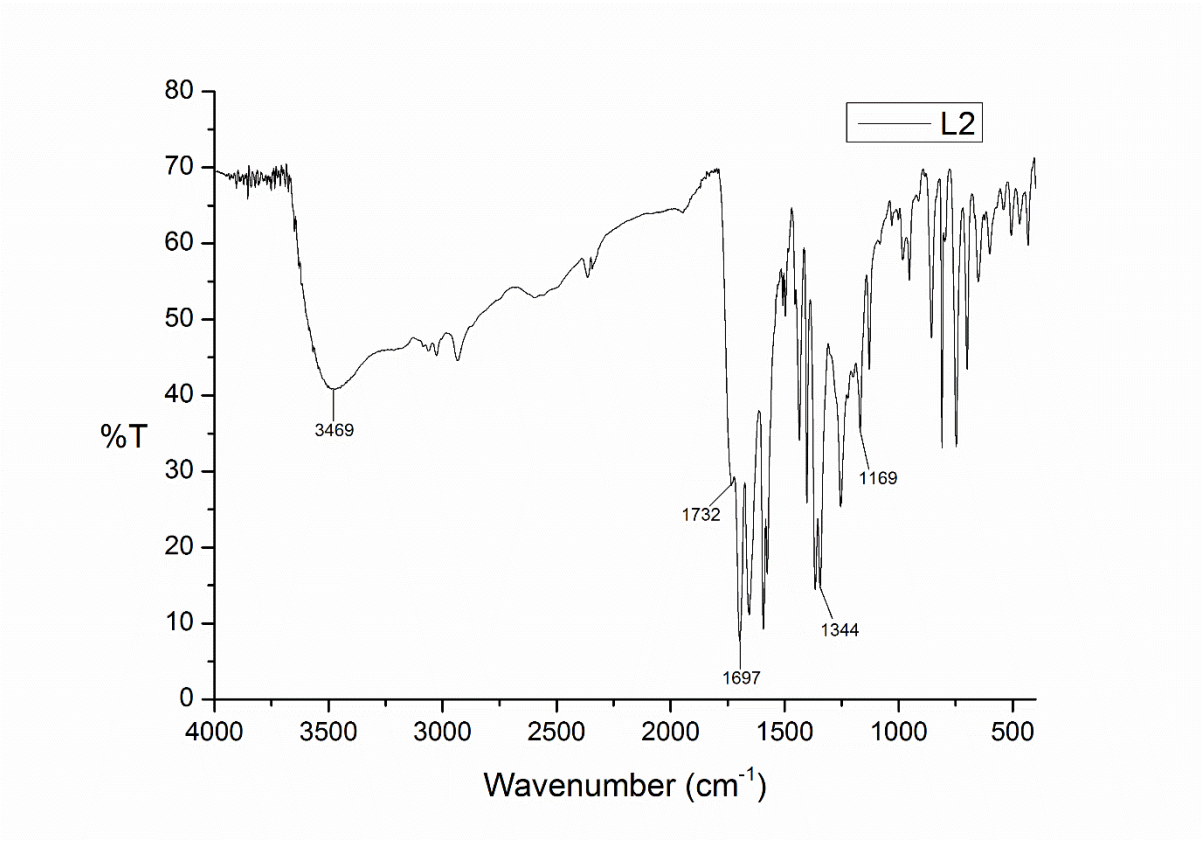

Figure 13. FTIR spectrum of L2.

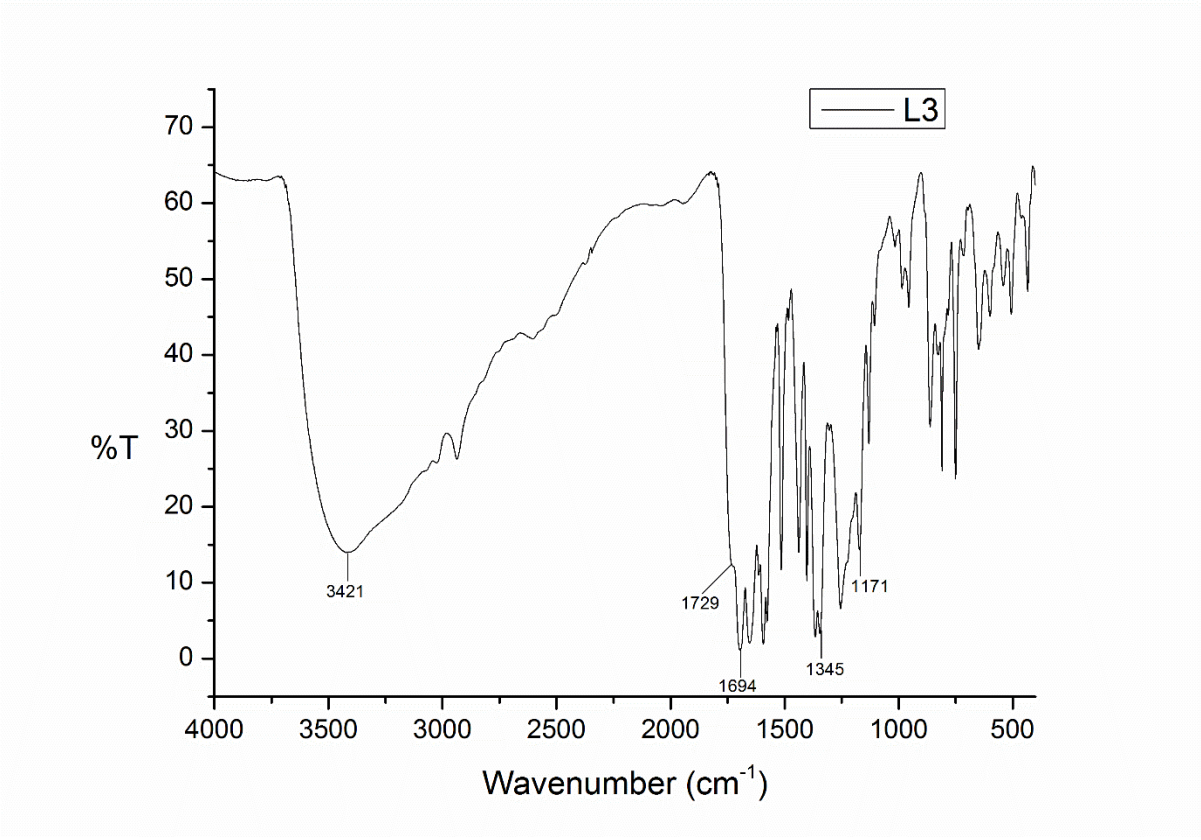

Figure 14. FTIR spectrum of L3.

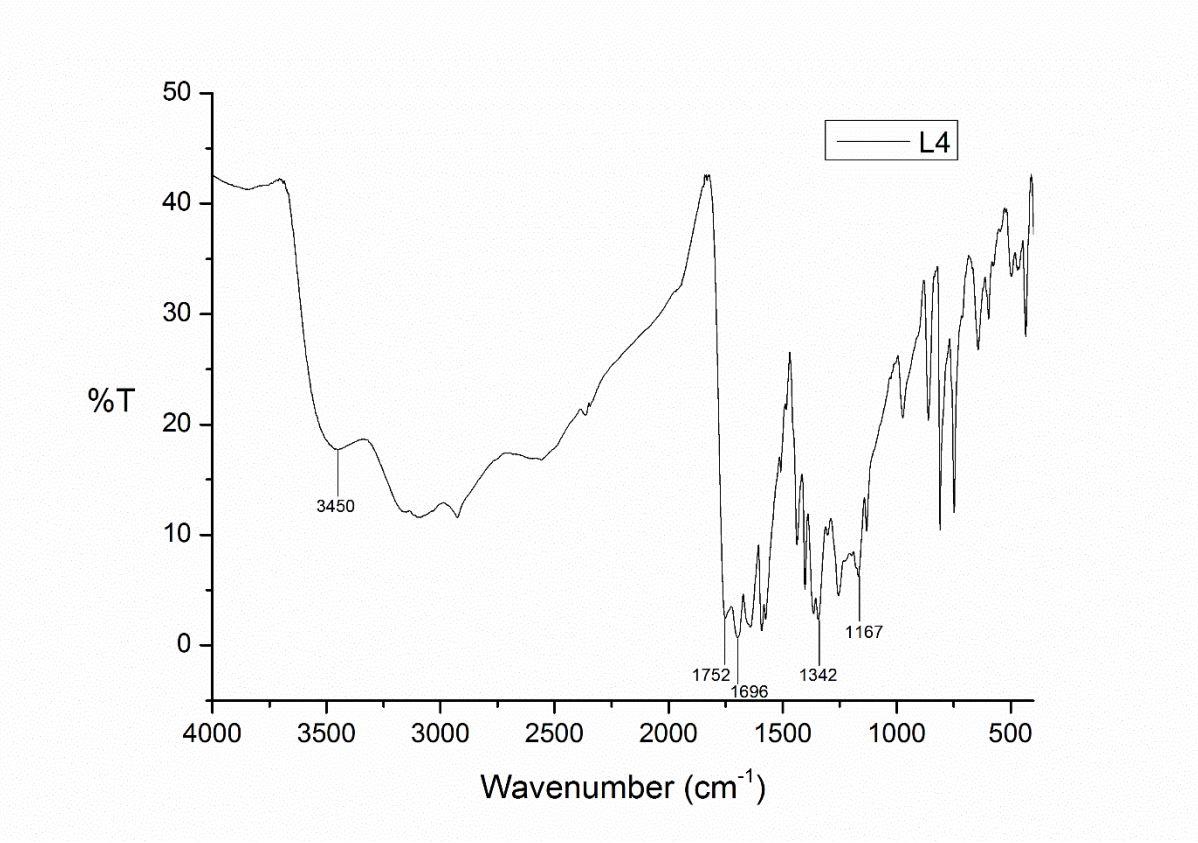

Figure 15. FTIR spectrum of L4.

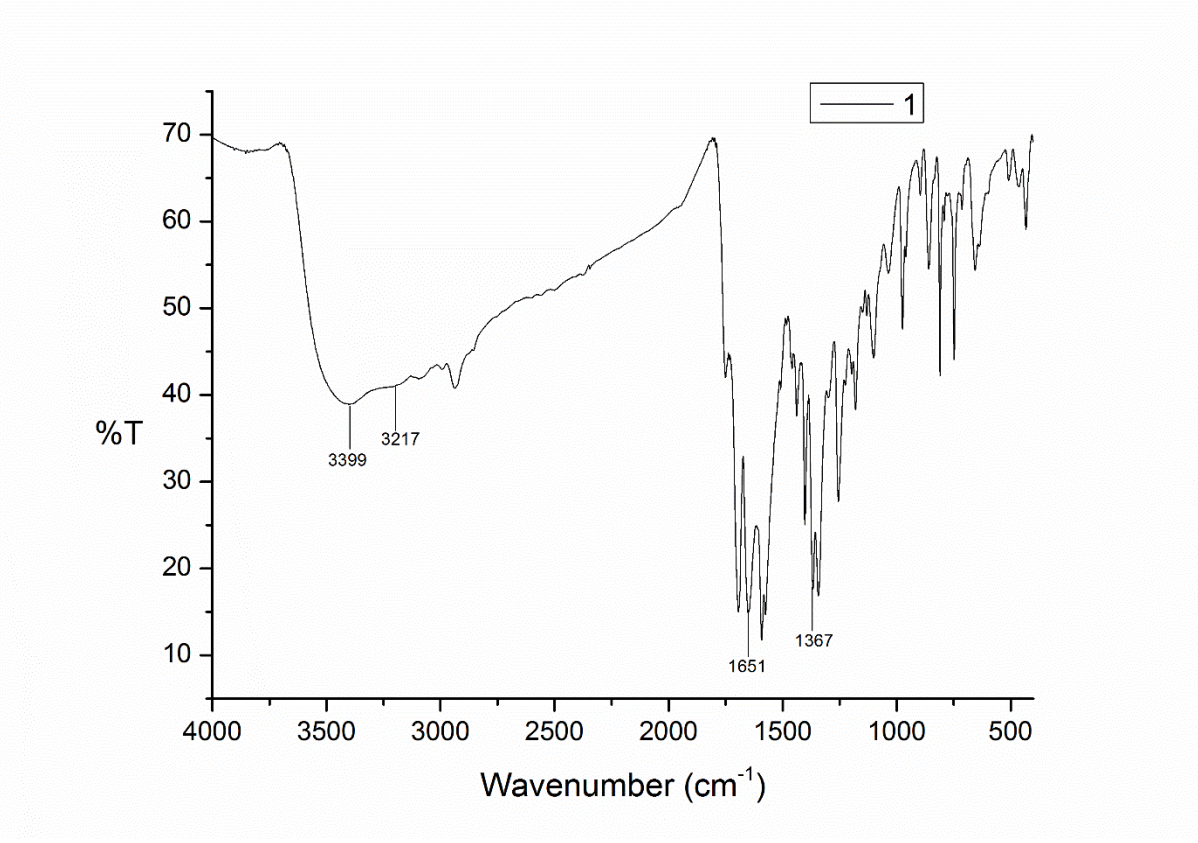

Figure 16. FTIR spectrum of $[Cu(Ala\text{-}Per)(H_2O)]_2 \cdot 6H_2O$ (**1**).

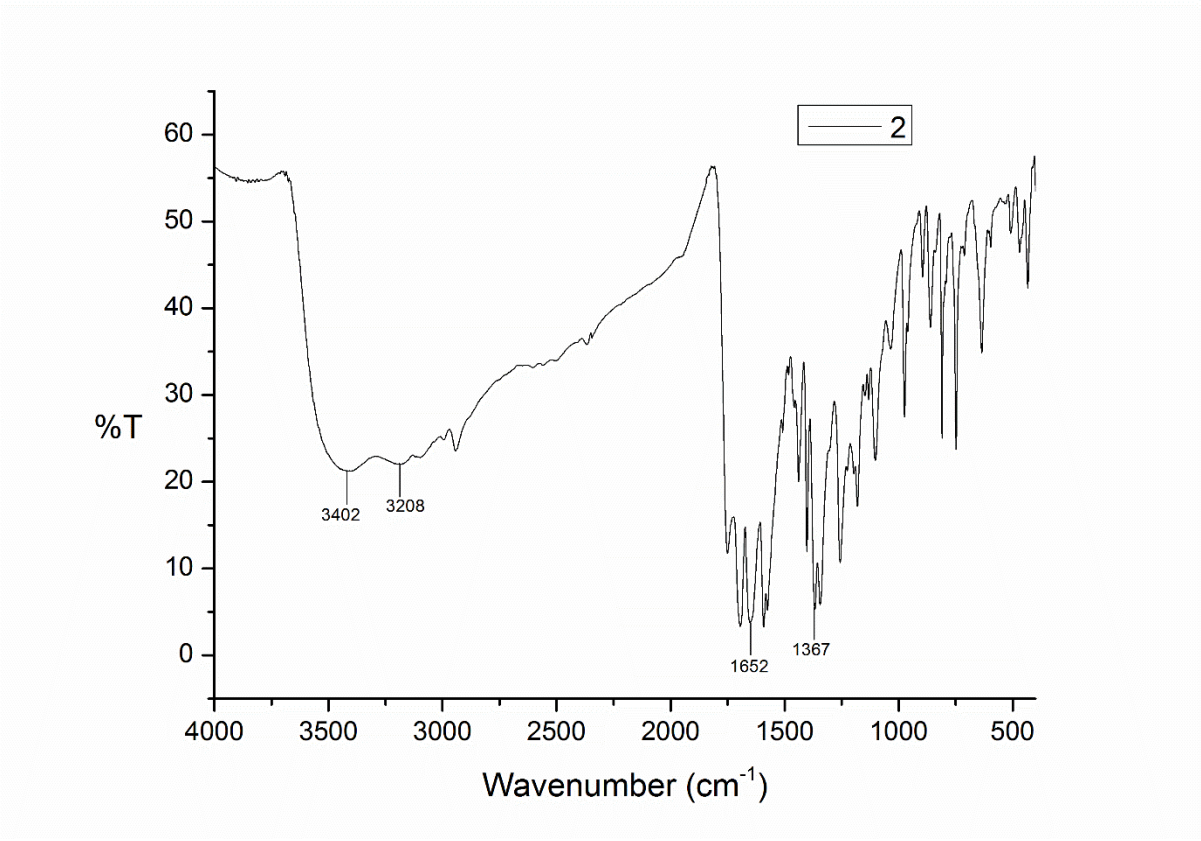

Figure 17. FTIR spectrum of $[Ni(Ala\text{-}Per)(H_2O)]_2 \cdot 3H_2O$ (**2**).

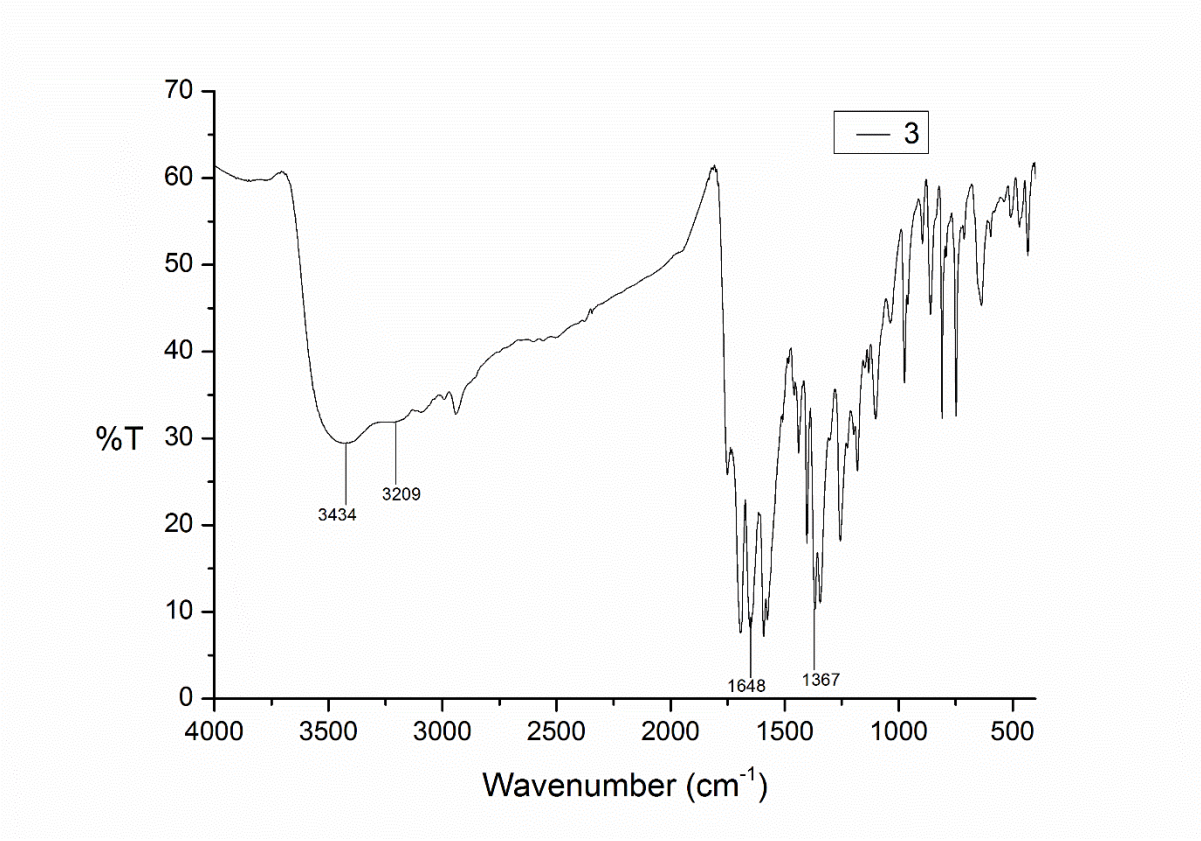

Figure 18. FTIR spectrum of $[Cd(Ala\text{-}Per)(H_2O)]_2$ (**3**).

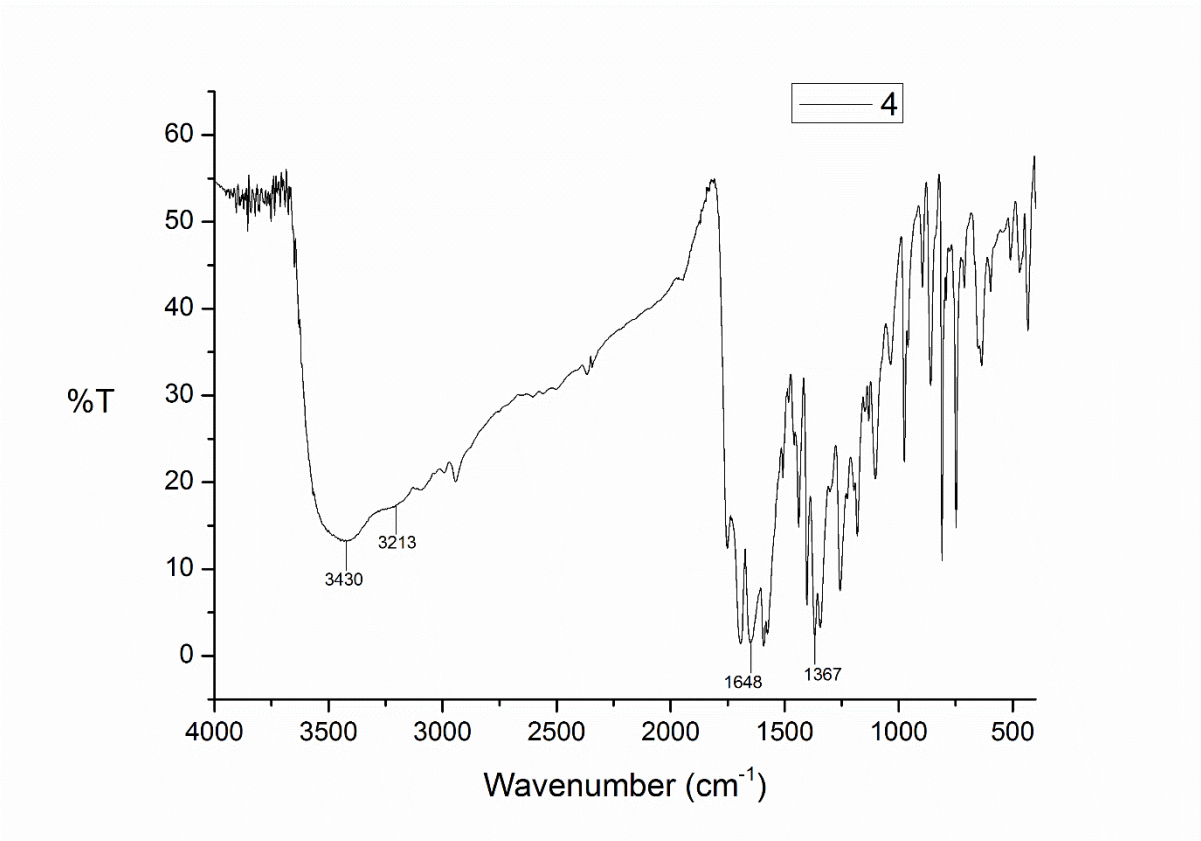

Figure 19. FTIR spectrum of $[Zn(Ala\text{-}Per)(H_2O)]_2 \cdot 4H_2O$ (**4**).

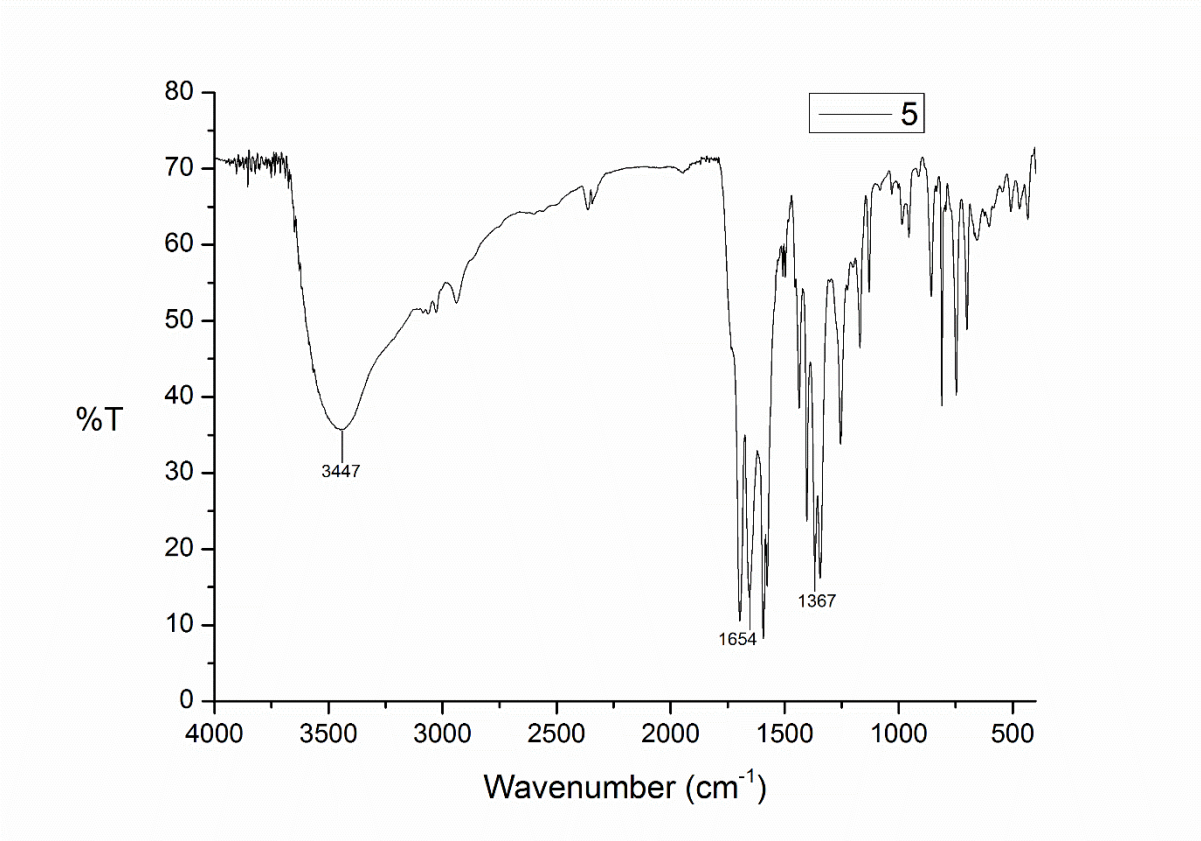

Figure 20. FTIR spectrum of $[Cu(Phe\text{-}Per)(H_2O)]_2 \cdot 5H_2O$ (**5**).

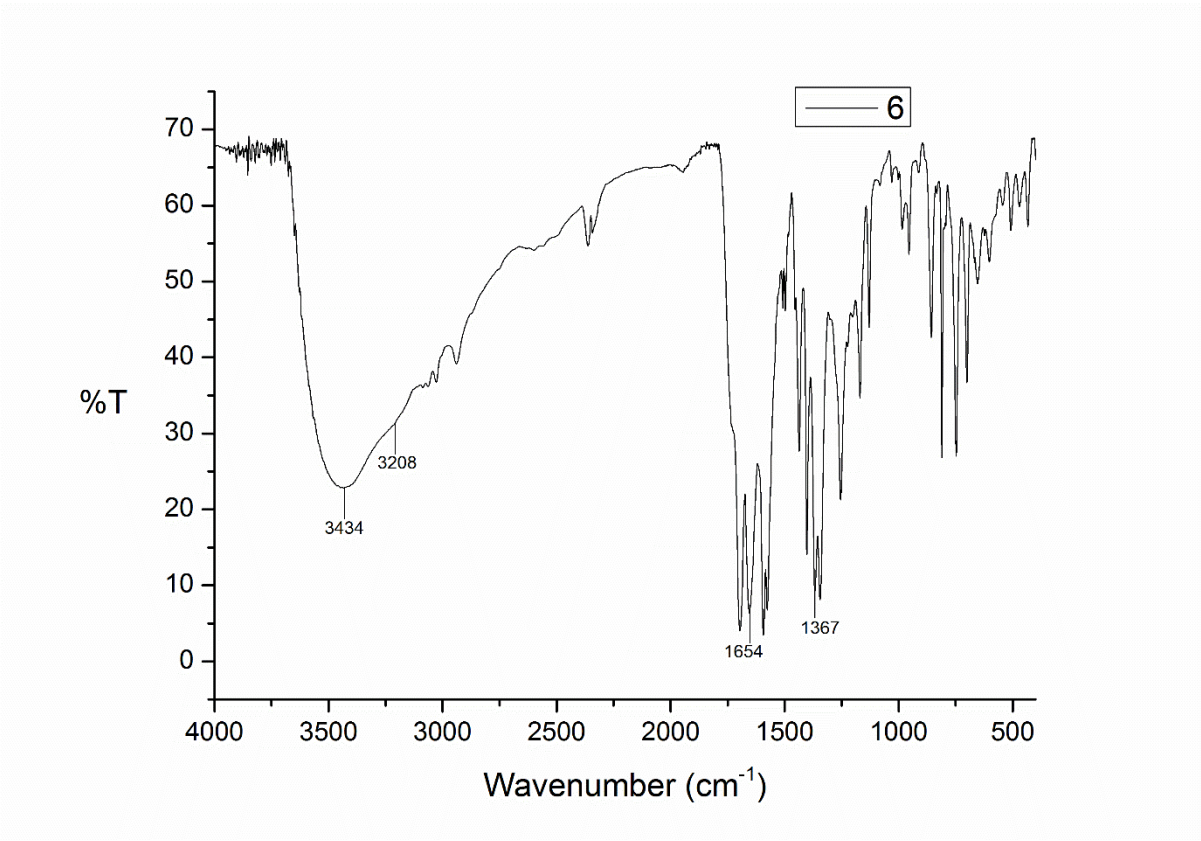

Figure 21. FTIR spectrum of $[Ni(Phe\text{-}Per)(H_2O)]_2 \cdot 6H_2O$ (**6**).

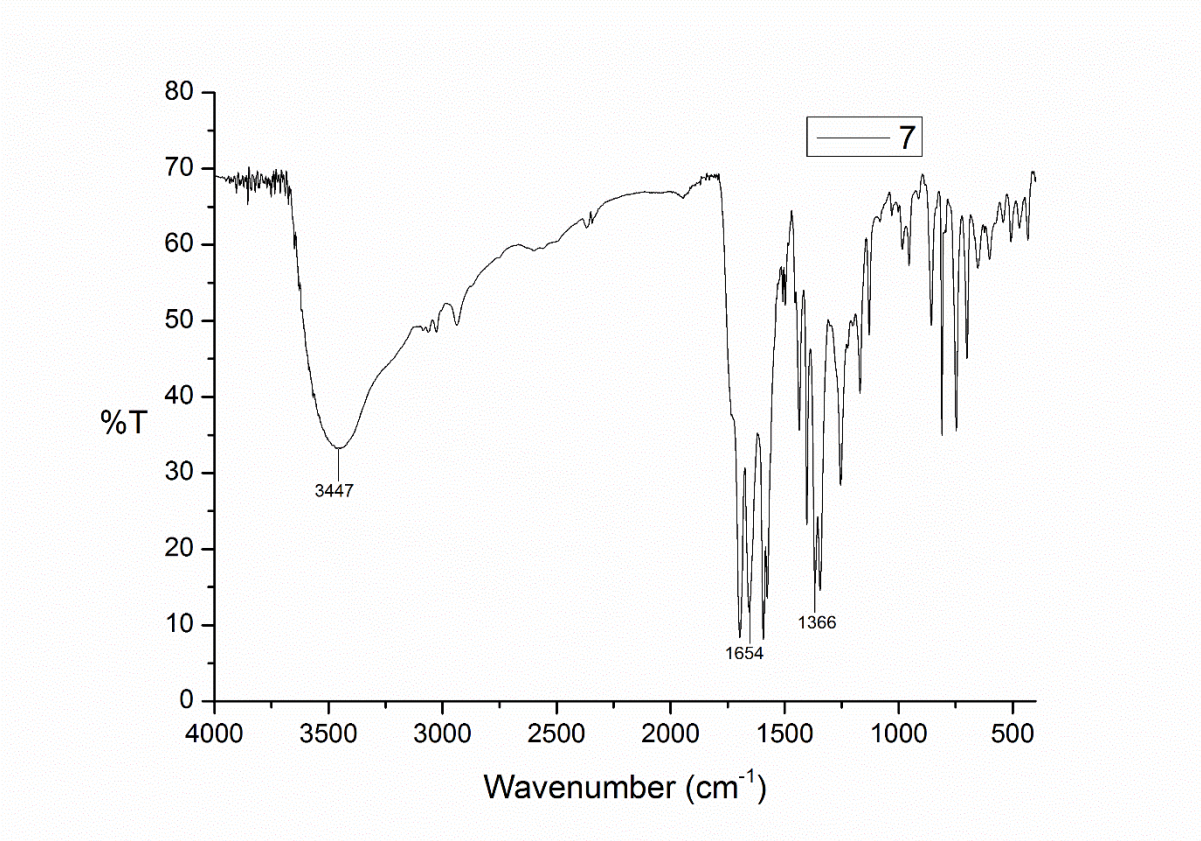

Figure 22. FTIR spectrum of $[Cd(Phe\text{-}Per)(H_2O)]_2$ (**7**).

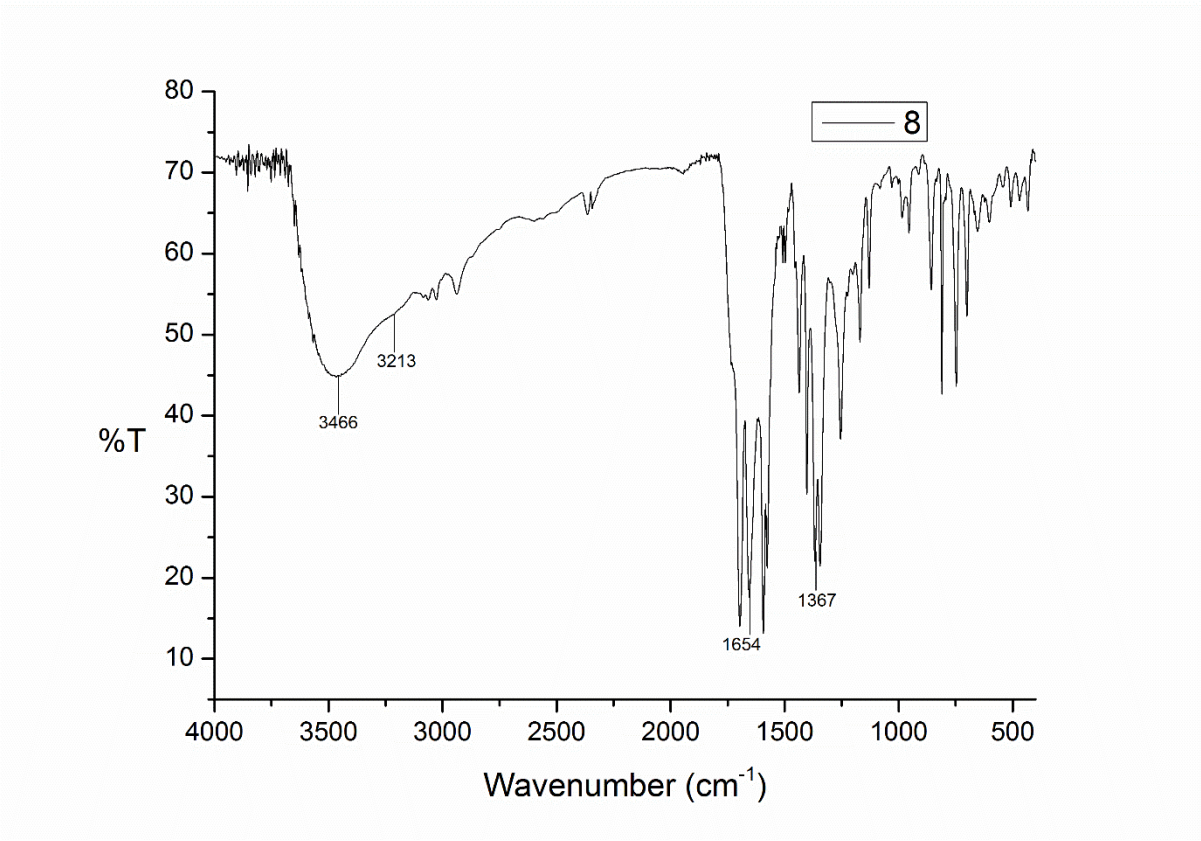

Figure 23. FTIR spectrum of $[Zn(Phe\text{-}Per)(H_2O)]_2 \cdot 2H_2O$ (**8**).

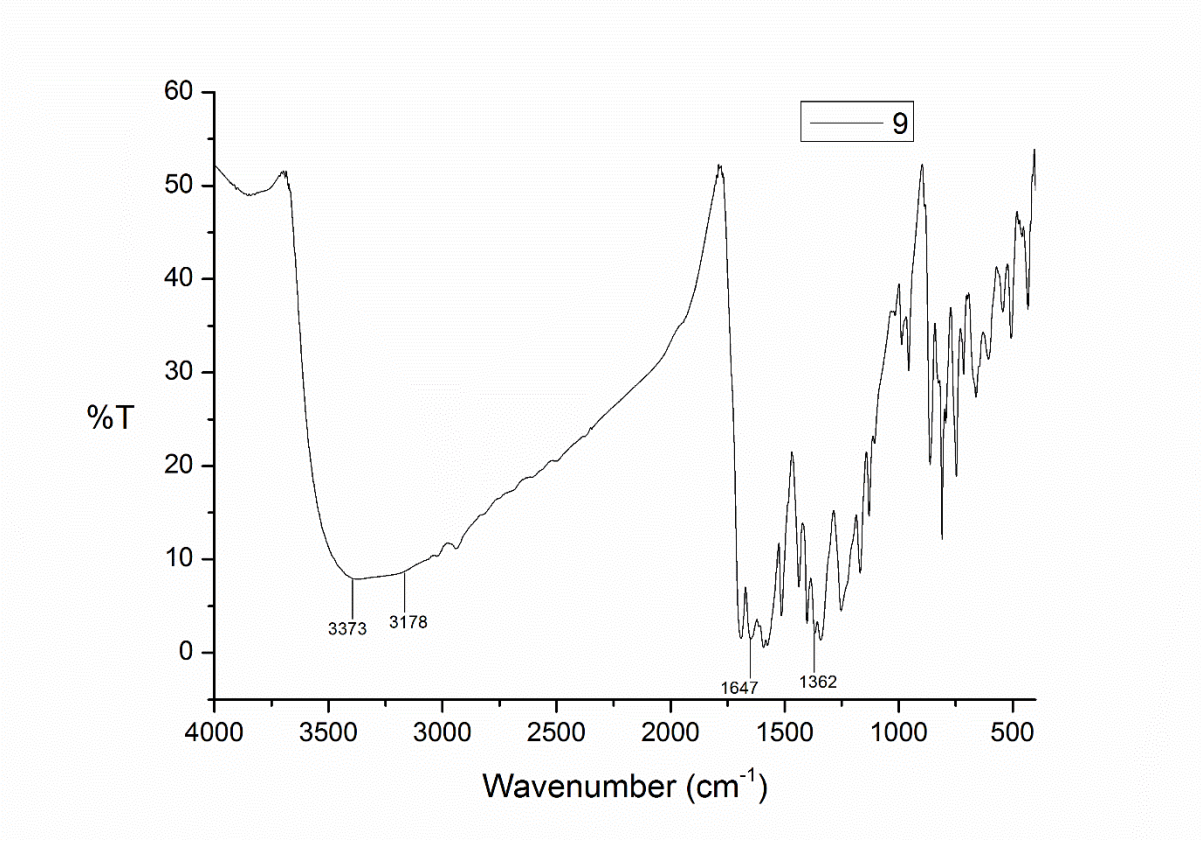

Figure 24. FTIR spectrum of $[Cu(Tyr\text{-}Per)(H_2O)]_2 \cdot 8H_2O$ (**9**).

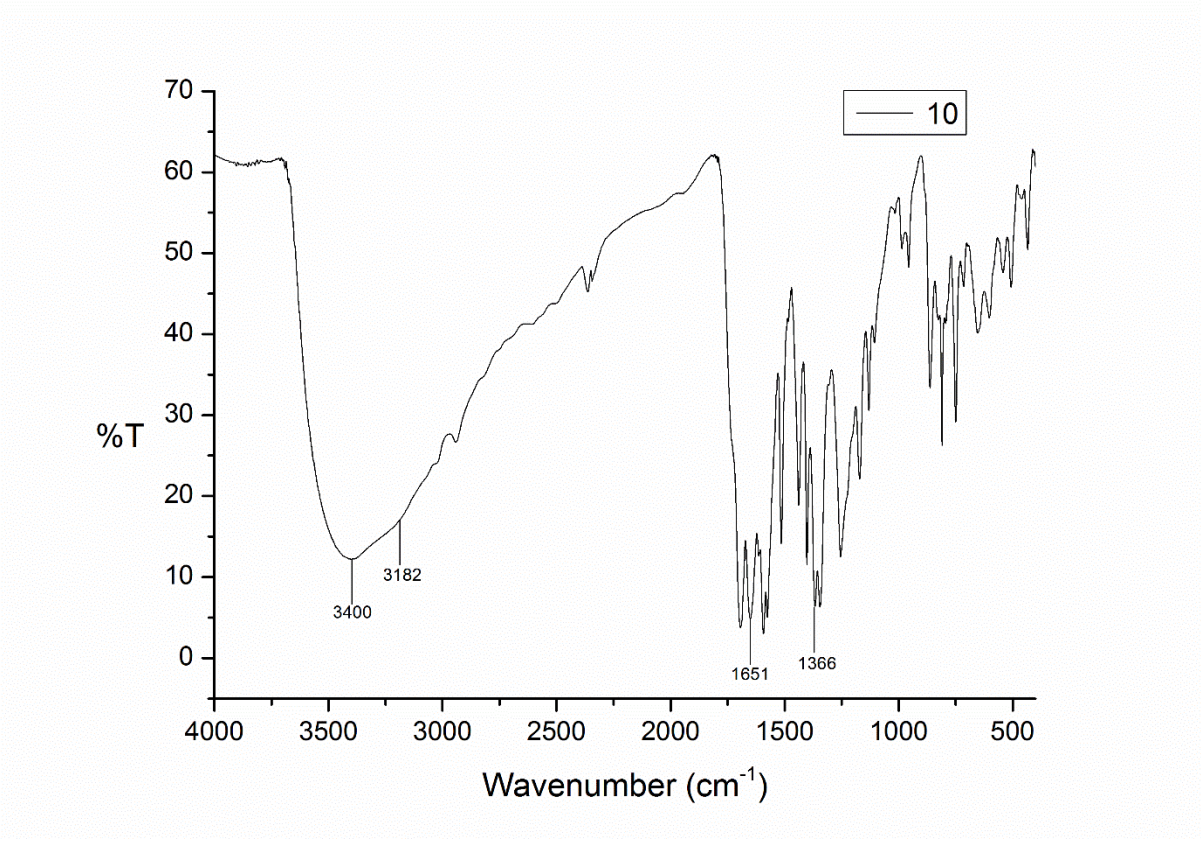

Figure 25. FTIR spectrum of $[Ni(Tyr\text{-}Per)(H_2O)]_2 \cdot 8H_2O$ (**10**).

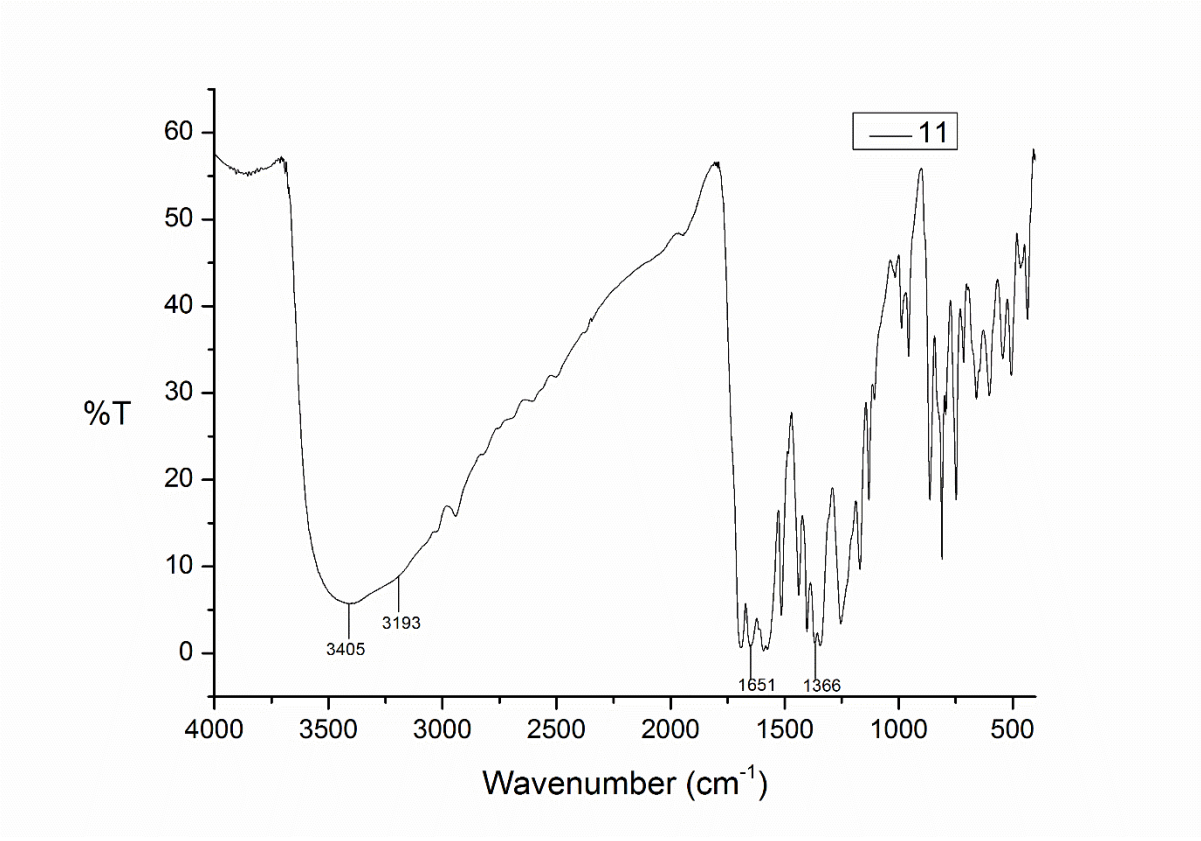

Figure 26. FTIR spectrum of $[Cd(Tyr\text{-}Per)(H_2O)]_2 \cdot 7H_2O$ (**11**).

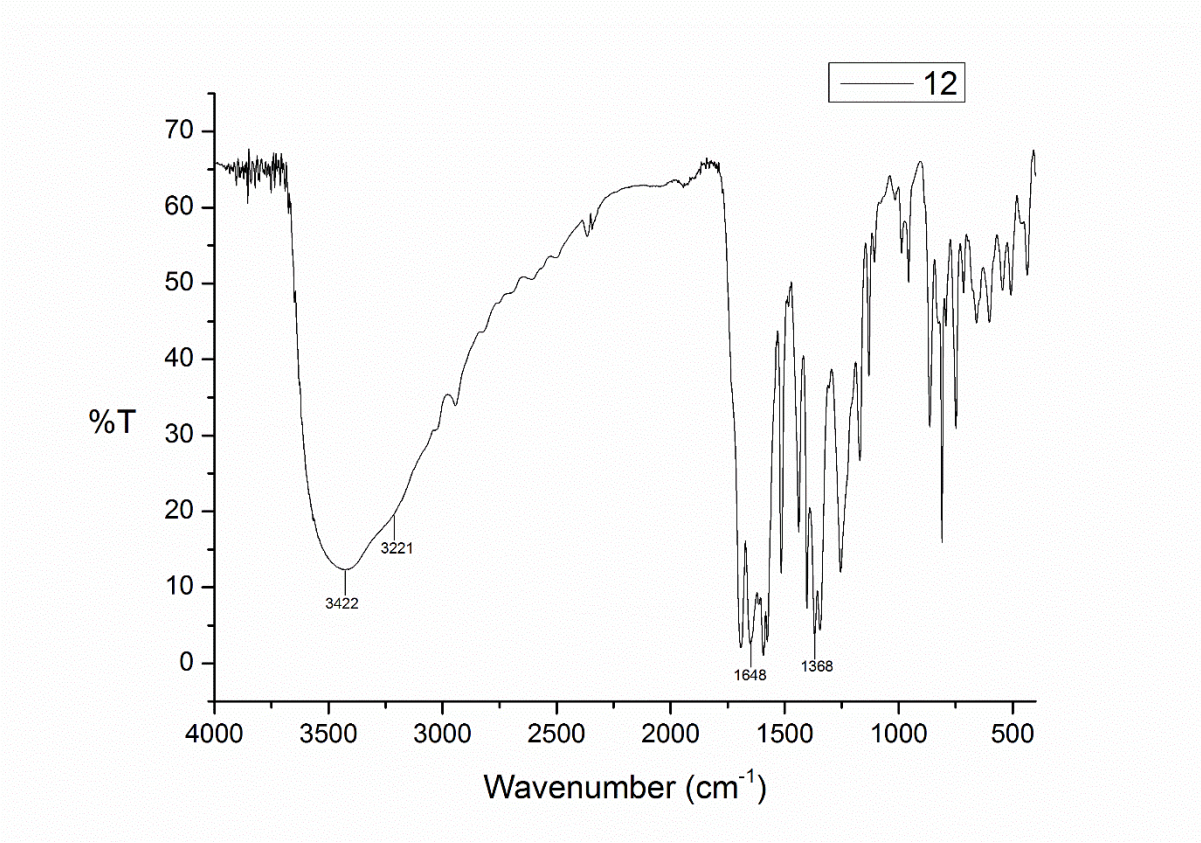

Figure 27. FTIR spectrum of $[Zn(Tyr\text{-}Per)(H_2O)]_2 \cdot 8H_2O$ (**12**).

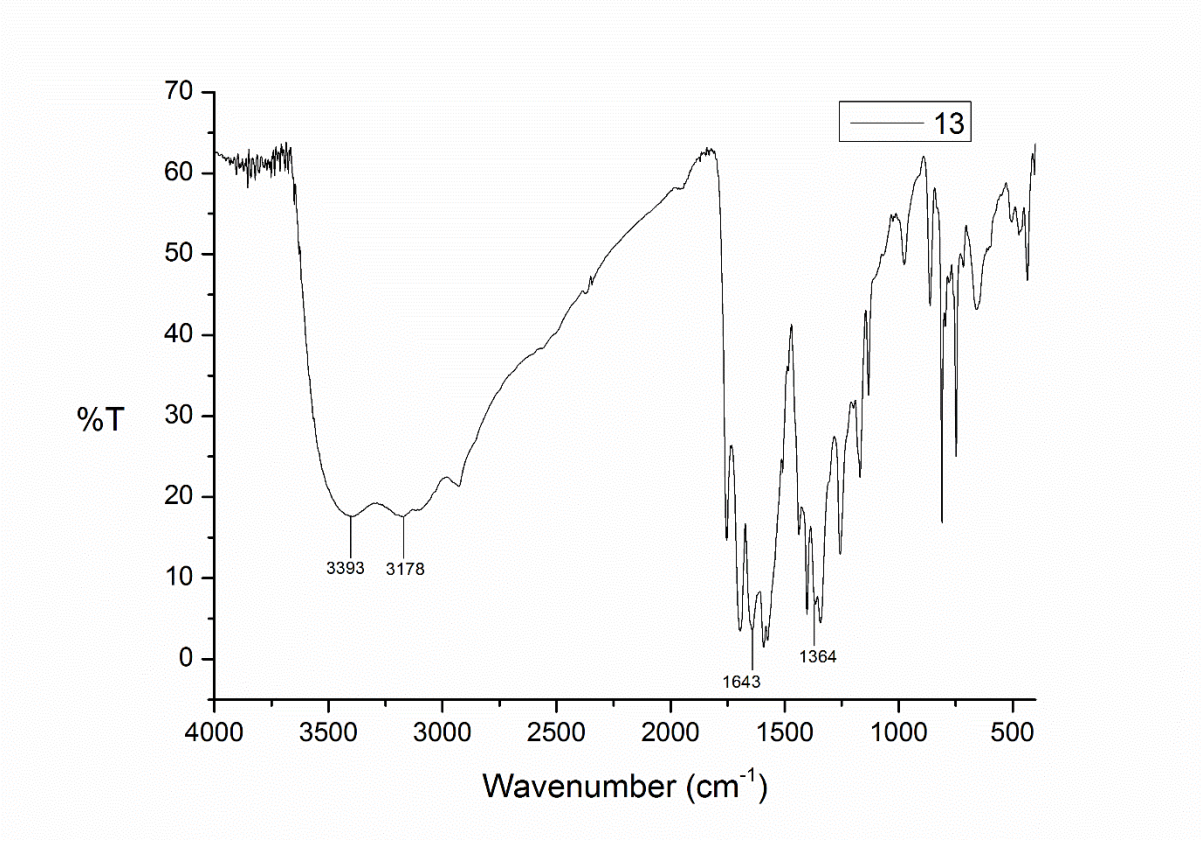

Figure 28. FTIR spectrum of $[Cu_2(Glu\text{-}Per)(H_2O)_2]_2 \cdot 5H_2O$ (**13**).

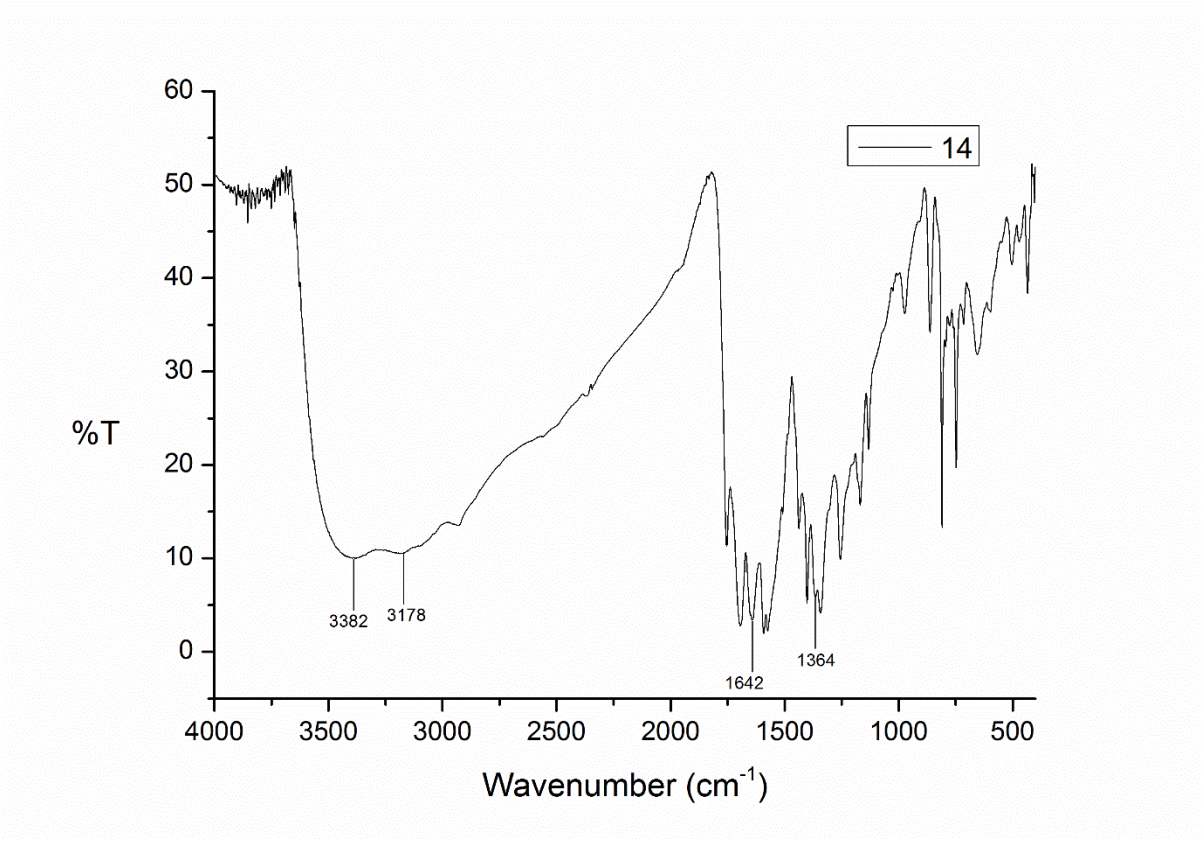

Figure 29. FTIR spectrum of $[Ni_2(Glu\text{-}Per)(H_2O)_2]_2 \cdot 7H_2O$ (**14**).

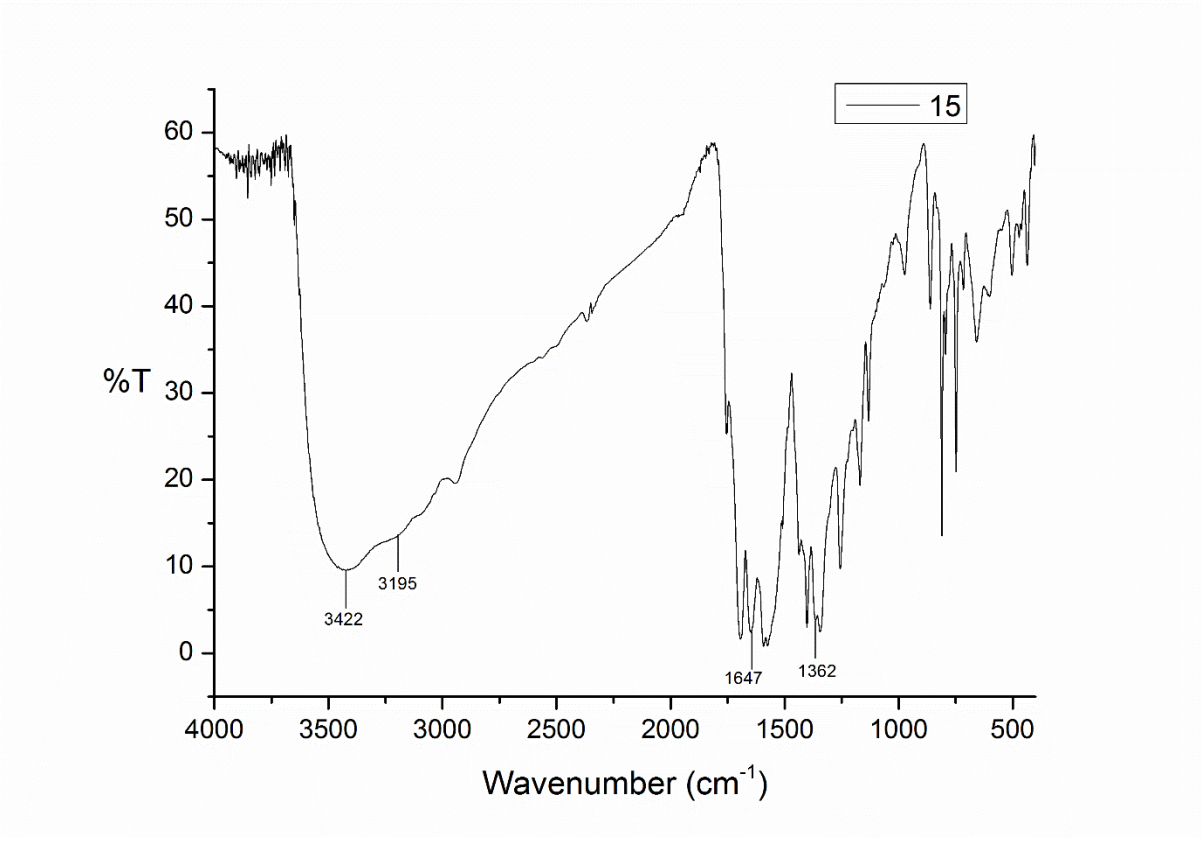

Figure 30. FTIR spectrum of $[Cd_2(Glu\text{-}Per)(H_2O)_2]_2 \cdot 5H_2O$ (**15**).

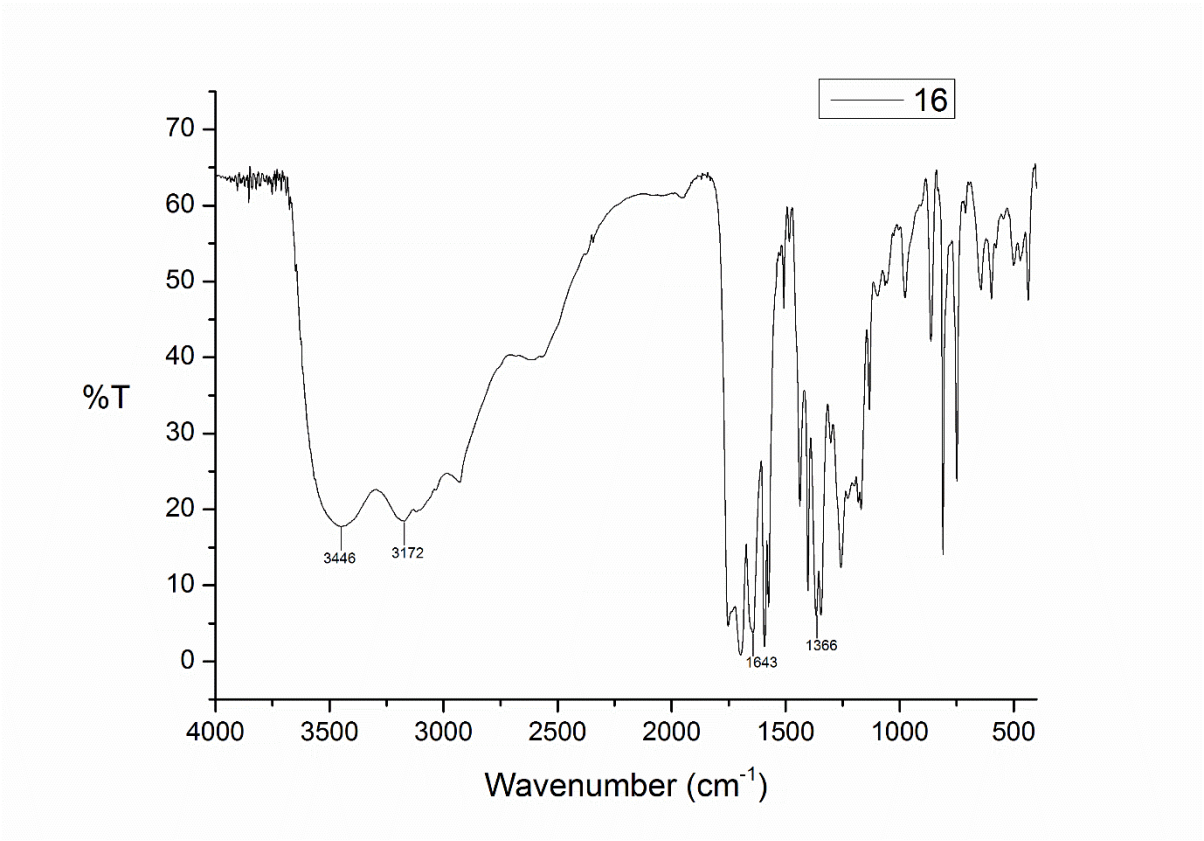

Figure 31. FTIR spectrum of $[Zn(Glu\text{-}Per)(H_2O)]_2 \cdot 3H_2O$ (**16**).

Solution State Fluorescence Studies

Fluorescence studies (solution state) were done for the linker L3 and its metal complexes **9**, **10**, **11** only because of solubility constraints. Fluorescence spectra were recorded on Perkin Elmer LS 55 fluorescence spectrometer. As expected, intensity was found maximum for free linker molecule. Quenching was observed for all the metal complexes following the order **9**>**10**>**11**. This can be attributed to the fact that in presence of metal centre the electron cloud in aromatic moiety responsible for fluorescence is now shared with the metal centre, leading to lowering of intensity. The presence of empty d orbitals in Cu^{+2} and Ni^{+2} lead to higher transfer of electron density from linker to metal centre, resulting in more quenching as compared to Cd^{+2} which has filled d orbitals. A red shift was observed for emission wavelength in all metal complexes.

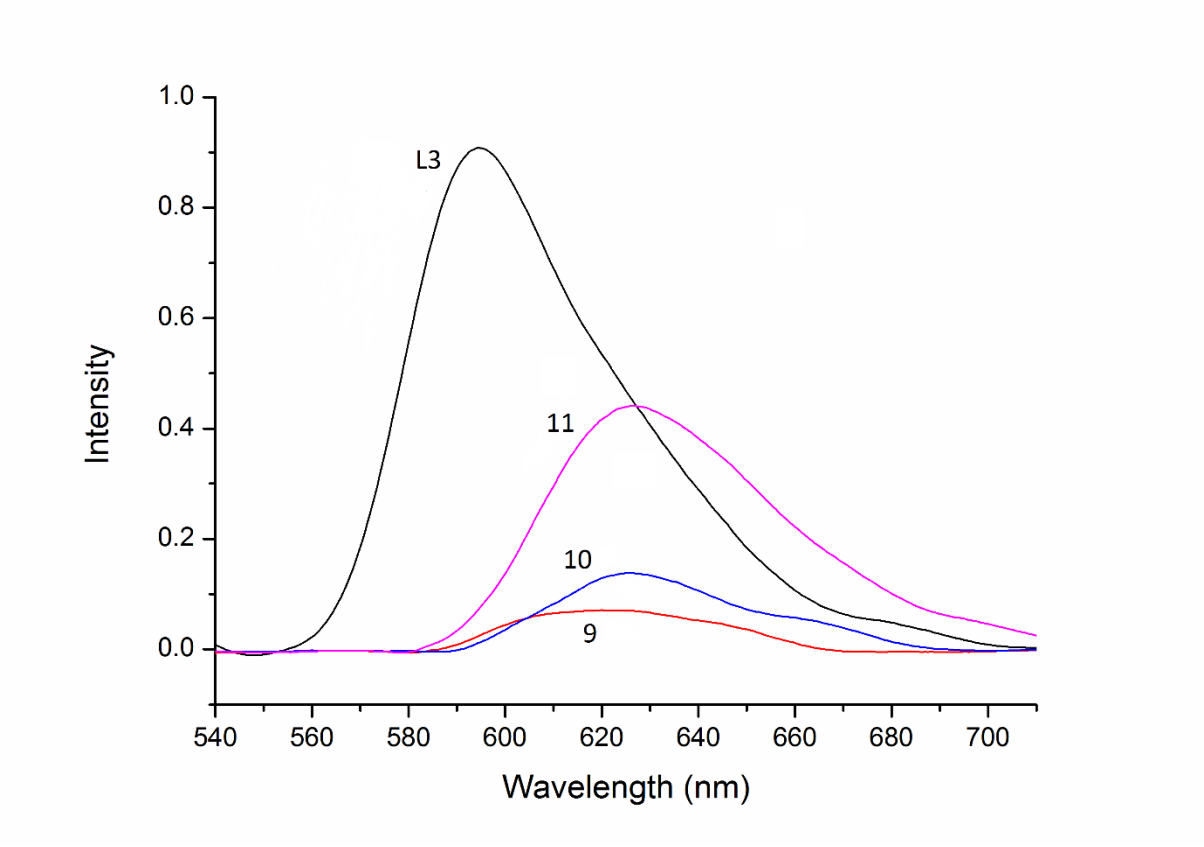

Figure 32. Emission spectra for L3 and metal complexes **9**, **10**, **11**; λ_{ex} = 410 nm.
λ_{em}(L3) = 594 nm; λ_{em}(**9**) = 616 nm
λ_{em}(**10**) = 627 nm; λ_{em}(**11**) = 628 nm

Solid State Fluorescence Studies

Fluorescence studies (solid state) were done for all complexes, as most of them faced solubility constraints. Samples were prepared by mixing the compound with KBr, similar to the case in FTIR, the difference being that the obtained powder was analysed as such, i.e. no pellet was made. Emission profile of every linker differs because of the presence of different R groups. However, spectra of the metal complexes of a linker do not differ much, showing the dominance of Perylene moiety. Emission profile of each compound is shown below.

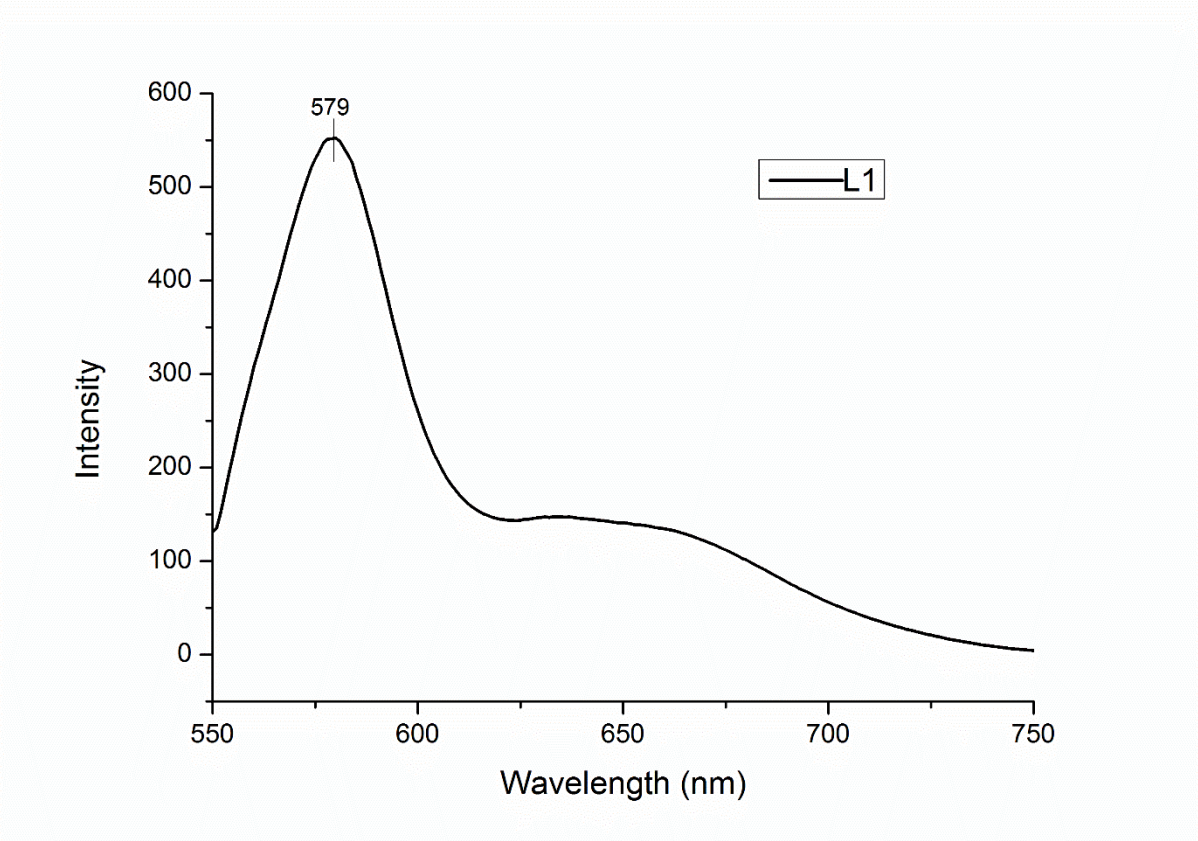

Figure 33. Emission spectrum of L1; λ_{ex} = 525 nm.

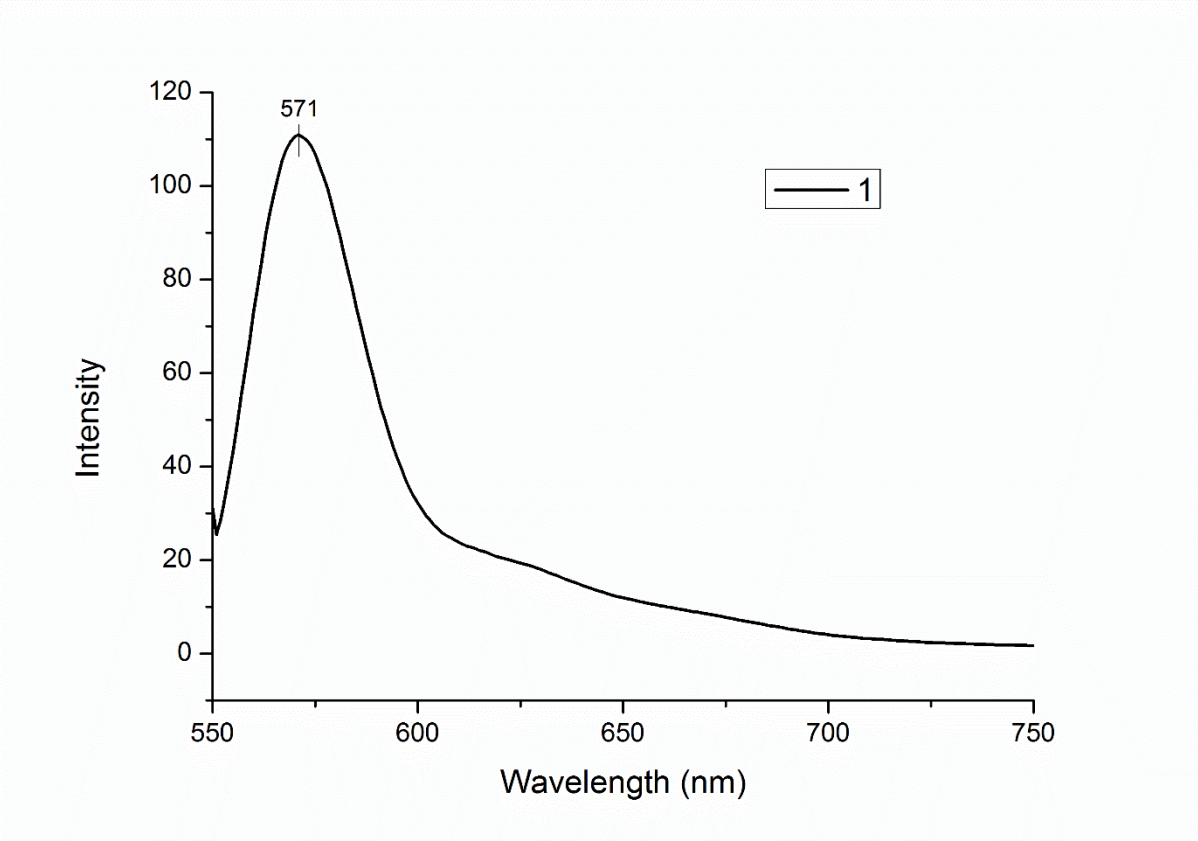

Figure 34. Emission spectrum of $[Cu(Ala\text{-}Per)(H_2O)]_2 \cdot 6H_2O$ (**1**); λ_{ex} = 525 nm.

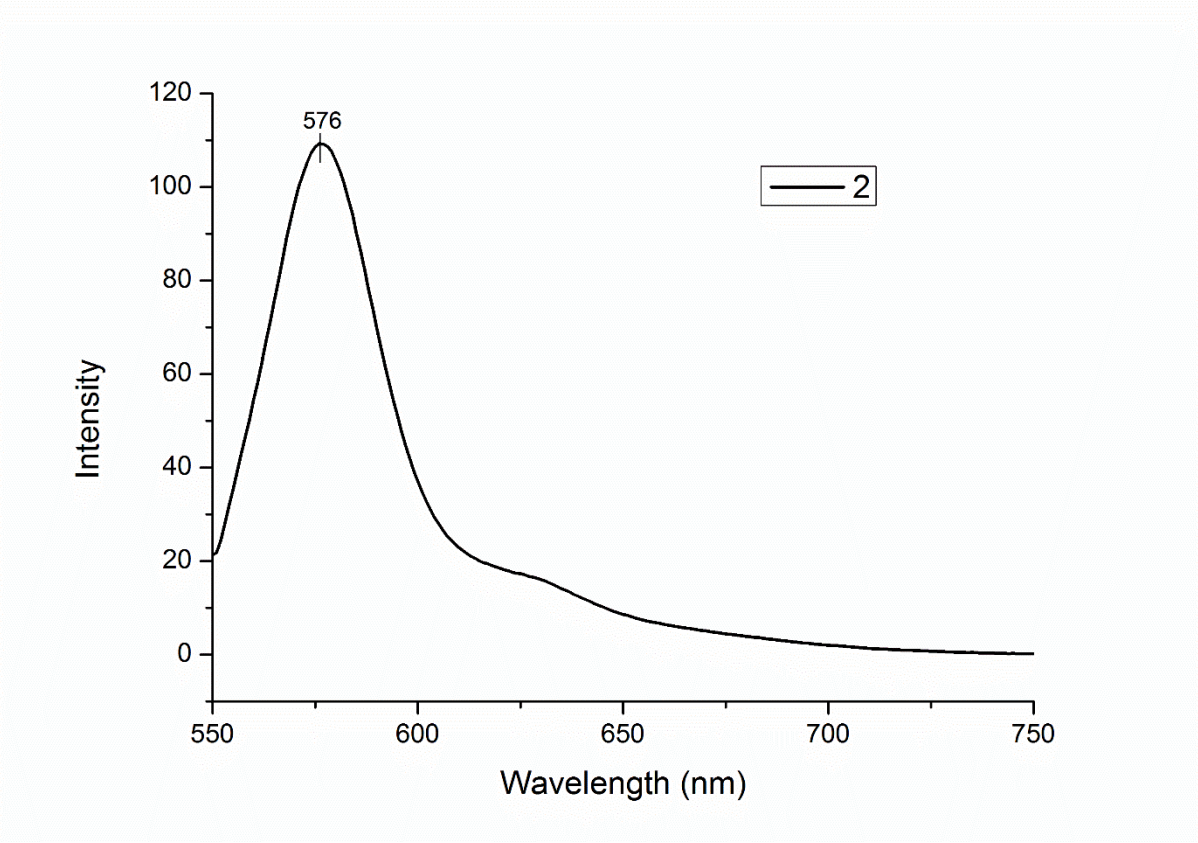

Figure 35. Emission spectrum of $[Ni(Ala\text{-}Per)(H_2O)]_2 \cdot 3H_2O$ (**2**); λ_{ex} = 525 nm.

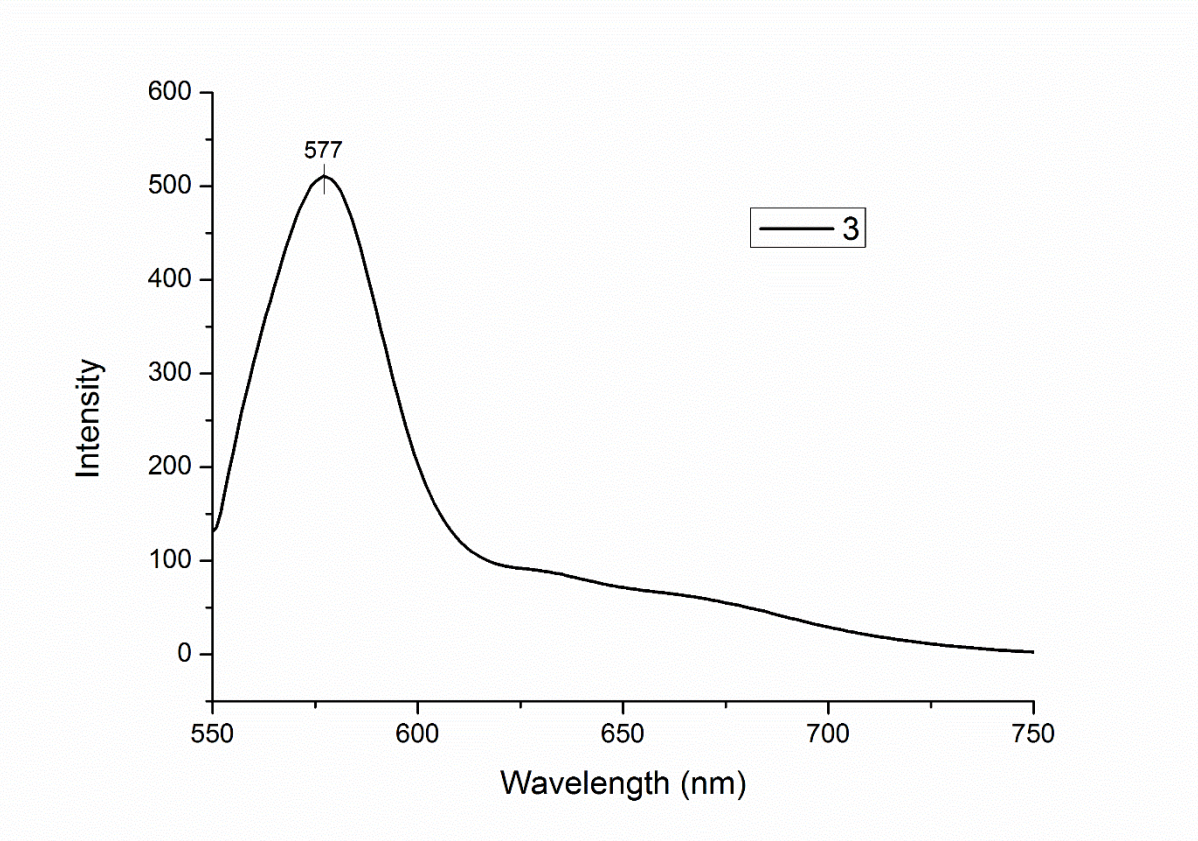

Figure 36. Emission spectrum of $[Cd(Ala\text{-}Per)(H_2O)]_2$ (**3**); λ_{ex} = 525 nm.

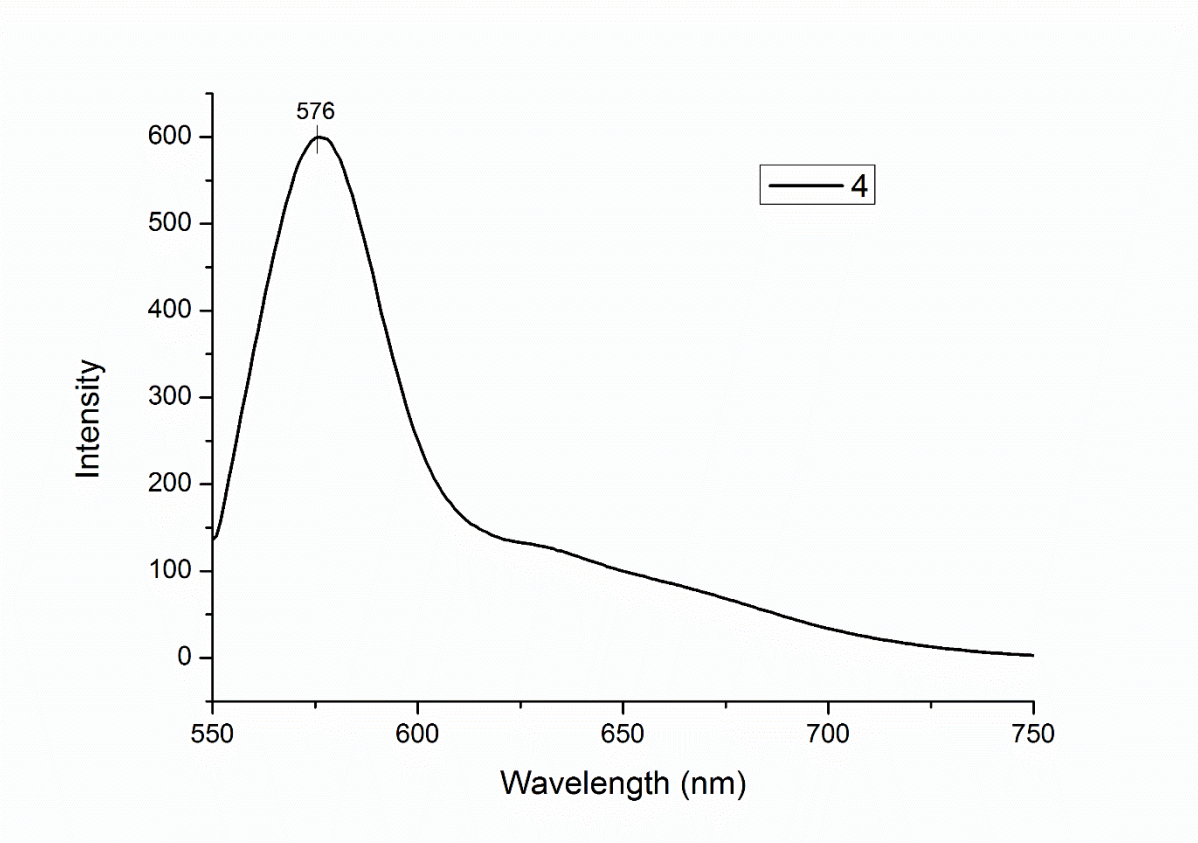

Figure 37. Emission spectrum of $[Zn(Ala\text{-}Per)(H_2O)]_2 \cdot 4H_2O$ (**4**); λ_{ex} = 525 nm.

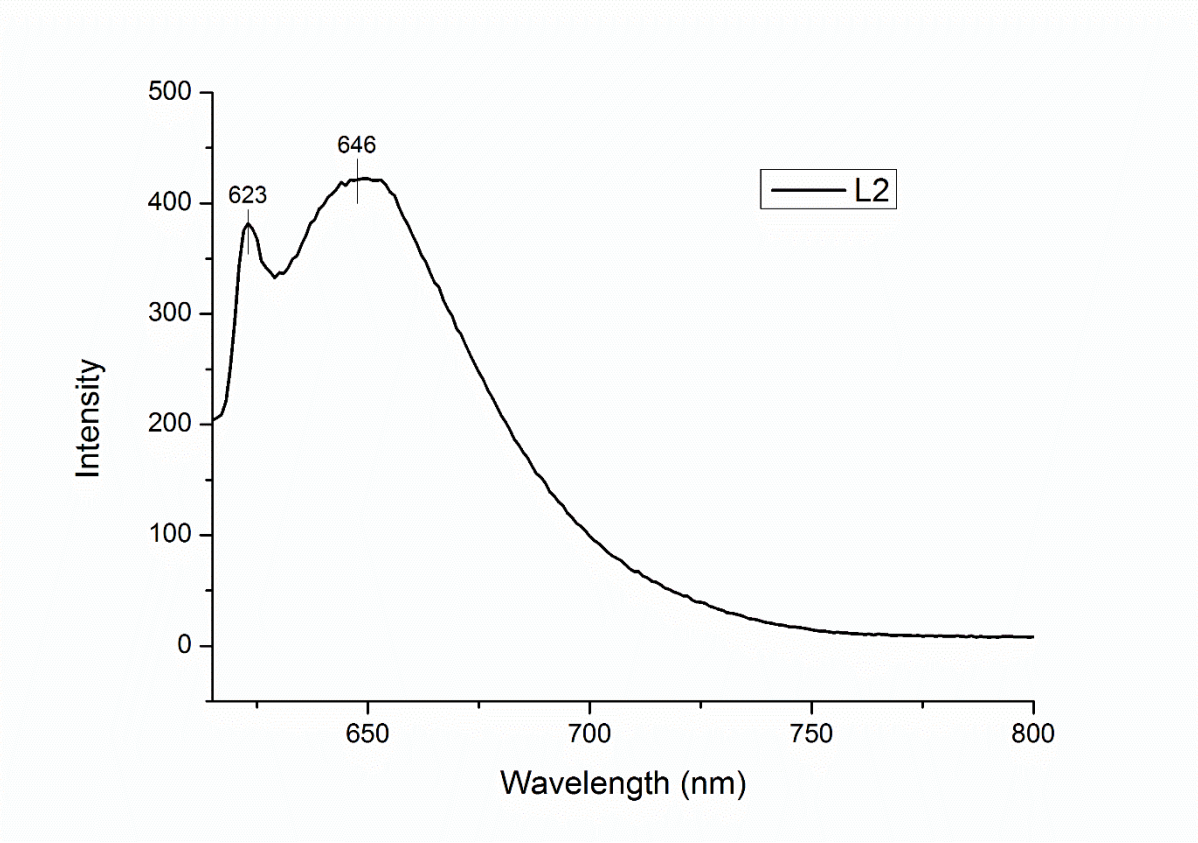

Figure 38. Emission spectrum of L2; λ_{ex} = 599 nm.

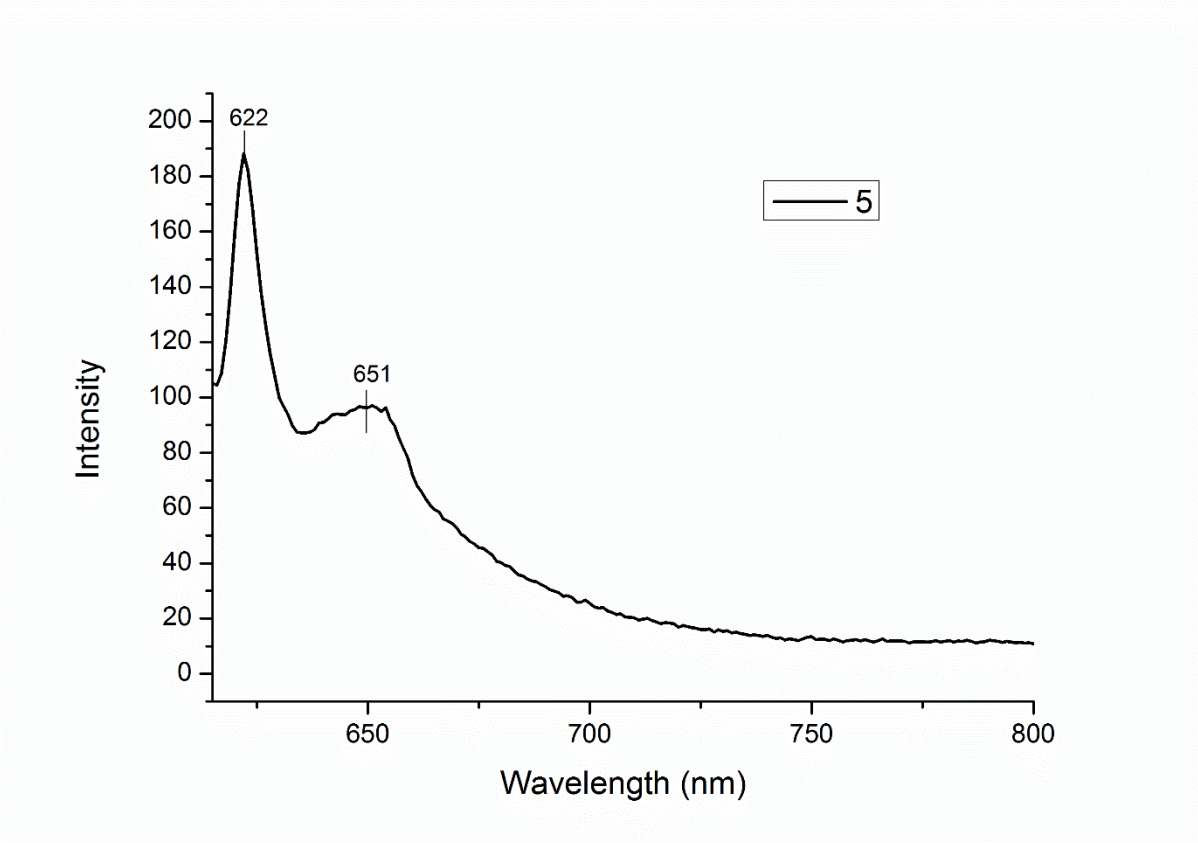

Figure 39. Emission spectrum of $[Cu(Phe\text{-}Per)(H_2O)]_2 \cdot 5H_2O$ (**5**); λ_{ex} = 599 nm.

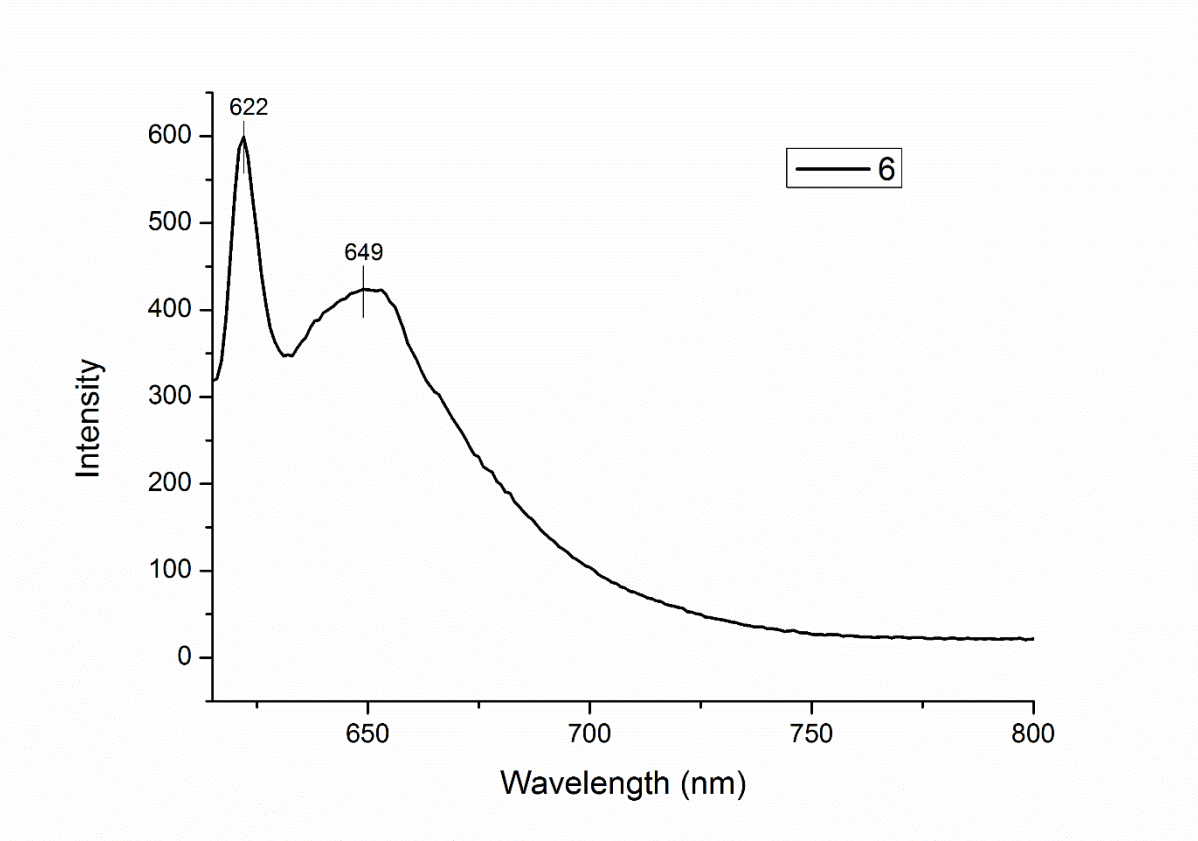

Figure 40. Emission spectrum of $[Ni(Phe\text{-}Per)(H_2O)]_2 \cdot 6H_2O$ (**6**); λ_{ex} = 599 nm.

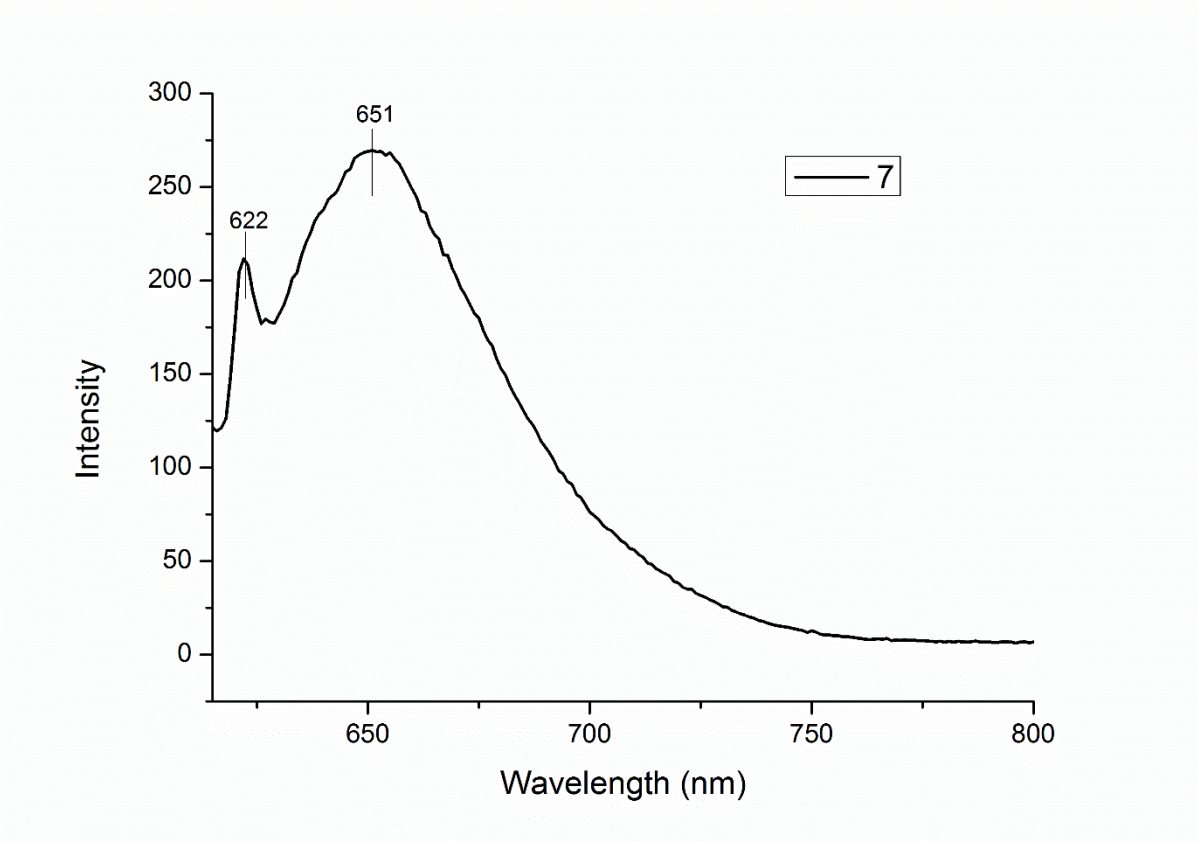

Figure 41. Emission spectrum of $[Cd(Phe\text{-}Per)(H_2O)]_2$ (**7**); λ_{ex} = 599 nm.

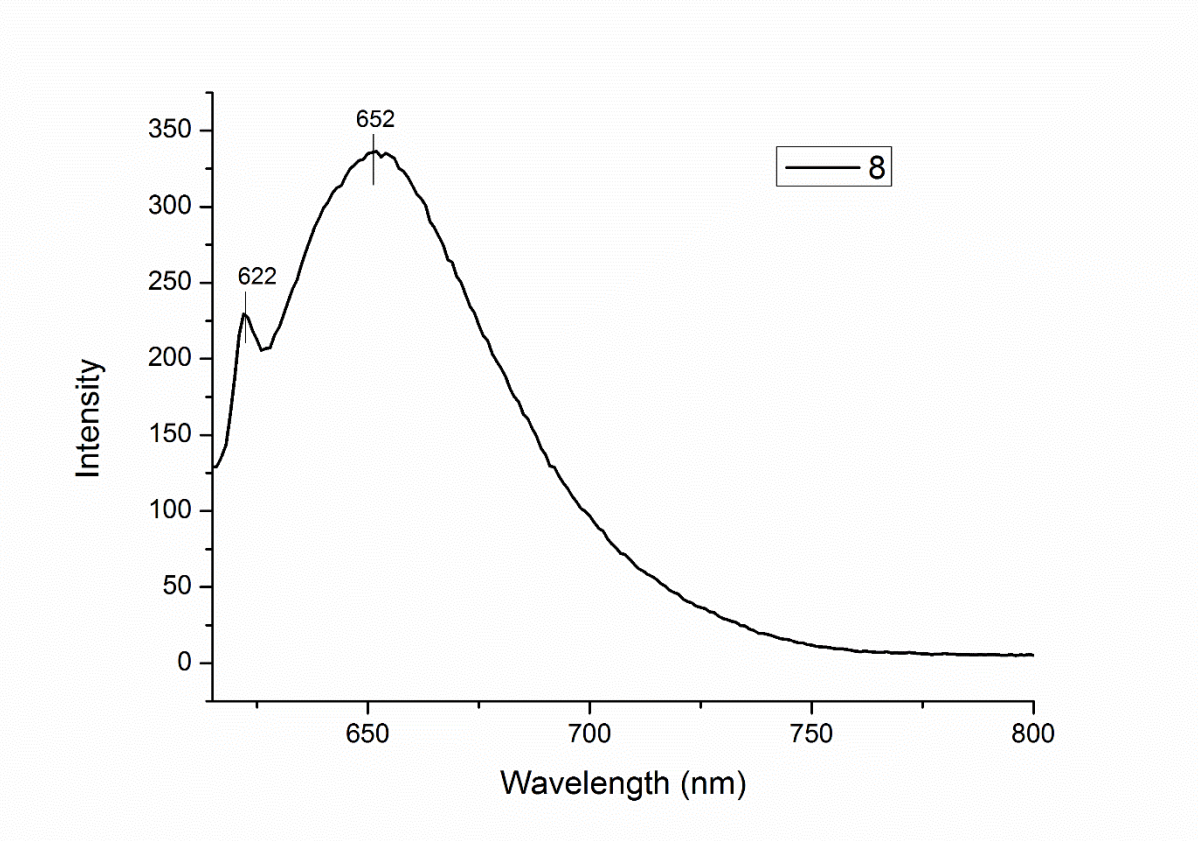

Figure 42. Emission spectrum of $[Zn(Phe\text{-}Per)(H_2O)]_2 \cdot 2H_2O$ (**8**); λ_{ex} = 599 nm.

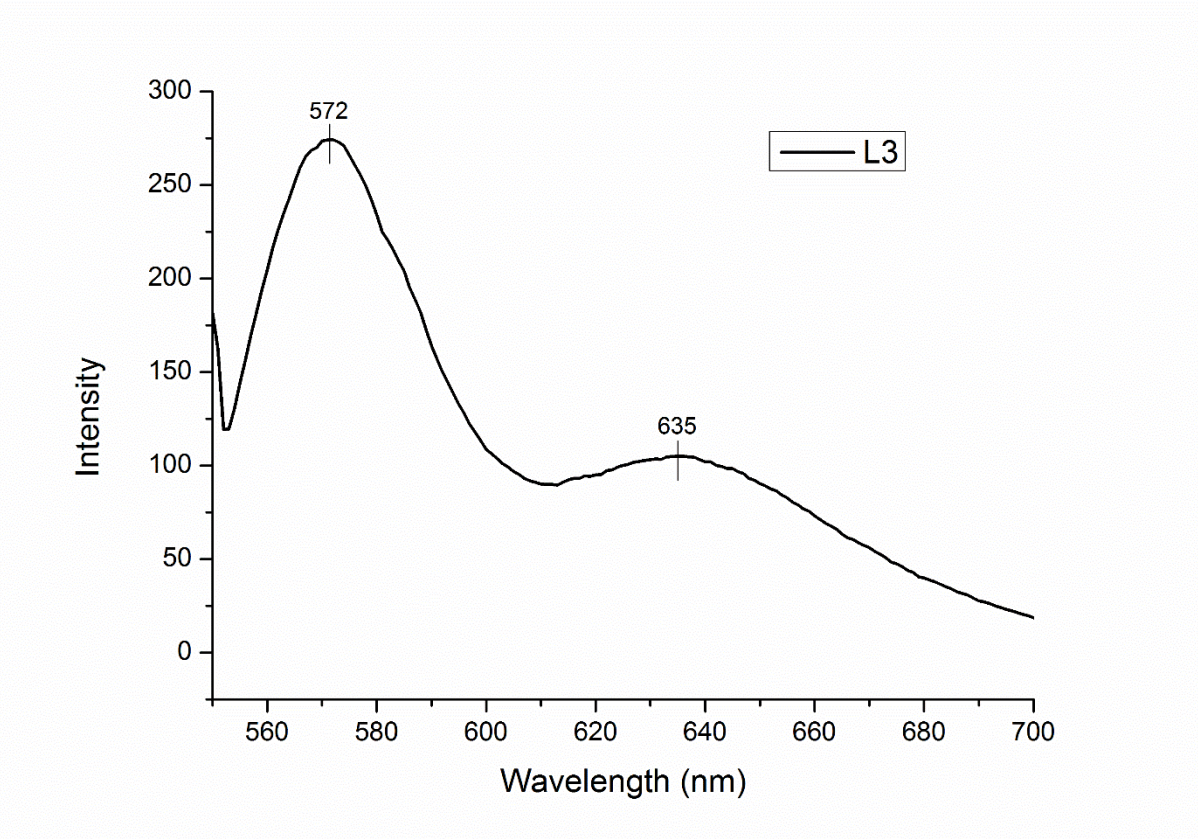

Figure 43. Emission spectrum of L3; λ_{ex} = 531 nm.

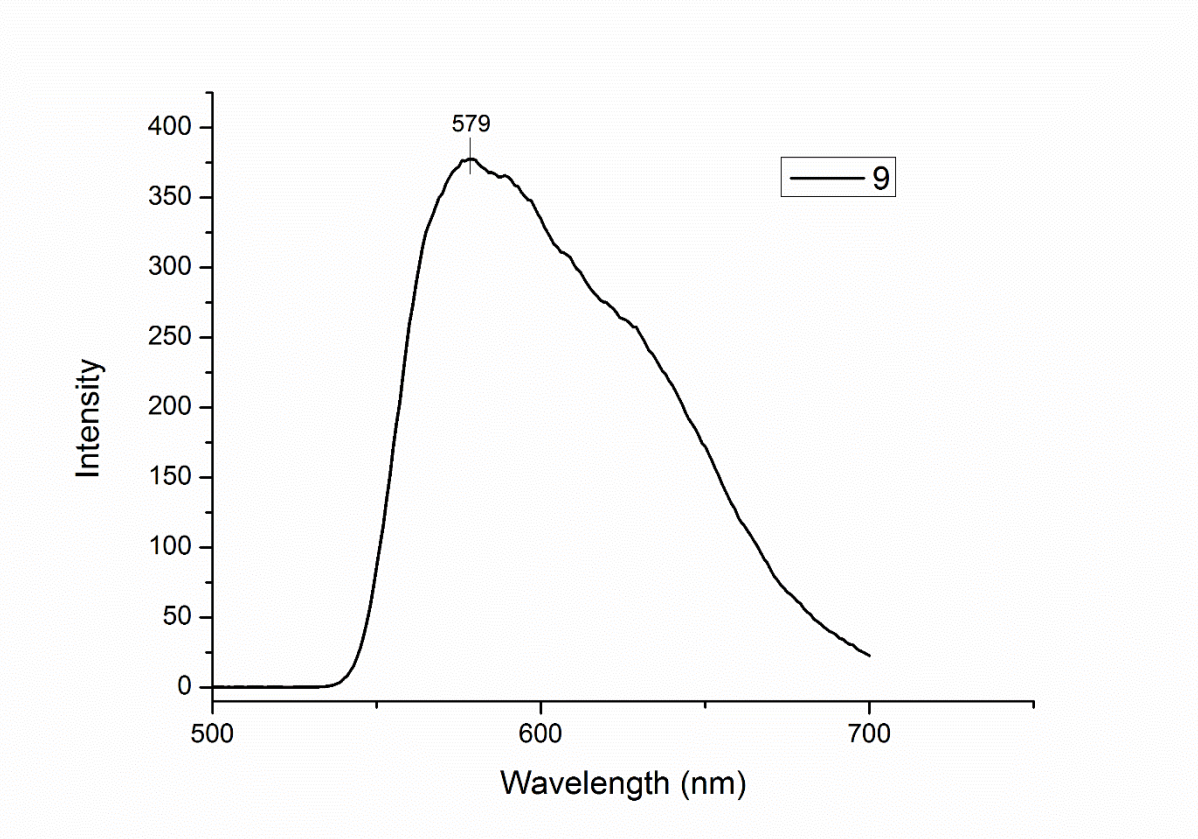

Figure 44. Emission spectrum of $[Cu(Tyr\text{-}Per)(H_2O)]_2 \cdot 8H_2O$ (**9**); λ_{ex} = 261 nm.

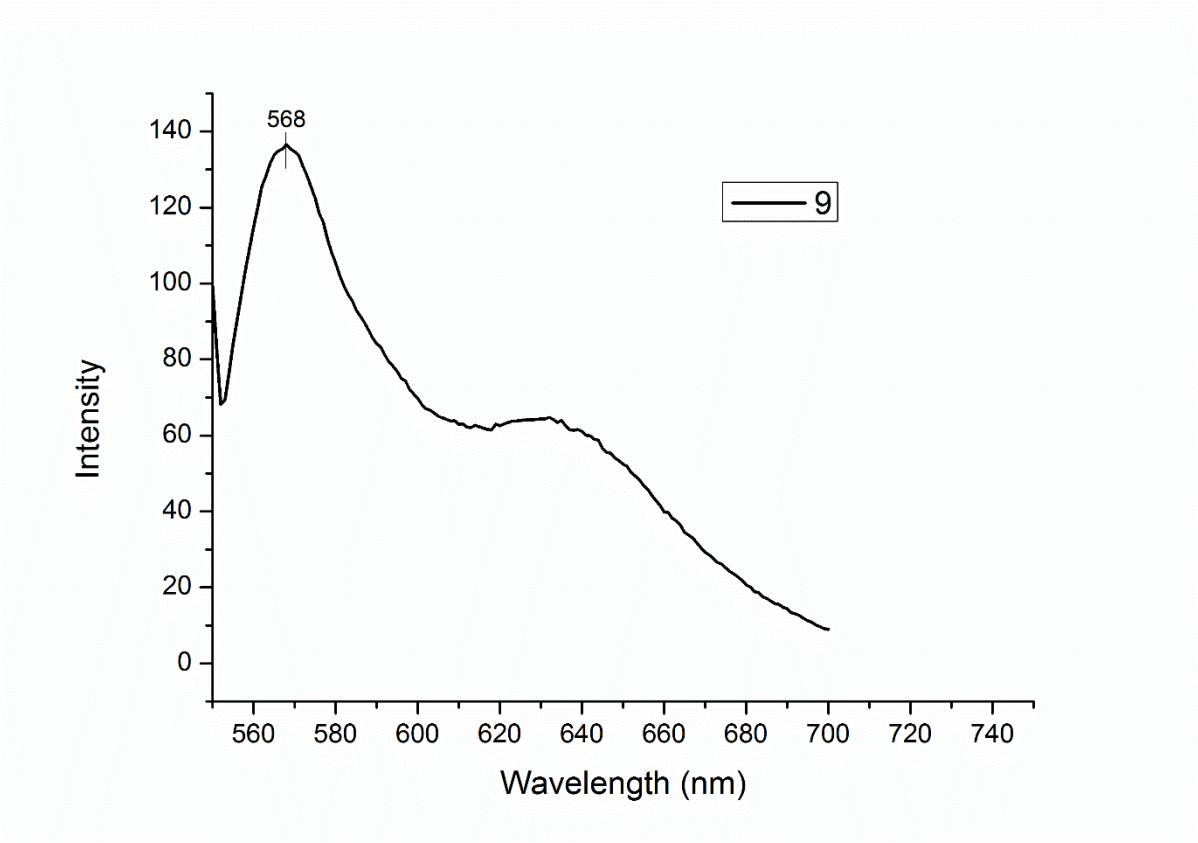

Figure 45. Emission spectrum of $[Cu(Tyr\text{-}Per)(H_2O)]_2 \cdot 8H_2O$ (**9**); λ_{ex} = 531 nm.

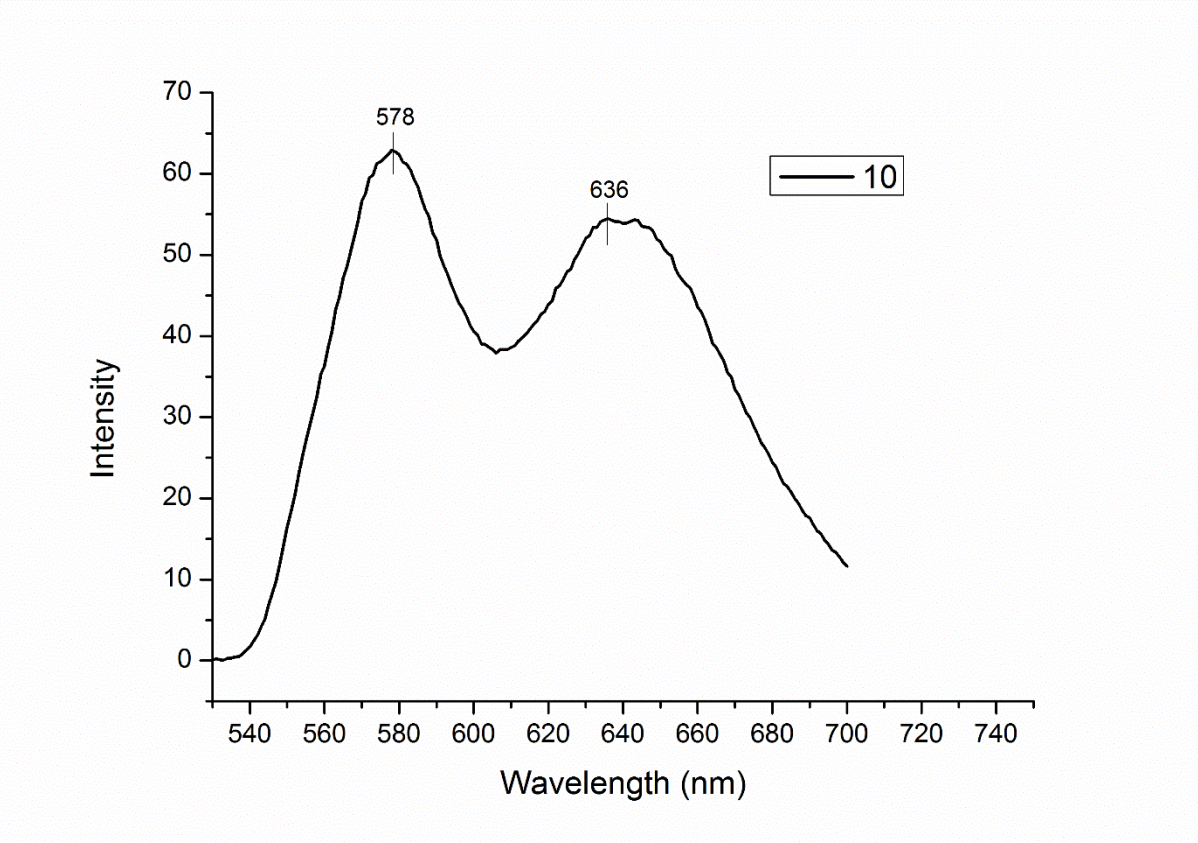

Figure 46. Emission spectrum of $[Ni(Tyr\text{-}Per)(H_2O)]_2 \cdot 8H_2O$ (**10**); λ_{ex} = 491 nm.

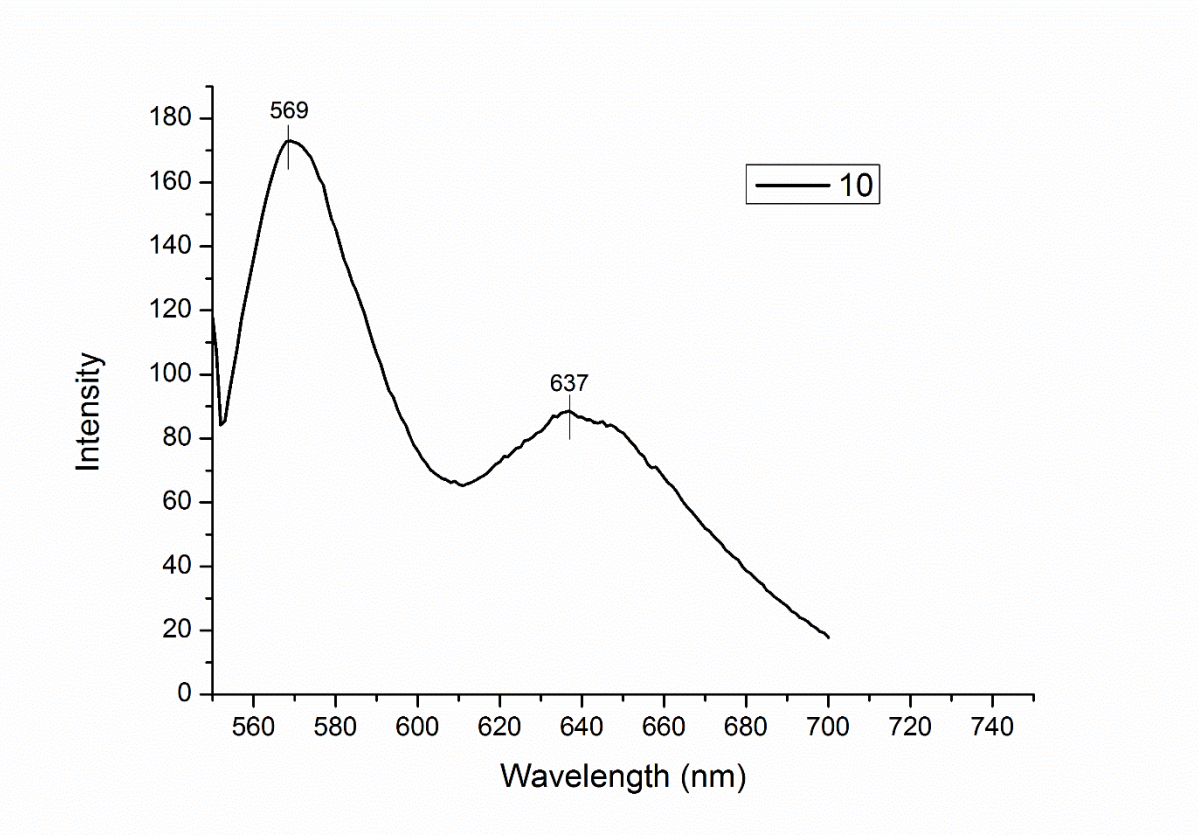

Figure 47. Emission spectrum of $[Ni(Tyr\text{-}Per)(H_2O)]_2 \cdot 8H_2O$ (**10**); λ_{ex} = 531 nm.

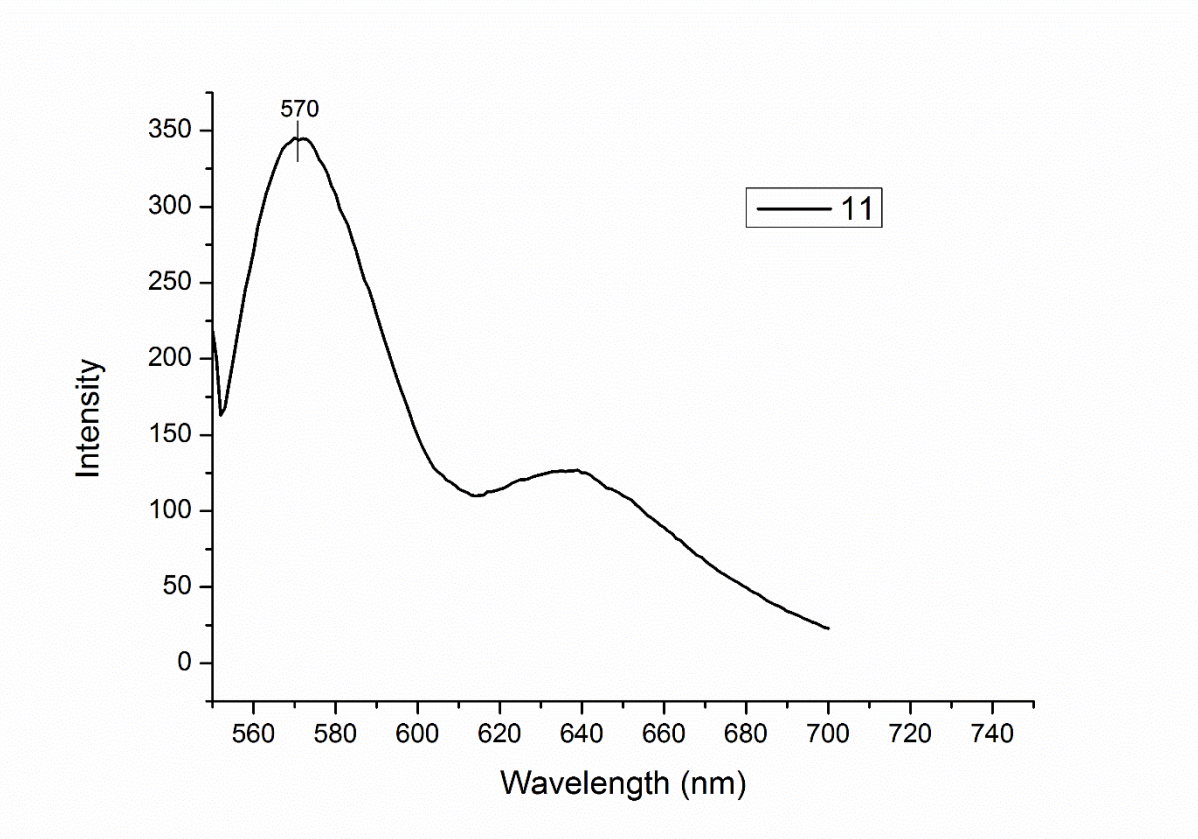

Figure 48. Emission spectrum of $[Cd(Tyr\text{-}Per)(H_2O)]_2 \cdot 7H_2O$ (**11**); λ_{ex} = 531 nm.

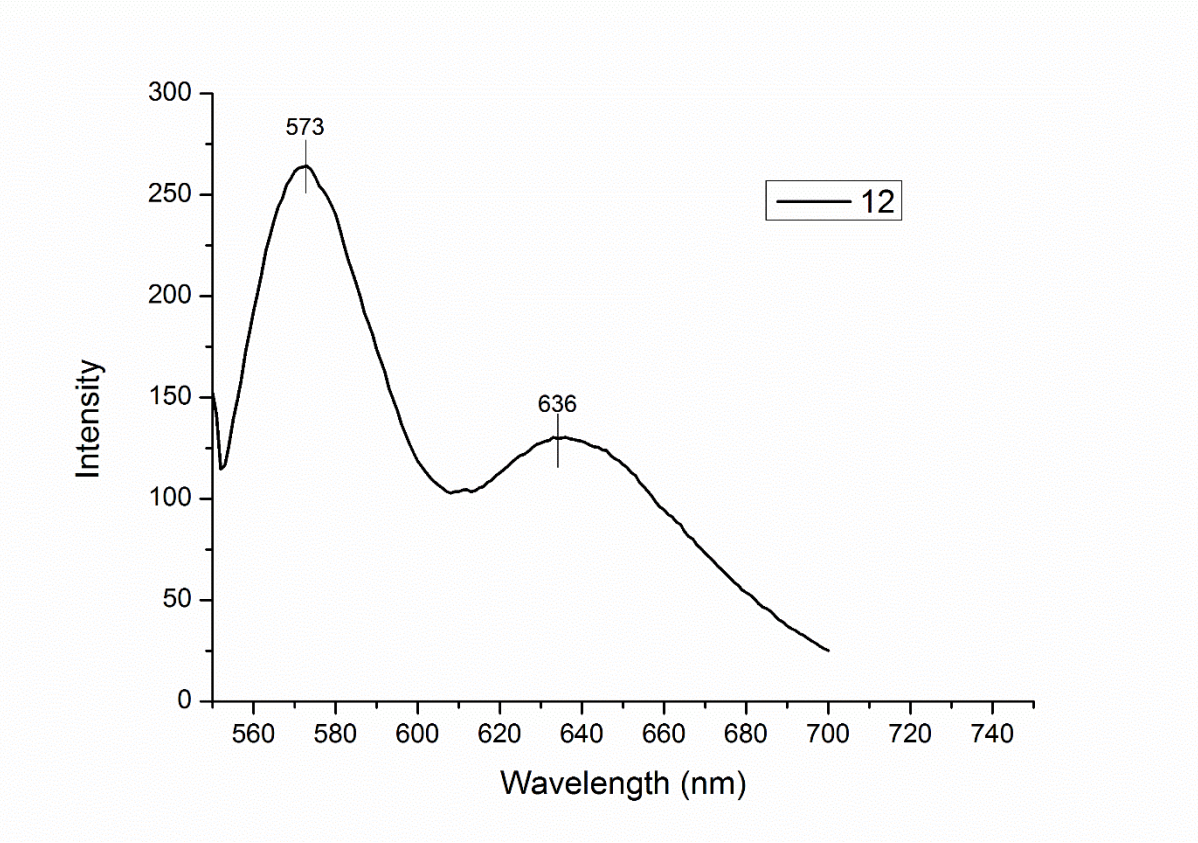

Figure 49. Emission spectrum of $[Zn(Tyr\text{-}Per)(H_2O)]_2 \cdot 8H_2O$ (**12**); λ_{ex} = 531 nm.

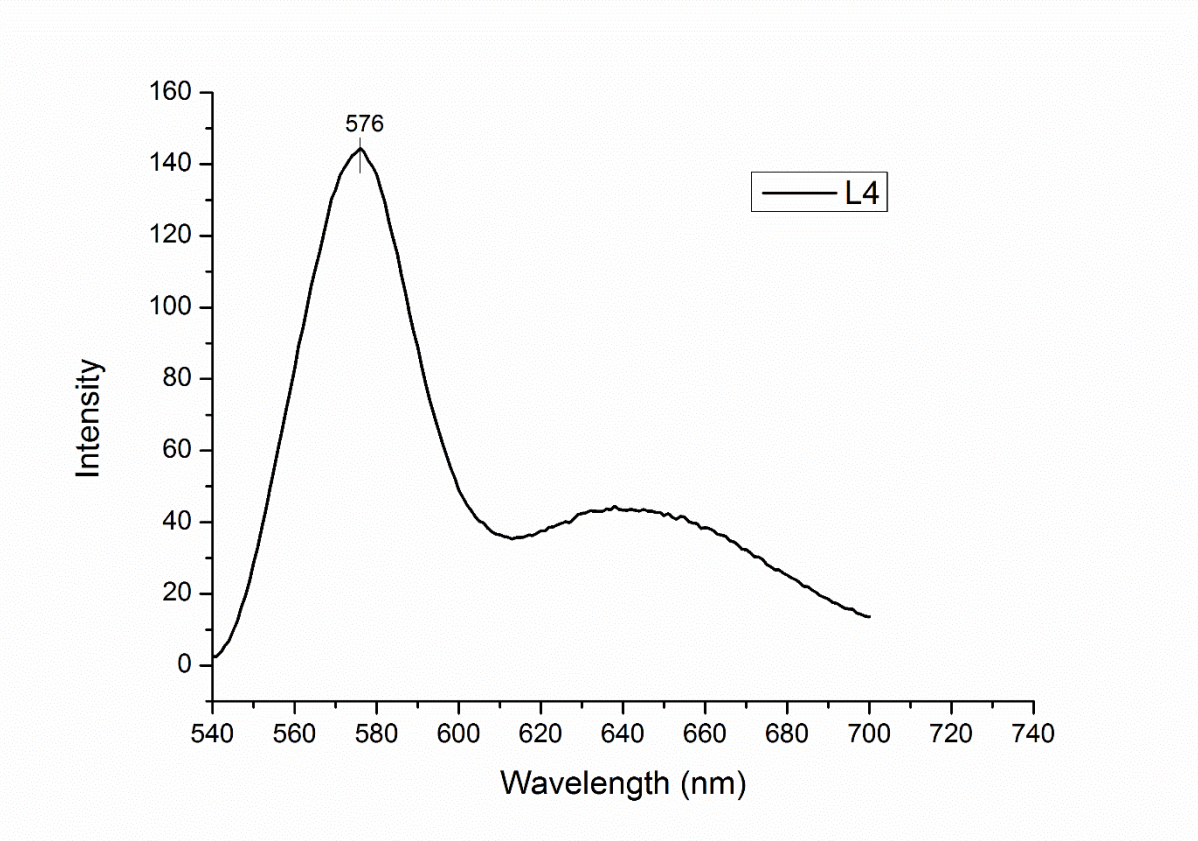

Figure 50. Emission spectrum of L4; λ_{ex} = 524 nm.

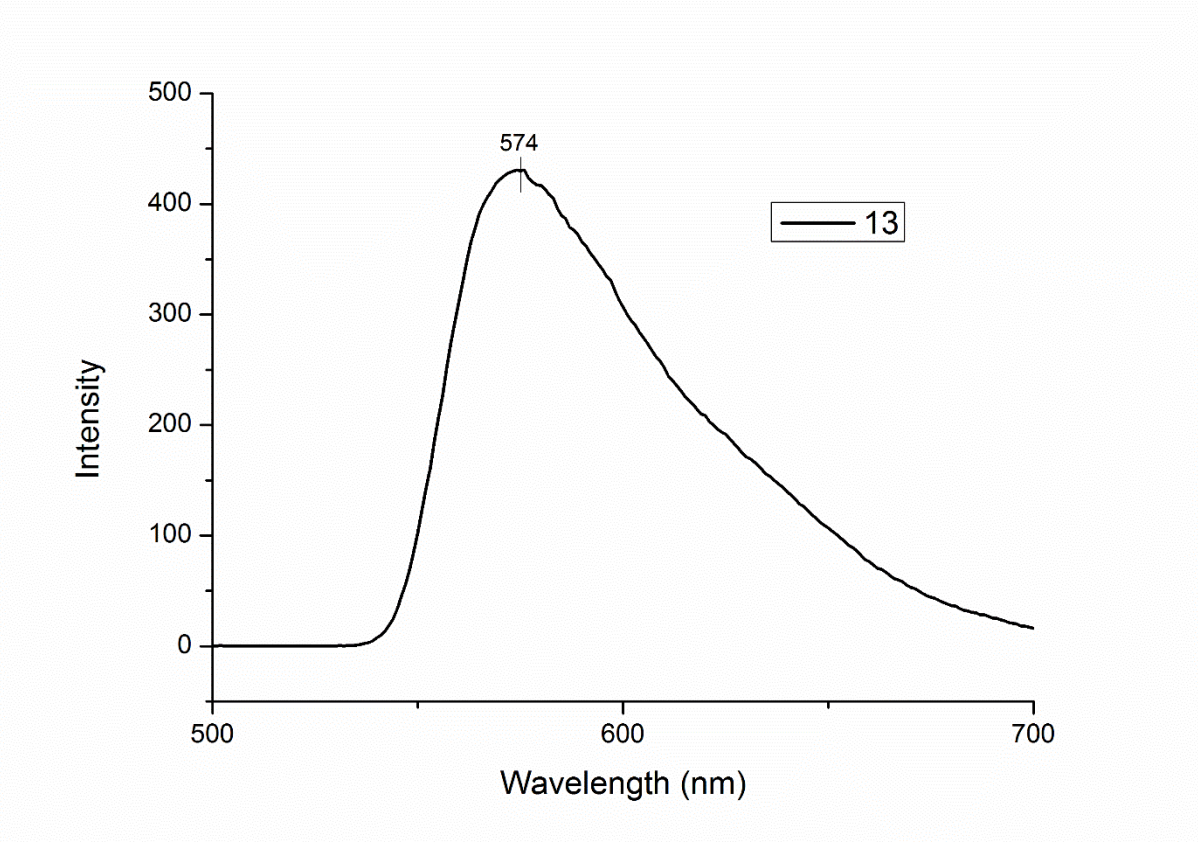

Figure 51. Emission spectrum of $[Cu_2(Glu\text{-}Per)(H_2O)_2]_2 \cdot 5H_2O$ (**13**); λ_{ex} = 254 nm.

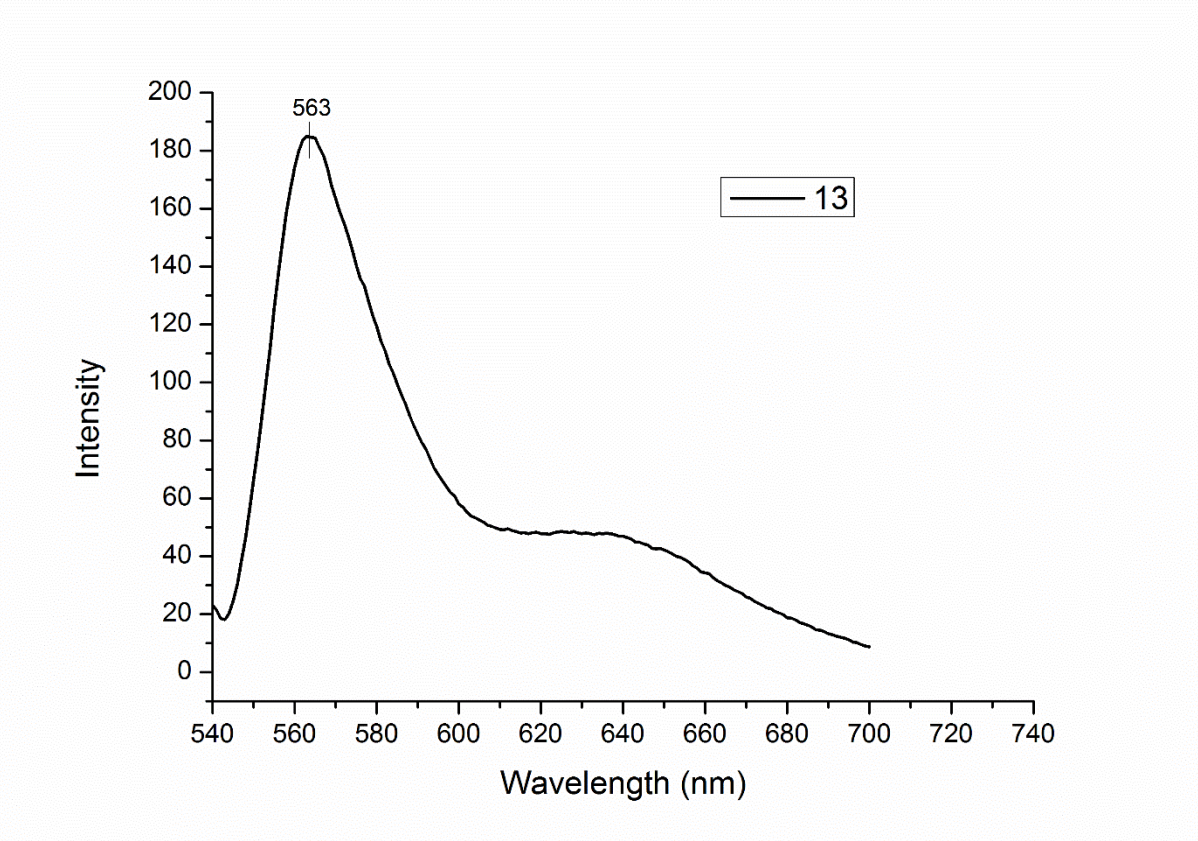

Figure 52. Emission spectrum of $[Cu_2(Glu\text{-}Per)(H_2O)_2]_2 \cdot 5H_2O$ (**13**); λ_{ex} = 524 nm.

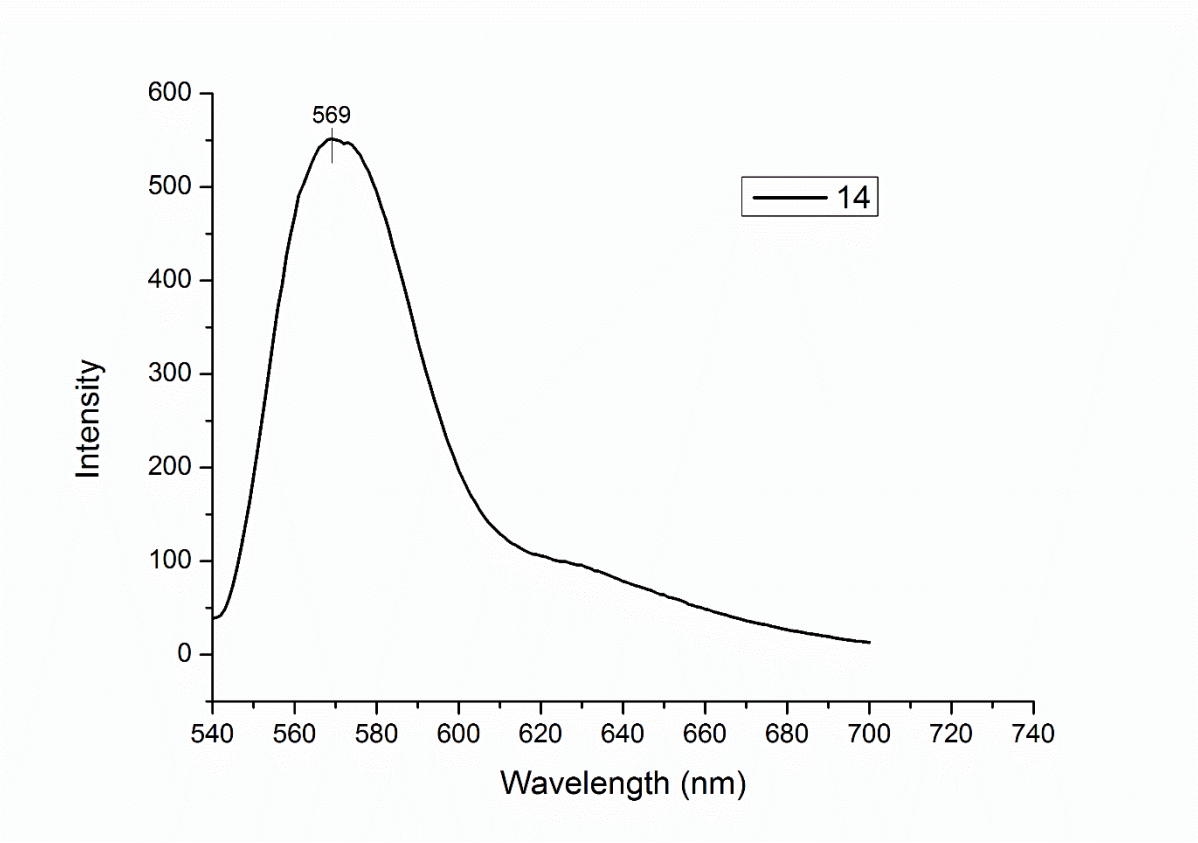

Figure 53. Emission spectrum of $[Ni_2(Glu\text{-}Per)(H_2O)_2]_2 \cdot 7H_2O$ (**14**); λ_{ex} = 524 nm.

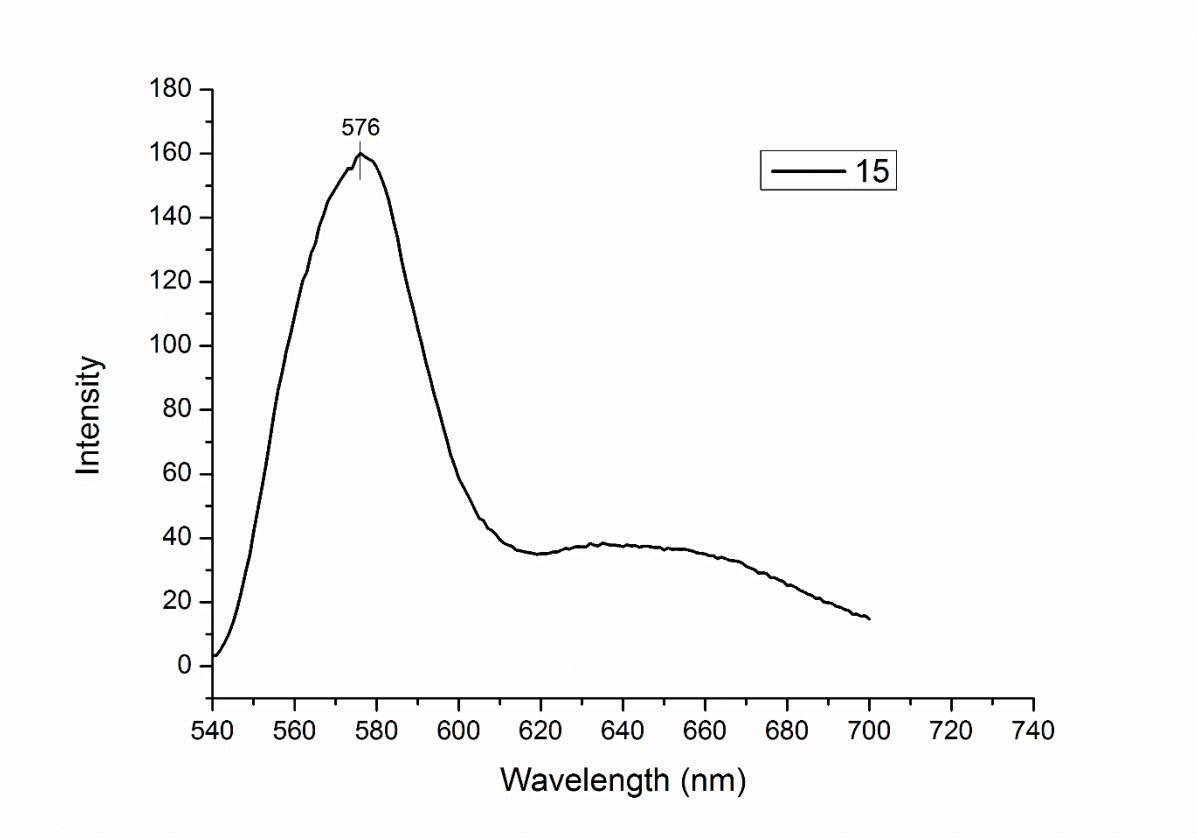

Figure 54. Emission spectrum of $[Cd_2(Glu\text{-}Per)(H_2O)_2]_2 \cdot 5H_2O$ (**15**); λ_{ex} = 524 nm.

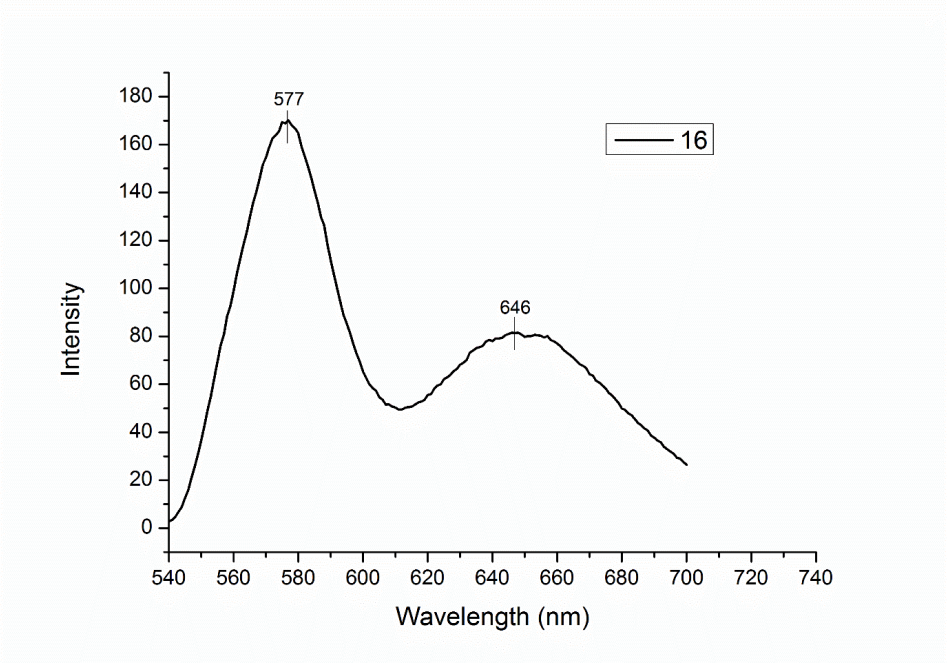

Figure 55. Emission spectrum of $[Zn(Glu\text{-}Per)(H_2O)]_2 \cdot 3H_2O$ (**16**); λ_{ex} = 524 nm.

Circular Dichroism

Circular dichroism (CD) spectra were recorded on Appliedphotophysics Chirascan CD spectrophotometer. Positive and negative cotton effects were observed in all the cases with inflection point coming around 540 nm, which indicated that the thus obtained molecule is chiral. Due to solubility constraints the analysis was done only for L3 and its metal complexes **9**, **10** and **11**.

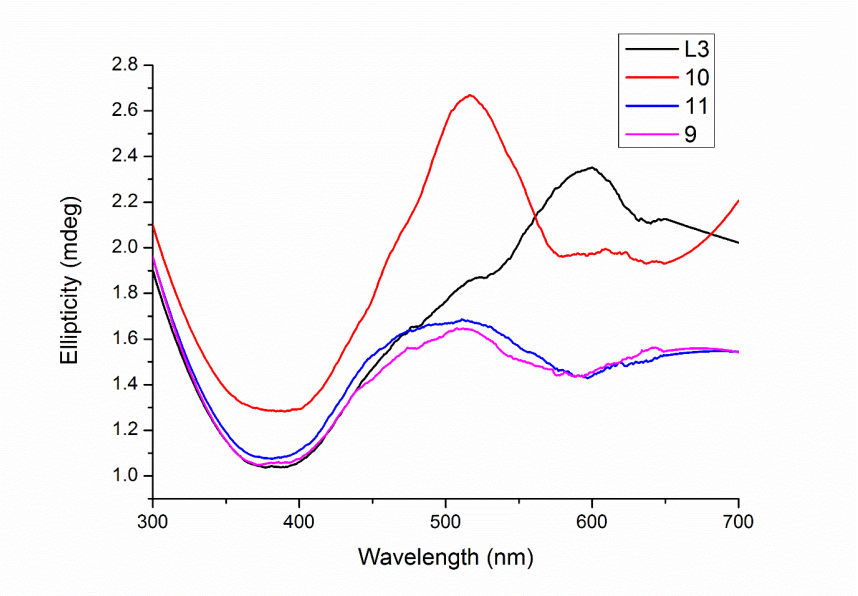

Figure 56. CD spectra for L3 and metal complexes **9**, **10** and **11**.

Powder X-ray Diffraction Studies

Each sample was placed on a glass sample holder that was placed on the sample rotation stage (120 rpm) attachment. The data were collected over an angle range 5° to 50° with a scanning speed of 2° per minute. It was found that few broad peaks were observed in each case but the intensity was quite low which means that crystalline nature is very limited. Also, on comparison of linker and its metal complexes it was observed that patterns are pretty much similar suggesting isostructural nature.

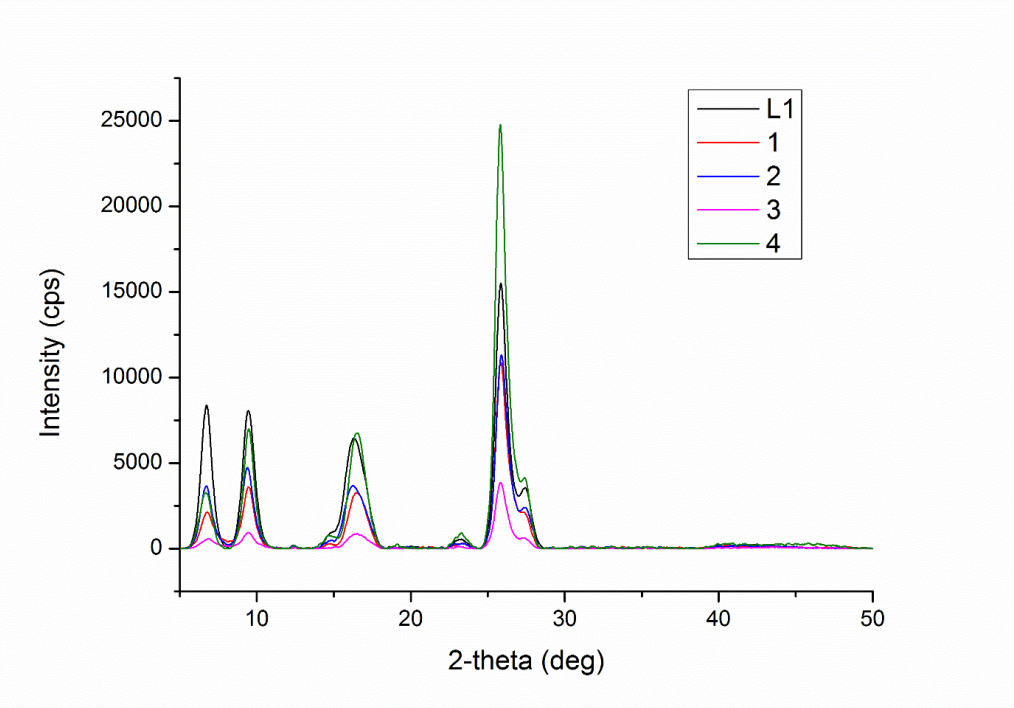

Figure 57. PXRD patterns of L1 and metal complexes **1-4**.

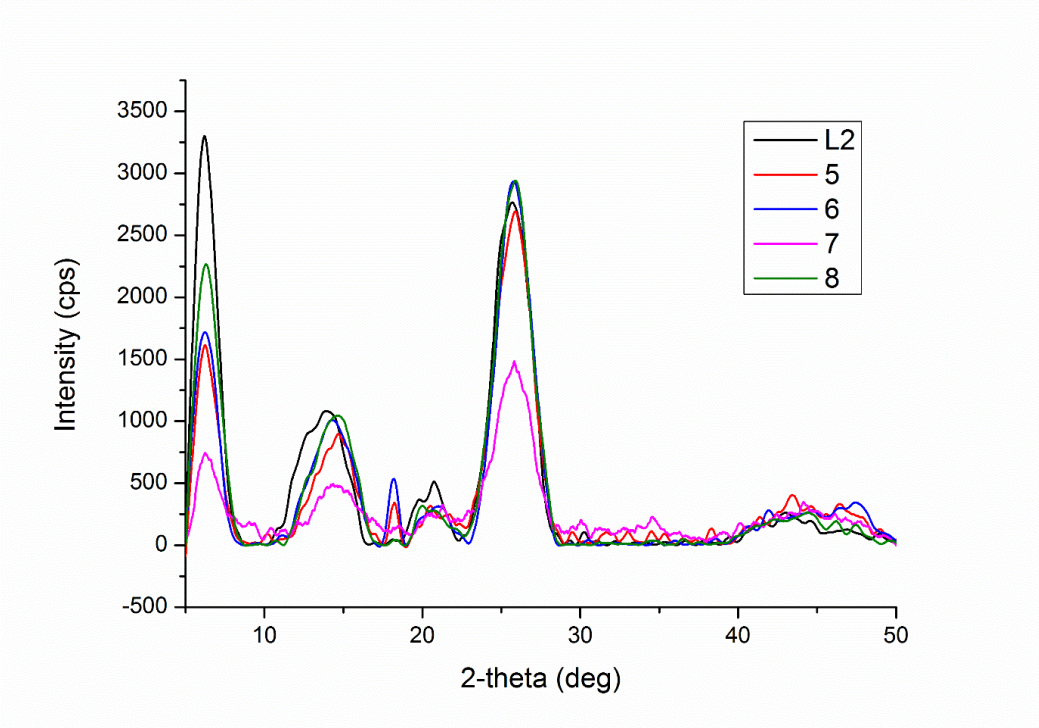

Figure 58. PXRD patterns of L2 and metal complexes **5-8**.

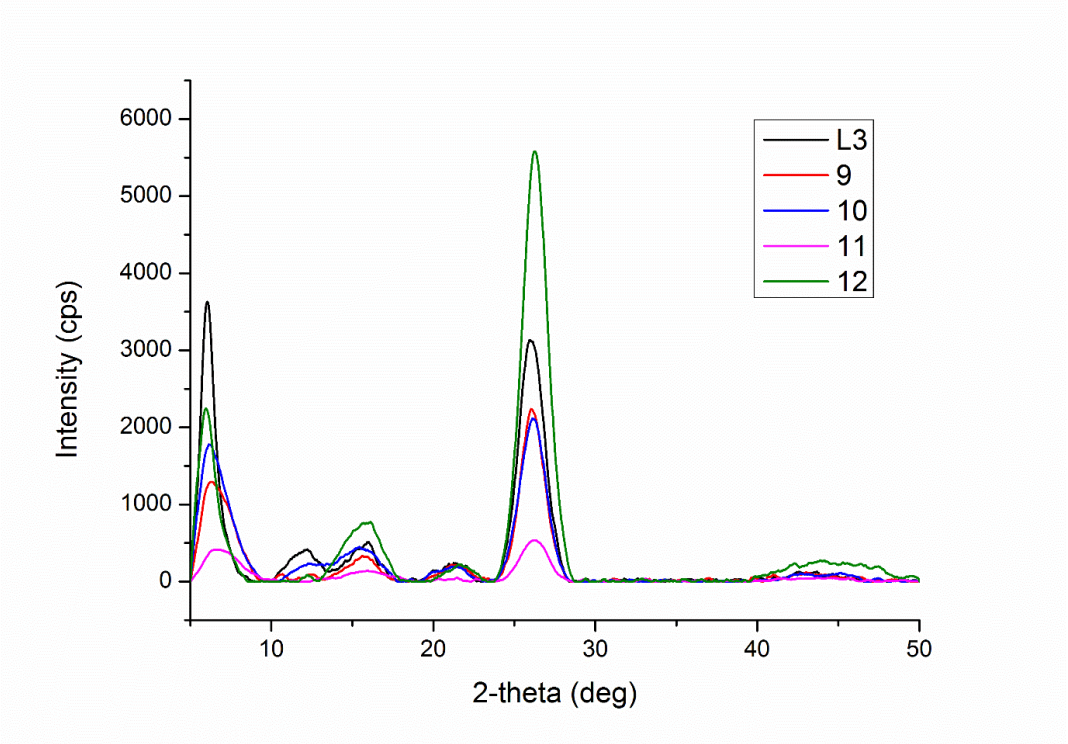

Figure 59. PXRD patterns of L3 and metal complexes **9-12**.

Chapter IV

CONCLUSION AND FUTURE DIRECTIONS

A generalized synthetic procedure for the formation of four Perylene-3,4,9,10-tetracarboxylic dianhydride based linkers in excellent yields and high purity is developed. Sixteen metal complexes of these linkers with transition metal ions, such as Cu(II), Ni(II), Cd(II) and Zn(II) have been synthesized and characterized by various analytical techniques. Solution state fluorescence studies showcase the quenching effect in case of metal complexes. Solid state fluorescence was performed for most of the samples which illustrates the emission profile. Solubility constraints have limited the crystal growth of the metal complexes. Structural elucidation through single crystal X-ray diffraction (SCXRD) analysis of the complexes is required to gain insight into the three dimensional structure and determine the structure-property relationships. The complexes can be studied for various photoluminescence based sensing applications where electron donating or accepting analyte molecule alters the existing π electron cloud leading to an enhancement or quenching of the fluorescence intensity. Other aspects, such as chiral catalysis, gas storage, can also be explored.

References

1. Zhou, H. C.; Long, J. R.; Yaghi, O. M. *Chem. Rev.* **2012**, *112*, 673.
2. Janiak, C. *Dalton Trans.* **2003**, 2781.
3. Tranchemontagne, D. J.; Mendoza-Corte´s, J. L.; O'Keeffe, M.; Yaghi, O. M. *Chem. Soc. Rev.* **2009**, *38*, 1257.
4. Li, H.; Eddaoudi, M.; O'Keeffe, M.; Yaghi, O. M. *Nature* **1999**, *402*, 276.
5. Kitagawa, S.; Kitaura, R.; Noro, S. *Angew. Chem. Int. Ed.* **2004**, *43*, 2334.
6. Ferey, G.; Serre, C. *Chem. Soc. Rev.* **2009**, *38*, 1380.
7. Ma, L.; Abney, C.; Lin, W. *Chem. Soc. Rev.* **2009**, *38*, 1248.
8. Lee, J. Y.; Farha, O. K.; Roberts, J.; Scheidt, K. A.; Nguyen, S. T.; Hupp, J. T. *Chem. Soc. Rev.* **2009**, *38*, 1450.
9. Yoon, M.; Srirambalaji, R.; Kim, K. *Chem. Rev.* **2012**, *112*, 1196.
10. Allendorf, M. D.; Bauer, C. A.; Bhakta, R. K.; Houk, R. J. T. *Chem. Soc. Rev.* **2009**, *38*, 1330.
11. Kreno, L. E.; Leong, K.; Farha, O. K.; Allendorf, M.; Duyne, R. P. V.; Hupp, J. T. *Chem. Rev.* **2012,** *112*, 1105.
12. Cui, Y.; Yue, Y.; Qian, G.; Chen, B. *Chem. Rev.* **2012**, *112*, 1126.
13. Hu, Z.; Deibert, B. J.; Li, J. *Chem. Soc. Rev.* DOI: 10.1039/c4cs00010b.
14. Czaja, A. U.; Trukhan, N.; Muller, U. *Chem. Soc. Rev.* **2009**, *38*, 1284.
15. Murray, L. J.; Dinca, M.; Long, J. R. *Chem. Soc. Rev.* **2009**, *38*, 1294.
16. Suh, M. P.; Park, H. J.; Prasad, T. K.; Lim, D. *Chem. Rev.* **2012**, *112*, 782.
17. Li, J.; Sculley, J.; Zhou, H. *Chem. Rev.* **2012**, *112*, 869.
18. Zhang, X.; Ballem, M. A.; Hu, Z.; Bergman, P.; Uvdal, K. *Angew. Chem. Int. Ed.* **2011**, *50*, 5729.

19. Horcajada, P.; Gref, R.; Baati, T.; Allan, P. K.; Maurin, G.; Couvreur, P.; Ferey, G.; Morris, R. E.; Serre, C. *Chem. Rev.* **2012**, *112*, 1232.

20. Stock, N.; Biswas, S. *Chem. Rev.* **2012**, *112*, 933.

21. Huang, L.; Wang, H.; Chen, J.; Wang, Z.; Sun, J.; Zhao, D.; Yan, Y. *Microporous Mesoporous Mater.* **2003**, *58*, 105.

22. Tranchemontagne, D.; Hunt, J.; Yaghi, O. M. *Tetrahedron* **2008**, *64*, 8553.

23. Cravillon, J.; Munzer, S.; Lohmeier, S. J.; Feldhoff, A.; Huber, K.; Wiebcke, M. *Chem. Mater.* **2009**, *21*, 1410.

24. Rabenau, A. *Angew. Chem. Int. Ed.* **1985**, *24*, 1026.

25. Ni, Z.; Masel, R. I. *J. Am. Chem. Soc.* **2006**, *128*, 12394.

26. Mueller, U.; Puetter, H.; Hesse, M.; Wessel, H. WO **2005**/049892.

27. Meek, S. T.; Greathouse, J. A.; Allendorf, M. D. *Adv. Mater.* **2011**, *23*, 249.

28. Pichon, A.; Lazuen-Garay, A.; James, S. L. *Cryst. Eng. Comm.* **2006**, *8*, 211.

29. Friscic, T.; Fabian, L. *Cryst. Eng. Comm.* **2009**, *11*, 743.

30. Cohen, S. M. *Chem. Rev.* **2012**, *112*, 970.

31. Wang, Z.; Cohen, S. M. *Chem. Soc. Rev.* **2009**, *38*, 1315.

32. Ravon, U.; Domine, M. E.; Gaudillere, C.; Desmartin-Chomel A.; Farrusseng, D. *New J. Chem.* **2008**, *32*, 937.

33. Mueller, U.; Schubert, M.; Teich, F.; Puetter, H.; Schierle-Arndt, K.; Pastre´, J. *J. Mater. Chem.* **2006**, *16*, 626.

34. Maji, T. K.; Mostafa, G.; Chang, H. C.; Kitagawa, S. *Chem. Commun.* **2005**, 2436.

35. Mueller, T.; Ceder, G. *J. Phys. Chem. B* **2005**, *109*, 17974.

36. Rieter, W. J.; Taylor, K. M. L.; An, H.; Lin, W. *J. Am. Chem. Soc.* **2006**, *128*, 9024.

37. Qiu, L. G.; Li, Z. Q.; Wu, Y.; Wang, W.; Xu, T.; Jiang, X. *Chem. Commun.* **2008**, 3642.

38. Zou, X.; Zhu, G.; Hewitt, I. J.; Sun, F.; Qiu, S. *Dalton Trans.* **2009**, 3009.

39. Lan, A.; Li, K.; Wu, H.; Olson, D. H.; Emge, T. J.; Ki, W.; Hong, M.; Li, J. *Angew. Chem. Int. Ed.* **2009**, *48*, 2334.

40. Pramanik, S.; Zheng, C.; Zhang, X.; Emge, T. J.; Li, J. *J. Am. Chem. Soc.* **2011**, *133*, 4153.

41. Xu, H.; Rao, X.; Gao, G.; Yu, J.; Wang, Z.; Dou, Z.; Cui, Y.; Yang, Y.; Chen, B.; Qian, G. *Chem. Commun.* **2012**, *48*, 7377.

42. Icil, H.; Uzun, D.; Arslan, E. *Spectrosc. Lett.* **2001**, *34*, 605.

43. Langhals, H. *Heterocycles* **1995**, *40*, 477.

44. Langhals, H.; Blanke, P. *Dyes and Pigments* **2003**, *59*, 109.

45. Tian, H.; Liu, P.; Zhu, W.; Gao, E.; Wu, D.; Cai, S. *J. Mater. Chem.* **2000**, *10*, 2708.

46. Todd, E. K.; Wang, S.; Wan, X.; Wang, Z. Y. *Tetrahedron Lett.* **2005**, *46*, 587.

47. Zhou, Y.; Zhang, D.; Zhang, Y.; Tang, Y.; Zhu, D. J. *Journal of Organic Chemistry* **2005**, *70*, 6164.

48. Sun, R.; Xue, C.; Owak, M.; Peetz, R. M.; Jin, S. *Tetrahedron Lett.* **2007**, *48*, 6696.

49. Xu, Y.; Leng, S.; Xue, C.; Sun, R.; Pan, J.; Ford, J.; Jin, S. *Angew. Chem. Int. Ed.* **2007**, *46*, 3896.

50. Tuntiwechapikul, W.; Taka, T.; Bethencourt, M.; Makonkawkeyoon, L.; Lee, T. R. *Bioorg. Med. Chem. Lett*, **2006**, *16*, 4120.

51. Roy, S.; Maiti, D. K.; Panigrahi, S.; Basak, D.; Banerjee, A. *RSC Adv.* **2012**, *2*, 11053.